



Technical University Graz

Masterthesis

Institute for Chemistry (Karl-Franzens-University Graz)

Prof. Dr. Volker Ribitsch

***Functionalization of cellulose acetate surfaces for the
removal of endocrine disrupting compounds***

submitted by

Victoria Eleonore Reichel

Graz, January, 2012

Master Biotechnology (F 066 484)

EIDESSTATTLICHE ERKLÄRUNG

Ich erkläre an Eides statt, dass ich die vorliegende Arbeit selbstständig verfasst, andere als die angegebenen Quellen/Hilfsmittel nicht benutzt, und die den benutzten Quellen wörtlich und inhaltlich entnommene Stellen als solche kenntlich gemacht habe.

Graz, am

.....
(Unterschrift)

Englische Fassung:

STATUTORY DECLARATION

I declare that I have authored this thesis independently, that I have not used other than the declared sources / resources, and that I have explicitly marked all material which has been quoted either literally or by content from the used sources.

.....
date

.....
(signature)

Abstract

The pollution of water with endocrine disrupting compounds (EDCs), like natural and synthetic hormones, became an important problem in environmental technology. EDCs are known for influencing the sexual development of fish and amphibians even at trace concentrations (ng per liter). Moreover, EDCs in drinking water are suspected to be associated with the decreasing fertility of male population in western countries. Therefore the removal of this class of pollutants out of waste- and surface water is a hot topic in water purification. One of the most promising strategies is the degradation of EDCs using enzymes, which are highly active under environmental conditions. One of the most promising candidates is the robust and widely used horseradish peroxidase. We have screened the activity of novel, genetically designed horseradish peroxidase isoenzymes against 17 α Ethinylestradiol, an estrogen which is used for contraception (anti-baby-pill). The most promising isoenzyme was then produced and purified in a fermentation process using the yeast *Pichia pastoris* as expression system. The produced and purified enzymes shall be immobilized onto the surface of cellulose acetate hollow fiber membranes used in water purification.

In order to make the membrane surface accessible to enzyme immobilization, nanostructured coatings consisting of functional polysaccharides and novel functional polysaccharide composite nanoparticles (developed by our working group), were developed to the membrane surfaces in a very specific manner. Their application procedure was optimized (Sarfus, AFM, QCM) and the surface properties were analyzed (contact angle, zeta-potential) using CA model surfaces. Finally they will be applied to the surface of hollow fibre membranes.

A novel analytical procedure to observe bacterial growth on surfaces, basing on real-time PCR, was set up in order to evaluate the fouling properties of the nanostructured cellulose acetate surfaces.

Solely biodegradable materials basing on renewable resources were used in this work.

Kurzfassung

Die Verschmutzung des Wassers mit endokrin wirksamen Stoffen (EDCs), zu denen natürliche und synthetische Hormone gehören, stellt ein enormes Problem in der Umwelt dar. Auch in geringsten Konzentrationen beeinflussen EDCs die sexuelle Entwicklung von Fischen und Amphibien (ng pro Liter). EDCs gelangen auch in das Trinkwasser und stehen mit der abnehmenden Fruchtbarkeit der männlichen Bevölkerung in den westlichen Ländern in Verbindung. Daher ist die Entfernung dieser Schadstoffe aus Abwasser- und Oberflächenwasser ein heißes Thema in der Wasseraufbereitung. Eine der vielversprechendsten Strategien ist der Abbau von EDCs mit Hilfe von Enzymen, die sehr aktiv unter Umgebungsbedingungen sind. Einer der vielversprechendsten Kandidaten ist die robuste und weit verbreitete Meerrettichperoxidase. Wir haben die neuartigen, genetisch entwickelten Meerrettichperoxidase Isoenzyme verwendet, um 17α Ethinylestradiol zu degradieren. 17α Ethinylestradiol ist ein synthetisches Östrogen, das zur Empfängnisverhütung (Anti-Baby-Pille) verwendet wird. Die vielversprechendsten Isoenzyme wurden hergestellt und in einem Fermentationsprozess unter Verwendung der Hefe *Pichia pastoris* als Expressionssystem aufgereinigt. Die gereinigten Enzyme sollen auf der Oberfläche der Celluloseacetat Hohlfasermembranen immobilisiert werden und in der Wasseraufbereitung eingesetzt werden. Um die Membran-Oberfläche zugänglich für die Enzymimmobilisierung zu machen, wurden nanostrukturierte Beschichtungen aus funktionellen Polysacchariden und neuartige funktionelle Polysaccharid Composite-Nanopartikel hergestellt (entwickelt von unserer Arbeitsgruppe), um die Membranoberflächen in einer ganz bestimmten Art und Weise zu entwickeln. Diese Applikation wurde optimiert (SARFUS, AFM, QCM) und die Oberflächeneigenschaften wurden analysiert (Kontaktwinkel, Zeta-Potential). Verwendet wurden CA Modell Oberflächen. Diese Applikationen können an der Oberfläche von Hohlfasermembranen eingesetzt werden.

Ein neuartiges analytisches Verfahren mittels real time PCR, um das Wachstum von Bakterien auf Oberflächen zu erfassen, wurde entwickelt. Dadurch können die anti-fouling Eigenschaften auf den nanostrukturierten Celluloseacetat Oberflächen bewertet werden. Rein biologisch abbaubare Materialien auf Basis nachwachsender Rohstoffe wurden in dieser Arbeit verwendet.

Danksagung

An erster Stelle möchte ich mich bei meinem Professor Dr. Volker Ribitsch bedanken, durch den es für mich erst möglich wurde dieses Diplomarbeitsthema zu bearbeiten und der mich sehr gefördert und in jeder Hinsicht unterstützt hat. Ein unbeschreiblich großer Dank geht auch an meinen Diplomarbeitbetreuer und wunderbaren Freund Martin Kulterer, der mir die interessanten Seiten der Forschung gezeigt hat und der mir immer bei allen Fragen und Problemen zu meiner Arbeit zur Seite gestanden ist. Als ich man manchmal verzweifelt bin, dass sich z.B. etwas einfach nicht lösen will, hat er mir gut zuredet und mir Mut gemacht nicht aufzugeben. Ein großer Dank geht auch an die gesamte Arbeitsgruppe, die sich zu einem tollen Team entwickelt hat. Es wurden auch viele Freundschaften geknüpft und die Hilfsbereitschaft ist immer vorhanden. Dafür bedanke ich mich besonders bei Rupi, Geri, Tamil, Stefan S., Stefan K., Ivana, Hölli, Simon, Verena, Andrea, Karin, Conny, Theresa, Phino, Doris, Heike, Sylvia, Helga, Birgit, Anna, und Andrea.

Weiteres möchte ich mich auch herzlich bei Prof. Dr. Anton Glieder und seinem Team bedanken, die mich in allen Fragen zur Enzymtechnologie beraten haben und mir einiges in der Biotechnologie zeigten. Ganz besonderer Dank geht an Florian Krainer, der nicht nur ein guter Freund sondern auch ein wunderbarer Kollege geworden ist. Vielen Dank auch an Laura Näätäsaari und Inge Eiteljörg zur lieben Hilfe im Labor.

Ich möchte mich auch ganz herzlich bei Prof. Dr. Koraimann und seiner lieben Kollegin Karin Bischof bedanken, die mir eine große Hilfe auf der Seite der Mikrobiologie waren.

Ein herzliches Dankeschön geht auch an Prof. Dr. Karin Stana-Kleinschek und ihrem Team in Maribor, mit denen wir eine sehr gute Kooperation pflegen.

Ein großes Dankeschön möchte ich auch der Firma Pentair X-Flow und dem EU-Projekt Surfucell aussprechen, durch die die Arbeit auch erst ermöglicht wurde und ich einen tollen Einblick in großtechnische und angewandte Forschung bekommen habe. Besonderer Dank geht an Jens Potreck und Stefan Köhl, die mir einen sehr interessanten Aufenthalt bei X-Flow und viel Wissen zur Membrantechnologie und Wasseraufbereitung ermöglicht haben.

Besonders möchte ich mich natürlich bei meinen wunderbaren Eltern Sonja Reichel und Erich Reichel bedanken, die es mir überhaupt ermöglicht haben mein Studium zu wählen und mich in der ganzen Zeit bis dahin und auch während des ganzen Studiums großartig unterstützt haben. Ohne euch hätte ich das alles nie geschafft!

Ein riesiges Dankeschön geht natürlich an meine beste Freundin Sarah Poguntke, die mich schon seit der Schulzeit durch Dick und Dünn begleitet und auch in den Studienjahren immer für Spaß, Freude und gemeinsame Stunden bereit stand!

Auch herzlich bedanken möchte ich mich bei meiner „Babyfreundin“ Franziska Hütter, die ich seit über 25 Jahren kenne und die einfach ein wunderbarer Teil meines Lebens ist.

Anschließend möchte ich mich auch bei meiner tollen „Biorunde“ (Nelli, Claudia, Sandra, Alex und Flo) bedanken, durch die ich eine lustige, interessante und lernreiche Studienzeit erlebt habe.

Zuletzt möchte ich mich bei meiner gesamten Familie und meinem Freundeskreis bedanken, dass alle immer ein offenes Ohr für mich haben und immer für mich da sind.

Table of acronyms

<i>%wt</i>	<i>weight percent</i>
<i>ABTS</i>	<i>2',2'-azino-bis(3-ethylbenzthiazoline-6sulphonic acid)</i>
<i>AC</i>	<i>Amino cellulose</i>
<i>AFM</i>	<i>Atomic force microscopy</i>
<i>AVI1</i>	<i>Avicell carboxymethyl cellulose</i>
<i>BCA assay</i>	<i>bicinchoninic acid protein assay</i>
<i>BMGY</i>	<i>Buffered glycerol-complex medium</i>
<i>BSA</i>	<i>Bovine serum albumin</i>
<i>BSM</i>	<i>Basal salt medium</i>
<i>CA</i>	<i>Cellulose acetate</i>
<i>CAA</i>	<i>activated cellulose acetate</i>
<i>CaCl₂</i>	<i>calcium chloride</i>
<i>CaSO₄</i>	<i>calcium sulphate</i>
<i>CMC</i>	<i>Carboxymethyl cellulose</i>
<i>CoCl₂</i>	<i>cobalt chloride</i>
<i>CuSO₄</i>	<i>copper sulphate</i>
<i>DA</i>	<i>degree of acetylation</i>
<i>DS</i>	<i>degree of substitution</i>
<i>DP</i>	<i>degree of polymerization</i>
<i>EE2</i>	<i>17 α Ethinylestradiol</i>
<i>EtOH</i>	<i>ethanol</i>
<i>FeSO₄</i>	<i>iron sulphate</i>
<i>H₃PO₄</i>	<i>phosphoric acid</i>
<i>HEC</i>	<i>Hydroxyethylcellulose</i>
<i>HRP</i>	<i>Horseradish peroxidase</i>
<i>H₂O</i>	<i>water</i>
<i>H₂O₂</i>	<i>hydrogen peroxide</i>
<i>H₂SO₄</i>	<i>sulfuric acid</i>

K_2SO_4	<i>potassium sulfate</i>
<i>kDa</i>	<i>kilo Dalton</i>
<i>KOH</i>	<i>potassium hydroxide</i>
<i>LbL</i>	<i>layer-by-layer</i>
<i>L-CHI</i>	<i>Low molecular weight chitosan</i>
<i>LLe</i>	<i>Liquid-Liquid-extraction</i>
<i>MeOH</i>	<i>methanol</i>
$MgSO_4$	<i>magnesium sulphate</i>
$MnSO_4$	<i>manganese sulphate</i>
<i>MQ</i>	<i>Milli-Q</i>
<i>NaI</i>	<i>sodium iodide</i>
Na_2Mo	<i>sodium molybdenum</i>
<i>NaOAc buffer</i>	<i>sodium acetate buffer</i>
<i>OD600</i>	<i>optical density at 600 nm</i>
pO_2	<i>oxygen partial pressure</i>
<i>PTM1</i>	<i>Trace salts solution</i>
<i>QCM-D</i>	<i>Quartz crystal microbalance with dissipation monitoring</i>
<i>rpm</i>	<i>rounds per minute</i>
<i>SEM</i>	<i>Scanning electron microscope</i>
<i>SPE</i>	<i>Solid phase extraction</i>
$ZnCl_2$	<i>zinc chloride</i>

Content

1. Introduction	12
2. Theoretical part	15
2.1 Polysaccharide materials	17
2.1.1 Cellulose	17
2.1.2 Cellulose Acetates (CA, CAP, and CAB)	18
2.1.4 Chitosan (CHI) and Chitin	20
2.2 Polyelectrolytes	21
2.3 Polyelectrolyte adsorption	21
2.4 Nanoparticle precipitation.....	22
2.5 X-Flow Hollow fibre membranes	23
2.6 Surface characterization methods.....	25
2.6.1 Spin coating techniques	25
2.6.2 Atomic Force Microscopy (AFM).....	26
2.6.2 Scanning electron microscopy (SEM).....	28
2.6.3 Sarfus™	31
2.6.4 Contact angle techniques	33
2.7 Spectroscopic methods	35
2.7.1 Absorption and Fluorescence	35
2.7.2 Fluorescence	36
2.7.3 Phosphorescence	36
2.7.4 Fluorescence spectroscopy	37
2.8 Biotechnological processing	38
2.8.1 Horseradish peroxidase (HRP)	38
2.8.2 Recombinant protein expression using <i>Pichia pastoris</i>	39
2.8.3 Expression of novel Horseradish peroxidase isoenzymes	41
2.8.4 Directed evolution.....	42
2.8.5 Fermentation	42
2.8.6 Fermenting <i>Pichia pastoris</i>	43
2.8.7 Purification of HRP.....	45
2.8.8 Fast Protein Liquid Chromatography (FPLC).....	45
2.8.8.1 Superdex™ columns.....	46
2.9 Solid phase extraction (SPE)	50
2.9.1 Supelco LC-18 SPE tubes (1ml).....	50
2.10 The electrical double layer and the Zeta-Potential	51
2.11 Real time polymerase chain reaction (RT-PCR)	54
3.1 Chemicals.....	55
3.2 Instruments.....	56
3.2.1 Atomic force microscope	56
3.2.2 Contact angle instrument	56

3.2.3 Dynamic and electrophoretic light scattering (DLS, ELS).....	56
3.2.4 Sarfus TM	57
3.2.5 Scanning electron microscopy (SEM).....	57
3.2.6 Spin coater.....	58
3.2.7 Death/Live fluorescence staining assay.....	58
3.2.8 Real-time polymerase chain reaction (RT-PCR).....	58
3.2.9 BIOSTAT CT fermenter.....	59
3.2.10 FPLC ÄKTA purifier system.....	59
3.2.11 Spectramax Plus 384 spectrophotometer.....	59
4.1 Methods.....	59
4.1.1 Hollow fibre membrane production process (X-Flow).....	59
4.1.2 Synthesis of CA nanoparticles.....	60
4.1.3 Preparation and activation of CA model films (CAA).....	62
4.2 Results and discussion.....	63
4.2.1 Polysaccharide composite nanoparticles.....	63
4.2.2 Effective zeta potential.....	66
4.2.3 Stability of composite CA nanoparticles.....	67
4.2.4 Modification of CA surfaces.....	67
4.2.5 Activation of CA surfaces.....	68
4.2.6 Polysaccharide coating.....	69
4.2.7 Coating with polysaccharide composite nanoparticles.....	70
4.3 Conclusions, problems, difficulties.....	71
5.1 Methods.....	72
5.1.2 Preparation of media, buffer, and bacteria suspensions.....	72
5.1.3 Sample surface preparation.....	72
5.1.4 Incubation procedure.....	73
5.2 Results and Discussion.....	73
5.2.1 Incubation and cultivation procedure.....	73
5.2.2 Live/Death fluorescence staining technique.....	74
5.2.3 Real Time (RT) PCR.....	75
5.2.4 Scanning electron microscopy (SEM).....	78
5.3 Conclusions, problems, difficulties.....	79
6.1 Methods.....	79
6.1.1 Preparation of 17 α Ethinylestradiol solution.....	79
6.1.2 Enzyme and hormone incubation procedure.....	79
6.1.3 Determination of the enzyme activity.....	80
6.2 Results and discussion.....	82
6.2.1 EE2 analysis.....	82
6.2.2 Sample clean up.....	83
6.2.3 Liquid-liquid extraction (LLe).....	83
6.2.4 Solid phase extraction (SPE).....	84
6.3 Conclusions, problems, difficulties.....	87
7.1 Methods.....	88

7.1.2 Media and buffer solutions.....	88
7.1.3 Fermentation process	89
7.1.4 Fermenter	90
7.1.5 Fermentation procedure	90
7.1.6 Measuring the enzyme activity.....	90
7.1.7 Harvesting process.....	91
7.1.8 Enzyme purification	92
7.2 Results and discussion	93
7.2.1 Preculturing	93
7.2.2 Fermentation process	94
7.2.3 Harvesting process.....	96
7.2.4 Purification.....	96
Materials and Methods	99
7.2.5 Conclusion, problems, difficulties	102
8. Summary	103
9. List of tables	104
10. List of figures	105

1. Introduction

Endocrine disrupting compounds (EDCs) are a class of organic substances including natural and synthetic hormones, and substances of hormone-like chemical structure. This substance class has become a hot topic in environmental science. These chemicals are biologically active even at trace concentrations. In particular, even lowest concentrations of EDCs (ng/l^1) are known for influencing the reproduction of fish and amphibians, and can cause spontaneous sex change of these animals². Moreover, EDCs are suspected to be associated with the decreasing fertility of the male population in western countries over the last 50 years³. Most of natural and synthetic hormones found in the environment originate from contraception pharmaceuticals, like the anti-baby pill. The pollutants access surface- and wastewater mostly via the urine of women, which are using these contraceptions⁴. The most prominent substances are naturally occurring 17β -estradiol, estrone, and estriol, and synthetic 17α -ethinylestradiol. Especially 17α -ethinylestradiol is very frequently used for contraception⁴. The removal of these substances from waste- and surface water is very critical, and none of the existing technologies⁵, has proven its applicability at a large scale. This is because most of EDCs are resistant against standard degradation techniques like ozone treatment or UV- irradiation⁶, and most adsorption techniques⁷ (like charcoal) show too low binding constants for removing EDCs at very low concentrations. Therefore, there is a need for alternative water purification and clean-up methods for the degradation/removal of EDCs. Very promising candidates are EDC degrading enzymes like laccase⁸ and horseradish peroxidase⁹, for example. Enzymes take advantage of degrading the target components instead of binding them like aptamers or cyclodextrins¹⁰. The addition of hard chemicals is not required. Moreover, enzymes are able to react with EDCs even at lowest concentrations due to their high binding constants. Enzymes are usually utilized in solution, or in fixed bed reactors¹¹. The aim of this project is the immobilization of EDC degrading enzymes onto the surface of cellulose acetate hollow fiber membranes used for water purification (provided by Pentair X-flow Enschede, the Netherlands). Membrane based filtration techniques are commonly used for removing bacteria (microfiltration¹²), viruses (ultrafiltration¹³), ions (reverse osmosis¹⁴), or organic pollutants (nanofiltration¹⁵). Compared to classical water purification techniques, membranes take advantage of^{16,17}. Due to their sponge-like structure, hollow fiber membranes comprise a very large surface-to-

volume ratio¹⁸. Therefore, hollow fiber membranes are ideal candidates for immobilizing large amounts of active compounds in a relatively small volume.

For degrading EDCs, the plant enzyme horseradish peroxidase (HRP) was chosen. HRPs are very frequently used for sensor applications and fast analytics in medicine and live science, for example electrochemical sensors¹⁹, or ELISA test kits²⁰. The enzyme family HRP consists of more than 40 iso-enzymes, which vary in their isoelectric point, degree of glycosilation, stability, and activity. Commercial available HRPs are usually extracted directly from the horseradish plant. The main drawbacks of this source are seasonal changes of the quality (influence of growing conditions), and the expensive and time consuming purification. Besides that, the main limitation for the applicability of commercial available HRP in water purification is its dependency on hydrogen peroxide, which acts as electron acceptor in the reaction cycle²¹.

A promising route to overcome these limitations is the biotechnical production of HRP via expression through bacteria like *Escherichia coli*²², or yeasts like *Pichia Pastoris*²³. Besides providing high enzyme yields and easier purification, the biotechnological production allows modifying and optimizing the enzymes at the genetically level. In this work, novel, genetically engineered HRP isoenzymes (Institute of Molecular Bioscience, TU-Graz) were screened on their activity to degrade hormones in absence of hydrogen peroxide. As model substance, the estrogen 17 α -ethinylestradiol was chosen, which is frequently used in pharmacy. The most promising candidate was then produced via the expression through *Pichia Pastoris*, and purified.

Since the surface of cellulose acetate hollow fiber membranes is relatively inert, the development of a suitable way for making the cellulose acetate accessible for enzyme immobilization was required. This was performed via activating the surface followed by applying nanostructured coatings, consisting of functional polysaccharides and polysaccharide composite nanoparticles (recently developed by our group²⁴), onto the cellulose acetate surface. In particular, the cellulose acetate surface was first activated by cleaving ester bonds. Next, mono- and bi-layer of different functional polysaccharides (chitosan, carboxymethyl cellulose, hydroxyethyl cellulose) were adsorbed onto the activated surface. In the final step, polysaccharide composite nanoparticles were immobilized onto these surfaces. The coating procedure was developed and optimized using very well defined cellulose acetate thin films. These model surfaces were used in order to analyze the surface modification processes using SarfusTM, static contact angle measurements, quartz crystal microbalance (QCM), atomic force microscopy, and scanning electron microscopy (SEM).

Besides making the surface accessible to bind active biomolecules, these nanostructured coatings can be used for reducing biofouling on the membrane surface. Biofouling is the attachment and growth of bacteria in form of biofilms. In biofilms, bacteria of different species are embedded in a matrix, which mainly consists of proteins and polysaccharides. This sticky, slimy matrix is very robust, and protects bacteria from environmental influences, even antibiotics²⁵²⁶. These biofilms block the pores of membranes. Since biofilms are very robust, harsh chemical treatment is required to remove the bacteria from the surface. This treatment is expensive, negative for the environment, and limits the membrane lifetime because the chemicals damage the membrane material. The bacterial attachment and growth on surfaces can be reduced by following two strategies: An increase of the surfaces negative charge density and hydrophilicity makes it difficult for bacteria to attach to a surface, because tightly bound water molecules act as barrier, and negative surface charges repel the negatively charged surface of bacteria. The second strategy is the introduction of antimicrobial functionalities, which kill bacteria on the surface. For water purification, the number of possible coating materials is limited due to health risks. Biodegradable, eatable polysaccharides comprising the desired properties are therefore promising candidates for anti-fouling coatings in water purification.

The nanostructured coatings developed in this work comprise a mixed functionality, for example via applying two compounds: negatively charged, highly hydrophilic carboxymethyl cellulose, and antimicrobial chitosan composite nanoparticles²⁷.

The bacterial growth on surfaces is usually evaluated using scratching off / plating out techniques. These methods are time consuming, and often lack of reproducibility (ZIT). Therefore, we have set up a novel procedure for analyzing the bacterial growth on surfaces. In our approach, the total amount of bacteria on surfaces was determined by quantifying the amount of DNA using real-time polymerase chain reaction (RT-PCR). Additionally, we implemented a fluorescence staining assay in order to distinguish between death and alive bacteria on a surface. The test assembly was set-up using coated cellulose acetate model films. As model organism, biofilm forming Escherichia Coli MG 1655 R1-16 was used. The test results were validated by the direct analysis of the surface using scanning electron microscopy (SEM).

After optimizing the process, we could show that the test assembly is suitable for analyzing a broad variety of solid samples, like fibers and yarns.



Figure 1: Influence of hormones on fish fertilization rates²⁸.

2. Theoretical part

Endocrine disrupting compounds (hormones)

Steroid hormones

Hormones are physiological active substances which control many physiological processes, for examples gene expression and regulation, cell differentiation, and embryonic development ^{29, 30}. Organisms control specific actions, like growth regulation, reproduction, the maintenance of the inner milieu of cells, and metabolism adoptions on environmental changes through hormone distribution. Hormones are created and synthesized in cells which are produced in endocrine glands and endocrine organs, which are spread over the whole body of the organism.



Figure 2: Anti-baby pill³¹.

17 α Ethinylestradiol

17 α Ethinylestradiol (EE2) is a synthetic estrogen which is used in contraceptives (anti-baby pill). It was first synthesized in 1938 by Herloff Inhoffen and Walter Hohlweg at Schering AG in Berlin³². Taken orally, only the minor part of the hormone is taken up by the body. The major amount is excreted via

the urine and enters the water cycle. Therefore, EE2 gives rise to many health and environmental problems. Fish are sensitive to estrogens in water, even when the estrogen amounts are very low (ng/l)³³.

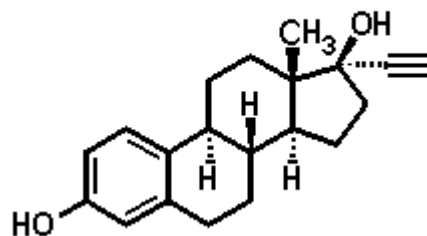


Figure 3: 17 α Ethinylestradiol³¹.

Biofilm formation and antimicrobial properties

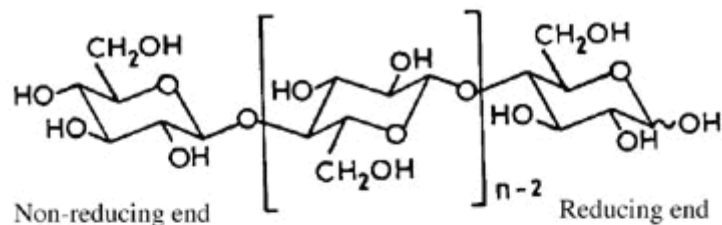
The bacterial growth and biofilm formation on surfaces is today one of the major problems in medicine (i.e. wound and implant infections) and technology (membrane fouling)³⁴. Biofilms are complex mixtures of different bacteria species, which are embedded in a matrix executed by the bacteria consisting mostly of polysaccharides and proteins. This matrix protects bacteria from environmental impacts, also antibiotics³⁵. Therefore, it is very difficult to kill and/or remove bacterial biofilms from surfaces. The bacterial growth on solid supports is commonly evaluated by plating out techniques. Here bacteria are manually collected from the surfaces, usually by manual scratching. The collected bacteria are then cultivated, and the colony forming units are counted manually³⁶. These tests are often problematic. It is difficult to ensure a satisfying accuracy and reproducibility because of the large number of manual steps. Therefore the operator has a huge influence on the obtained results³⁶. Moreover, it is not possible to distinguish between death and alive bacteria on the surface. A promising alternative are fluorescence staining techniques³⁷. Commercial available staining KITS, which include two different fluorescent dyes, allow quantifying and distinguishing death and alive bacteria on a surface³⁷. However, the quantitative use of such techniques is hampered by the fact that different bacteria strains show different accessibility for the fluorescent stains. Moreover, fluorescence microscopes are used for detection, which show limited sensitivity and reproducibility (influence of temperature, humidity, etc.). Therefore, we were aiming for an alternative technique, which allows on the one hand the quantification of the total amount of bacteria growing on a surface, and on the other hand gives semi-quantitative information about the amount of death and alive bacteria on a surface. For the quantification of bacteria on a surface, RT-PCR technique was used. The method allows

detecting and quantifying the amount of bacterial DNA³⁸. RT-PCR provides short detection times, high sample throughput, lowest detection limits, broad linear ranges, and high reproducibility³⁸. For distinguishing death and alive bacteria, a two fluorescent dye KIT was chosen, which allows selectively staining of death and alive *E.coli* bacteria. The obtained results were evaluated using SEM, which is a standard method for evaluating bacterial growth on surfaces³⁹. Additionally, the amount of bacteria in the incubation solution was determined by measuring the OD₆₀₀⁴⁰, in order to investigate the influence of the antimicrobial surface modifications on the bacterial growth in the surrounding.

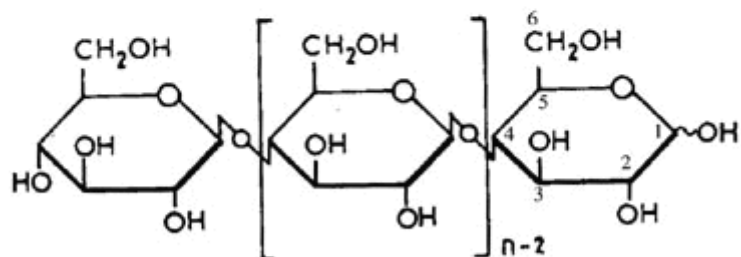
2.1 Polysaccharide materials

2.1.1 Cellulose

Cellulose is a linear polymer consisting of 1, 4-D-glycopyranose molecules. One monomer contains three accessible OH groups. At the C2 and C3 position secondary hydroxyl groups are arranged in equatorial position. The primary OH at C5 position is arranged in the thermodynamically preferred tans-gauche position. The properties of cellulose vary with its degree of polymerization (n). In general, the material is poorly soluble in most solvents (also water), and cannot be converted in the melted state before degradation^{41,42}. Cellulose is the most occurring biopolymer in nature. Pure cellulose is produced from many sources, it builds up plant cell walls for example, and occurs as a composite with pectins, lignin, hemicellulose, etc... Therefore, to achieve pure cellulose from plants, the other constituents have to be separated. In contrast, bacterial cellulose is naturally available in a pure state. One of the most important chemical and technical processing of cellulose undergoes the regeneration of cellulose in the viscose process. Cellulose is converted to cellulose xanthogenate. Cellulose xanthogenate is dissolved in aqueous sodium hydroxide, and the secondary fractions are separated. For the precipitation, not environmentally friendly heavy metals and CS₂ are used. Because of its large number of available OH groups, cellulose is easy to functionalize and modify. Esterification and etherification are two of the most important technical cellulose derivatization processes. The derivatization of *cellulose does not happen completely during heterogeneous reactions. The OH-groups at position C2, are favoured, followed by the C6 and the C3 hydroxile groups. Principally, substitution takes place in a statistically manner. The degree of substitution (DS) is the average number of substituted OH groups per glucose unit. A maximum DS of 3 can be achieved, because each anhydroglucose unit contains three free hydroxide groups*^{41,42}.



Sometimes shown as



Cellulose

Figure 1: Cellulose⁴³.

2.1.2 Cellulose Acetates (CA, CAP, and CAB)

Many cellulose esters are important for industrial purposes. Some examples of these esters are cellulose acetate (CA), cellulose acetate propionate (CAP) and cellulose acetate butyrate (CAB). These cellulose acetates are widely used in industry and pharmacy, for example as tablet extender, flat screens, textiles, sunglasses, home furnishings, membranes⁴⁴, e.g. X-Flow hollow fibre membranes, and slip covers. They are also used for creating composite materials⁴¹.

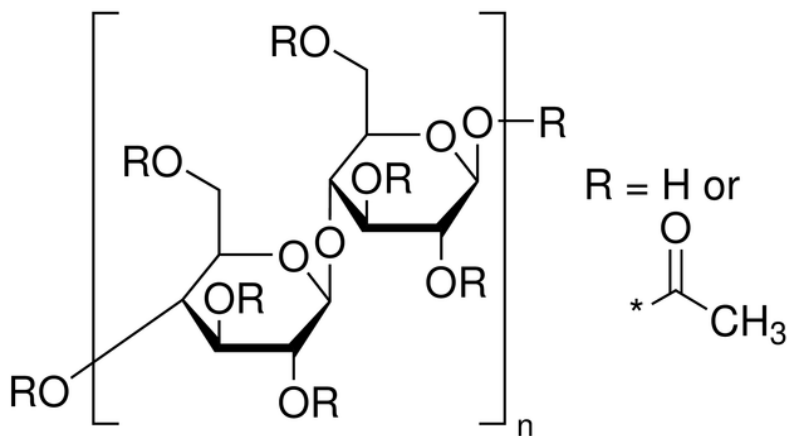


Figure 2: Cellulose acetate⁴⁵.

2.1.3 Carboxymethyl Cellulose (CMC)

Carboxymethyl cellulose is a very important cellulose derivative. It is used in food industry as emulsion stabilizer, as viscosity modifier, as water-based detergent, for papers, paints and lubricants⁴⁶. CMC is commonly used as sodium salt and it has very high water solubility. CMC is created through a slurry process of swollen cellulose which is treated with NaOH. Due to the substance chloroacetic, the alkali cellulose is etherified⁴¹. CMC's solution properties vary due to the differences in the CMC's molecular weight, the pH-value of the solution, and the CMC's degree of substitution. The pKa value of CMC lies between 4 and 5, which is also depending on the DS. When tuning the pH value of the solution, the charge of the polyelectrolyte is varied⁴⁷.

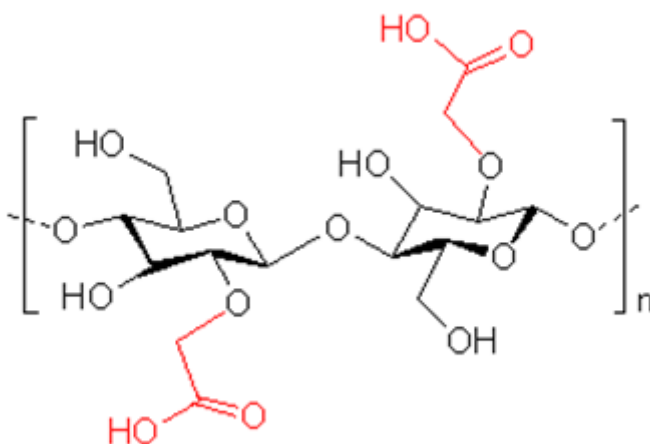


Figure 3: Carboxymethyl cellulose⁴⁸.

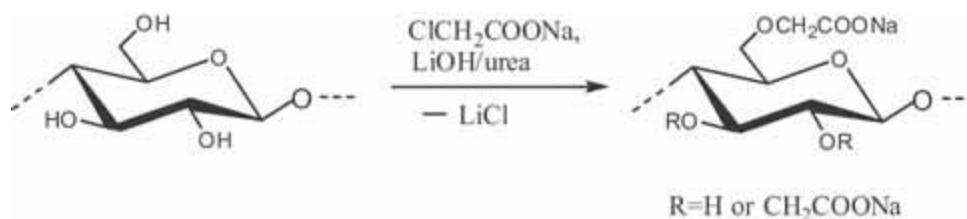


Figure 4: Reaction scheme of cellulose carboxymethylation in LiOH/urea aqueous solution.

2.1.4 Chitosan (CHI) and Chitin

Chitosan is a partly deacetylated form of chitin. Chitosan (CHI) and chitin can be found in insects, and fungi. But it is gained mostly through the alkaline deacetylation of chitin. Chitosan is a green polymer, because it is biodegradable and biocompatible. Chitin is insoluble and the deacetylation renders it selective even this is not completely achieved. Due to this fact, chitosan is a copolymer of deacetylated and acetylated 2-deoxy-D-glucopyranose units. Chitosan is a weak polycation with a pKa of 6,5. It is the only natural cationic polysaccharide. The degree of acetylation (DA) influences the charge density of this polymer. Also the pH-value of the solution is influencing its properties⁴⁹. The ionic strength of the solution, the solutions pH value, and the chitosan molecular weight are influencing the solubility of chitosan. Other biopolymers like lipids and proteins are negatively charged and can therefore easily interact with chitosan. Chitosan is an antimicrobial substance, which is able to act against viruses, fungi and bacteria. This is because of its cationic character, and its high nitrogen content. According to Begin and Calsteren, chitosan shows antimicrobial properties because of its positively charged protonated amino groups which can interact with the negatively charged membrane surfaces and shell proteins of bacteria, fungi and viruses⁵⁰. Ca^{2+} ions bind to chitosan, which therefore can attach to negatively charged membrane sites even at pH values below its pKa. The dimensional stability of cell membranes is therefore negatively affected and the cell collapses⁵¹.

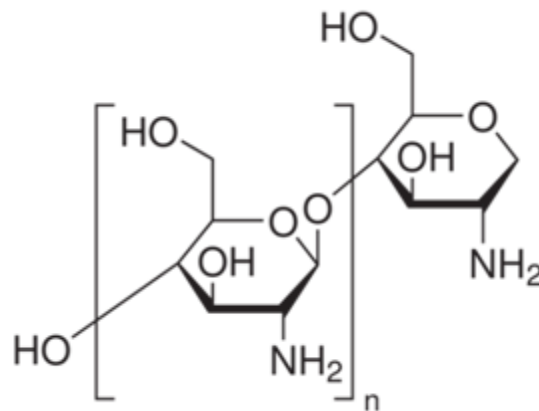


Figure 5: Chitosan⁴⁸.

2.2 Polyelectrolytes

Polyelectrolytes are water soluble macromolecules which carry repeating units of ionisable functional groups. Like electrolytes (e.g. salts), these polymers can be classified as strong or weak polyelectrolytes. Strong polyelectrolytes carry permanently charged functions. Weak polyelectrolytes carry dissociable functions, which are charged over a certain pH range⁵². The charges predominately influence the macromolecule's conformation in solution. The charge density of weak polyelectrolytes (degree of dissociation) can be adjusted by changing the pH. Moreover, charges can be shielded by the adsorption of counter ions. Hence, modifying the solution's ionic strength leads to conformational changes⁵³. Highly charged polyelectrolytes are in stretched conformation (maximal distance of charges of the same type). When charges are shielded, or the charge density is decreased by changing the pH, the conformation turns to a random coil (**Figure 6**)⁵⁴.

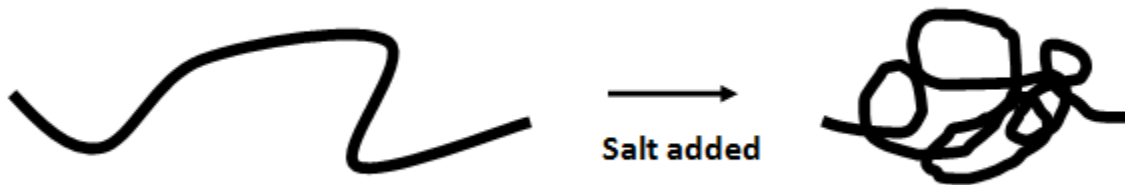


Figure 6: Influence of salt.

2.3 Polyelectrolyte adsorption

The accumulation of a gas, liquid, or solid on an interface is called adsorption. The Gibbs free energy (G) (**Equation 1**) describes the relation between temperature (T), entropy (S), and free enthalpy (H), and shows if a species adsorb on a surface, or not. Adsorption occurs when ΔG is negative.

$$\Delta G = \Delta H - T\Delta S$$

Equation 1

ΔH interaction energy.

$T\Delta S$ entropical term: a balance between decrease of entropy due to the reduced degree of freedom of an adsorbed polymer compound to an adsorbed one. The release of adsorbed H_2O molecules increase S .

When ΔG is zero, a system is in equilibrium state. This happens due to entropic and attractive forces. The adsorption and self assembly of polymers on surfaces can be used to generate functional nanostructures in a very specific manner. For example, one gain build of nanometric polymer multilayers by an alternating deposition of oppositely charged polyelectrolytes (layer-by-layer technique, LbL, see **Figure 7**)⁵⁵. The advantages of LbL technique are the easy applicability (dipping, spraying of the polyelectrolyte solution, and the enormous number of different natural and synthetic polymers, which can be used. These nano-structured thin films are widely used i.e. for designing antifouling /antimicrobial surfaces, sensors, and integrated optics⁵⁶

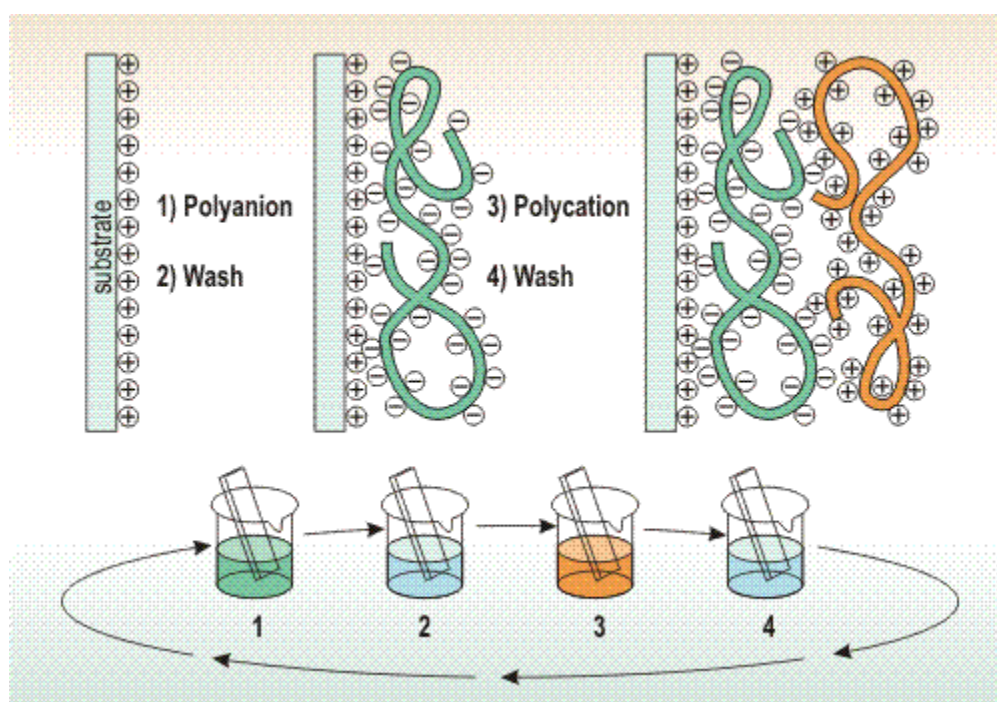


Figure 7: LbL technique: A negative charged polymer attaches on a positive charged surface, then a positive charged polymer can attach on this negative charged polymer. Double layer and bi-layer can be created⁵⁵.

2.4 Nanoparticle precipitation

The design and characterisation of nanoparticles has become a fast growing field of interest during the last decades. Typical applications are seen in drug delivery, food chemistry, surface coatings, sensors,

etc.⁵⁷. Through their small size, specific shape, and large surface to volume ratio, nanoparticles are very suitable for introducing new functions and huge accessible surface areas. A new method to prepare cellulose acetate (CA) nanoparticles by using nanoprecipitation technique was recently developed in our group by Martin Kulterer²⁷. Small, narrow size distributed NP could be generated by modifying the dispersive media with good solvents. In particular, best results were obtained with Tetrahydrofuran (THF), which was added to the non-solvent. Moreover, the influence of efficient agitation, sonication, temperature, pH value, and the stirrer shape and velocity on the particle formation process was investigated in this study. Under optimal conditions, spherical nanoparticles of 60 nm diameter, a Pdl of 0.19, could be generated with a yield of 87 %²⁷. Base on this method, we aimed for preparing functional composite nanoparticles from CA and variable hydrophilic polysaccharides.



Figure 8: Nanoparticle precipitation instruments in the laboratory scale.

2.5 X-Flow Hollow fibre membranes

The first artificial membranes were produced out of cellulosic materials, like nitrocellulose or cellophane. Since 1970, these materials were displaced by cellulose acetate or synthetic polymers like polyethersulfone. Hollow fibre membranes are produced in a solvent spinning process, which is in

principle similar to the CA nanoparticle precipitation process. The solvent (containing the polymer) and the non-solvent are mixed together via spraying in a metal tube, and the forming hollow fibre is directed in a precipitation bath⁵⁸. Membrane separation technologies are environmentally friendly processes with low chemical input and energy costs. The company Pentair X-Flow is worldwide known for their experience and expertise in water purification. Pentair X-Flow produces hollow fibre membrane filtration systems for cleaning waste- and surface water, and for purifying beverages, wine, and beer. The company produces a variety of different membrane types, ranging from micro- to nano-filtration systems¹⁸.



Figure 9: Pentair X-Flow water treatment¹⁸.

The hollow fibre membranes are produced in one step out of a single material. Ultrafiltration membranes are produced in capillary form, whereas microfiltration membranes are tubular shaped. The membranes are of asymmetric structure. Contrary to symmetric membranes of even pore size distribution, the pore size distribution of asymmetric membranes changes through the membrane wall. Pentair X-Flow hollow fibre membranes comprise a thin layer of small pores at the inner membrane wall, and large pores at the outside. Thus, the membranes allow filtering from inside out⁵⁹.



Figure 10: Hollow fibre membrane and hollow fibre membrane modules connected together to form the Megablock^{60, 61}.

2.6 Surface characterization methods

2.6.1 Spin coating techniques

Spin coating is an often used method for polymer coatings. It is based on the fast rotation of a substrate, which is covered with a solution of the coating substance. This solution is spread over the substrate when the substrate is rotated. A thin, homogeneous film is remaining on the substrate, and the coating substance precipitates in form of a thin layer due to evaporation of the solvent. The coating layer thickness and morphology can be influenced by adjusting coating substance concentration, viscosity and wettability, and changing the rotational speed, the acceleration, the rotation time, and the atmosphere⁶².

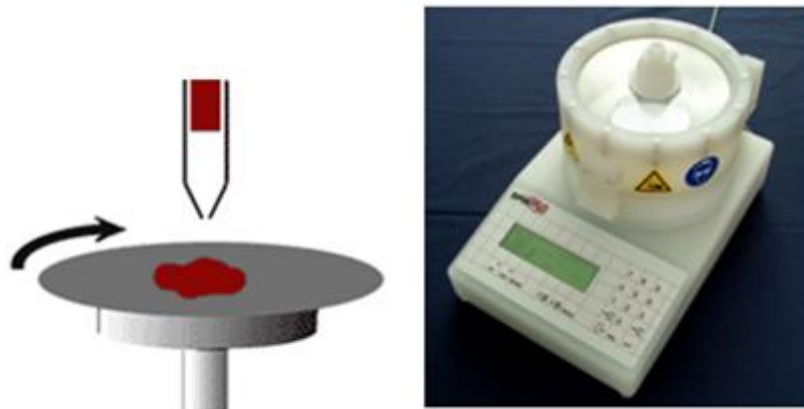


Figure 11: Spincoating procedure and Spincoater^{63, 64}.

2.6.2 Atomic Force Microscopy (AFM)

Atomic force microscopy (AFM) is a scanning probe technique (like scanning tunnelling microscopy) which allows, with atomic resolution, analysing surface morphologies, roughness, chemical structures, dominant interactions, and mechanical properties⁶⁵. A tip, which is placed at the end of a flexible cantilever, is sensing across a sample surface. 3D topographical and/or chemical informations are obtained by measuring the response of the tip. The method allows analysing various surfaces also under environmental conditions⁶⁶. In detail, the tip is fixed on the free end of the cantilever (**Figure 12**). The shape of the tip, and the cantilever used, depend on the sample characteristics and the measurement set-up. The forces acting between the tip and the sample surface results in a deflection of the cantilever (**Figure 12, B**). These forces depend on the surface chemistry, and the distance between tip and surface (surface topology). The deflection of the cantilever is measured using a laser beam. This laser beam is directed to the upper cantilevers surface, and gets reflected. The reflected beam is directed to a photodiode detector (**Figure 12, A-D**)². The surface information is finally obtained using an electronic feedback system (**Figure 12, F**).

The resolution ranges from atomic size to structures larger than 125 μm , which allows measuring also rough samples. In comparison to the scanning electron microscopy (SEM), the atomic force microscopy can reach much higher resolutions⁶⁵.

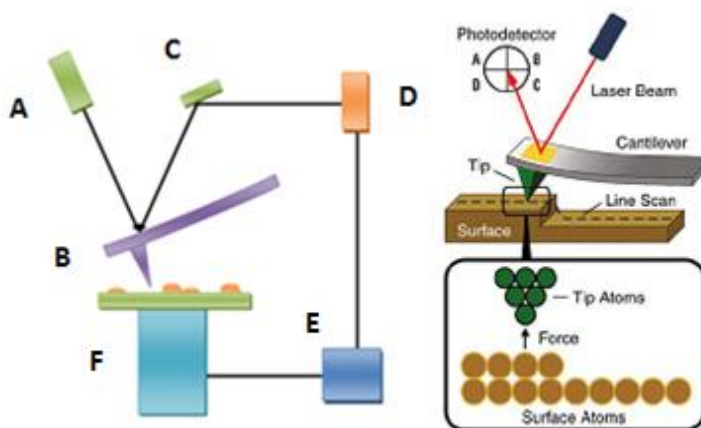


Figure 12: Schematic drawing of working principle: Laser diode (A), cantilever (B), mirror (C), position-sensitive photo detector (D), electronic feedback system (E), sample (F)⁶⁶.

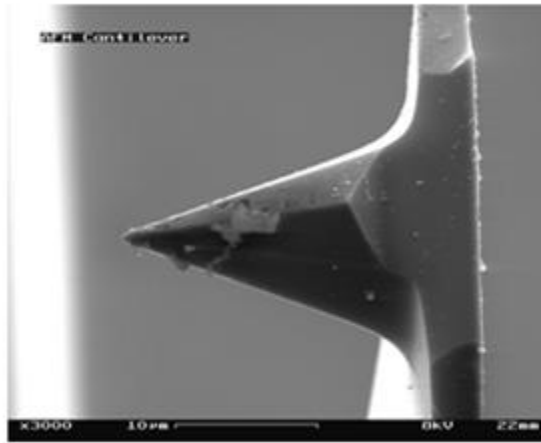


Figure 13: SEM image of an AFM tip⁶⁷

Modi in AFM

AFM can be performed in dynamic and static modi. When using static modi, the distance between the tip and the surface is held constant. The static modi therefore records static deflections of the cantilever with respect to the tip/surface distance. Static modi can therefore be used for determining attractive/repulsive forces in a distance-specific manner (**Figure 14**)⁶⁶.

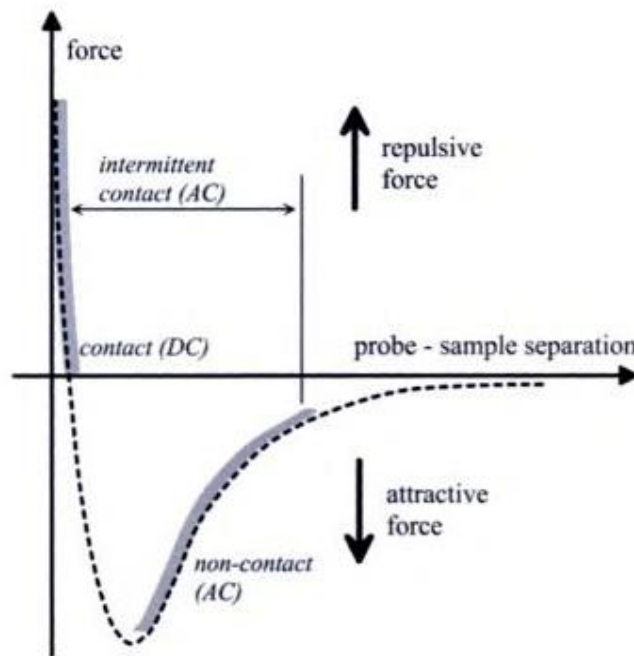


Figure 14: Forces between tip and sample with respect to the distance from the surface⁶⁶.

Static modi

Contact mode

The tip is in direct contact with the sample surface. Repulsion from electron shells of the atoms leads to an upward deflection of the cantilever. This mode is used for investigating rigid, flat sample surfaces⁶⁸.

Non-contact mode

The tip does not get in contact with the sample. The dominant forces acting on the tip can be screened by adjusting the tip-sample distance. The acting forces are much weaker, compared to the contact mode⁶⁹.

Dynamic modi

Intermittent contact mode (tapping mode)

In this mode the cantilever is oscillating, but the tip does not get in direct contact with surface. The oscillation frequency of the cantilever decreases when the tip is coming very close to the sample surface due to surface-tip interactions (**Figure 15**). Because of variations of the interaction potentials, the resonance frequency, phase frequency, and amplitude changes in a very specific manner. Hence, the data comprise information about the morphological, chemical and physical properties of the surface⁶⁶.

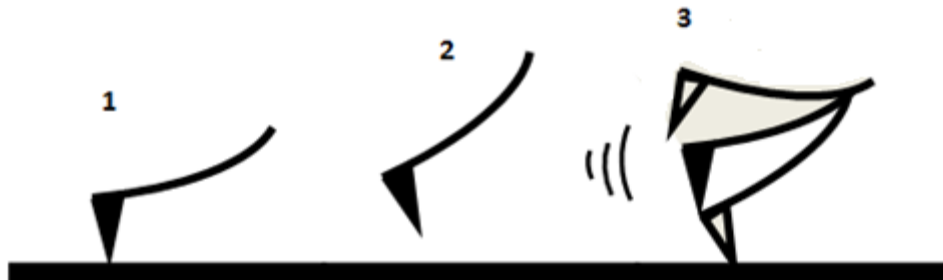


Figure 15: Different AFM modi: Contact mode (1), non-contact mode (2), tapping mode (3).

2.6.2 Scanning electron microscopy (SEM)

In the 1930s, the first transmission electron microscope (TEM) was developed. At these times, also the principle of scanning electron microscopy was invented. The first scanning electron microscope was engineered by Knoll and von Ardenne (1935). In the year 1963, Zworykin, McMullan and Oatley developed a better version of the scanning electron microscope (SEM). Today, instruments are able to

resolve up to 20 nm, with a magnification up to 200,000. In contrast to the TEM, which works in principle like optical transmission microscopes, SEM is a scanning technique. It can be used for three dimensional studies surfaces, which is not possible with TEM. Magnetic lenses are used for focusing an electron beam to one spot. This spot scans over the surface. On the surface is an electrically conductive specimen. The electron beam generates secondary electrons when hitting a conductive specimen. Isolators have to be covered with every thin layer of conductive material (often by "sputtering" with gold⁷⁰). These secondary electrons get collected using a secondary electron detector, and the signal gets converted into an image. Very important, the measurements have to be conducted under vacuum³⁹.

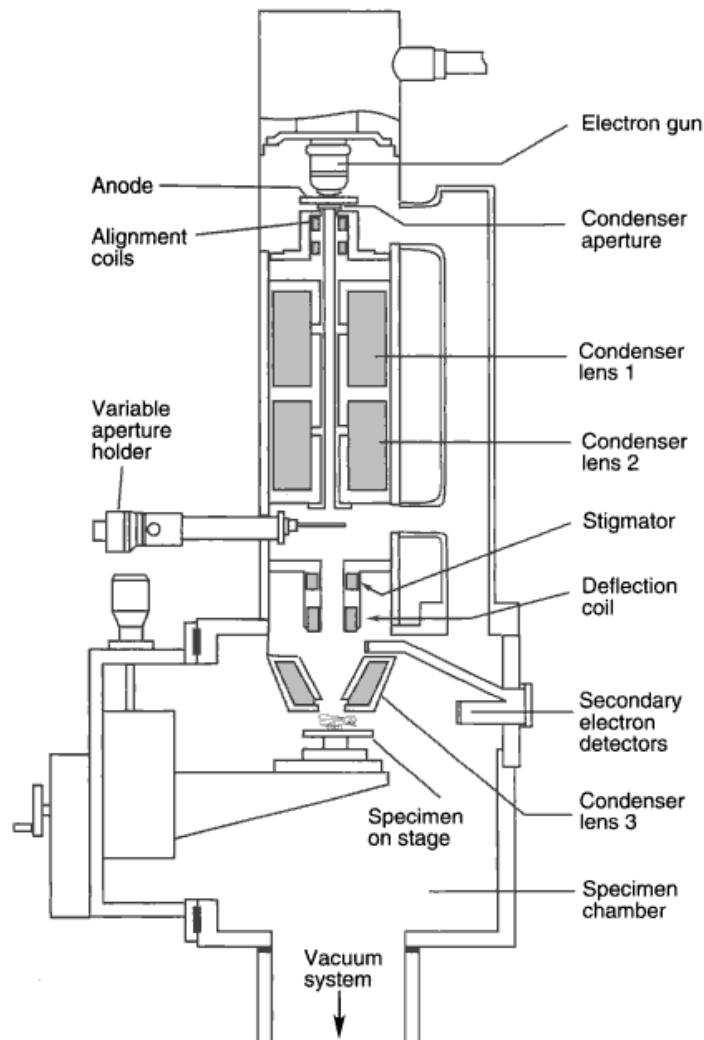


Figure 16: Column of SEM with major components⁷¹.



Figure 17: Modern, digital scanning electron microscope⁷¹.



Figure 18: SEM.

2.6.3 Sarfus™

Sarfus™ is an optical measurement technique for the determination of film thicknesses which was developed from the company nanoLANE. The enhanced contrast between a sample and the background is measured and leads to a high sensitive method in comparison to a conventional optical microscope. Therefore, the adsorption of monolayer of polyelectrolytes, nanoparticles or surfactants can be monitored. Supports (Surfs) made out of a silicon dioxide multilayer are used for the Sarfus™ microscopy. The uses of contrast-enhanced sample supports, so-called Surfs, are required for using this technique. These surfs are special multilayer coated silica supports, which comprise non-reflecting surfaces. The special multilayer coating enhances the contrast of about twice the magnitude, compared to plain silicon supports. The surfs can be decorated with material using spin coating, dip coating, or spray coating techniques⁷². The surfs can reflect the polarized light, without shifting the polarization plane. Silicon dioxide wafer can also be used for Sarfus™ microscopy. The contrast sensitivity with the silicon dioxide wafer is less than using surfs for this method. The incoming polarized light beam is totally reflected on the support (Surf). The state of polarization is remaining identically. By using a cross-polarizer in front of the detector, the background intensity can therefore be minimized. Samples, which are placed on the supports, interact with the polarized light. This leads to a change of polarization of the reflected light beam. When this shifted polarized light reaches the cross polarizer, a part of the light passes through and can be detected. **Equation 2** describes the correlation between the intensity I and the contrast C . I_1 is the object intensity and I_0 is the background intensity. Minimizing the background intensity increases the contrast⁷³.

$$C = \frac{I_1 - I_0}{I_1 + I_0}$$

Equation 2

The polarized light shift increases with increasing film thickness. Therefore, the film thickness can be correlated with the intensity of the detected light. Before measuring a sample, the system has to be calibrated by measuring a reference material with steps of defined high (**Figure 19**). On this Sarfus™ standard reference support, it can be seen that the steps are lighter when the film thickness is decreasing. Between the film thickness and the references intensity, a linear regression can be created between 10 nm and 80 nm⁷³. The technique gives images with high dimensional accuracy (< 1 nm), and roughness measurements, step high measurements and profile extraction can be performed⁷³.

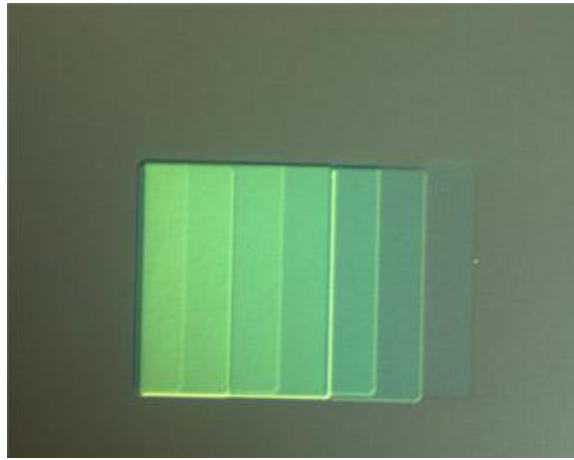


Figure 19: Sarfus standard⁷³.

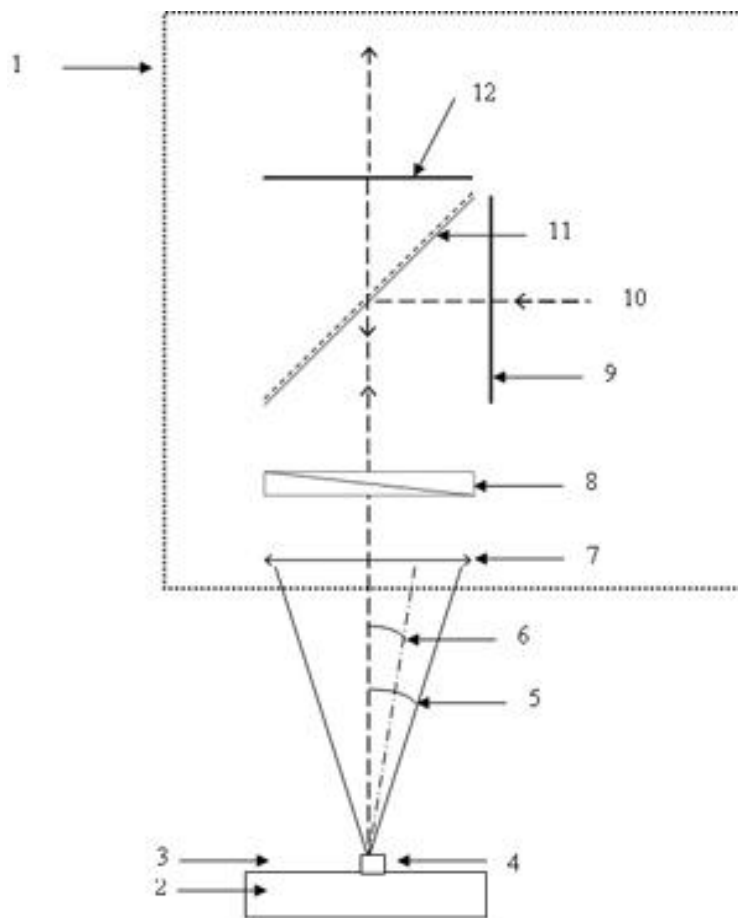


Figure 20: Optical polarizing microscope (1), Surf (2), Incident medium (3), Nanometric sample (4), $\Delta\theta$ (5), θ_0 (6), Objective (7), Differential Interference contrast device (8), Polarizer (9), Non-polarized white light beam (10), Mirror (11), Crossed polarizer = analyzer (12)⁷³.

2.6.4 Contact angle techniques

The surface analysis using contact angle θ measurements bases on the wettability of a solid by a liquid. The contact angel (θ) is formed at the three phase boundaries between a liquid, a solid surface and the gaseous environment. These boundaries are forming the wetting line. As lower the contact angle, as better is the wettability of the surface. For measuring the contact angle in a static way (sessile drop), a droplet of defined volume is placed onto the sample surface, and the contact angle is measured. A complete wetting is presented by a contact angle value of zero. The contact angle is influenced by, i.e. the affinity of the liquid to the solid, the surface morphology, swelling of the solid sample, dissolution of the solid surface, evaporation of the drop liquid, and physical parameters like temperature and pressure⁷⁴.

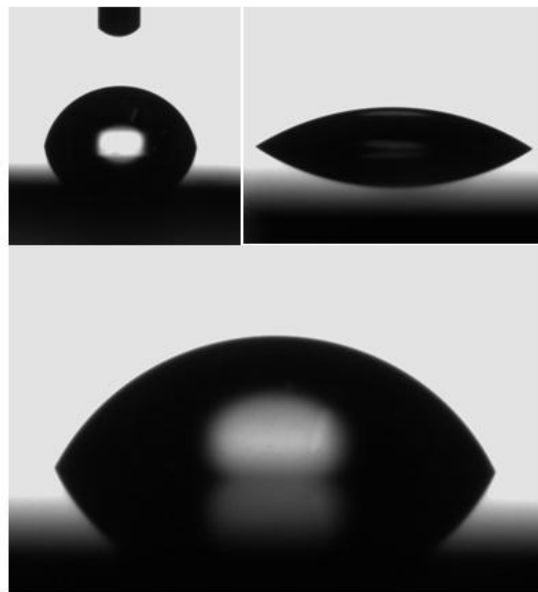


Figure 21: Different contact angle formations.

The physical work which is required to create a new surface, for example by dividing a liquid drop, is called the surface tension γ of a liquid. The minimization of the interfacial area which is energetically favourable is resulting in the phenomenon of surface tension. The work of cohesion W_{co} is defined as two times the surface tension when a body is separated into two parts.

$$W_{co} = 2\gamma$$

Equation 3

When a solid is separated from a liquid, which means the separation of two different materials, a new interface is formed. Now the work of adhesion is described through the equation of Dupre. γ_s is the surface tension of the solid, and γ_l is the surface tension of the liquid. γ_{sl} is the interfacial tension of the solid liquid interface.

$$W_{ad} = \gamma_s + \gamma_l - \gamma_{sl}$$

Equation 4

The interfacial tension between a solid and a liquid in an equilibrium state is the balance of forces at the three phase contact line of the materials. The result of this force balance is the contact angle (θ) of the liquid on the solid. It is described by the equation of Thomas Young (**Equation 4**).

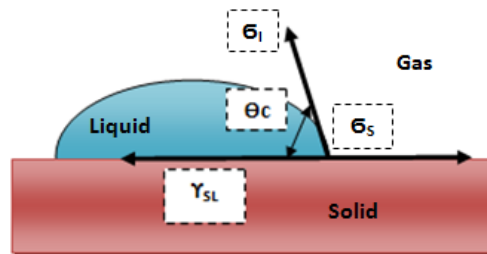


Figure 22: Liquid drop with the contact angel θ on a solid surface.

$$\gamma_s = \gamma_{sl} + \gamma_l \cos\theta$$

Equation 5

This equation compares the solid's surface tension with the liquid's surface tension and the contact angle (θ) of the liquid on the solid. Wettability is a result from the adhesive intermolecular forces between the solid and the liquid, and the cohesive intermolecular forces within the liquid and the solid.

The surface tension γ_s of the solid is higher than the interfacial tension γ_{sl} in the case of complete wetting. Hence the contact angel value is zero. In contrast, the contact angel value is 180° when the liquid does not wet the solid. Hydrophobic surfaces have water contact angles higher than 90° and hydrophilic surfaces have water contact angles lower than 90° .

$$W_{ad} = (1 + \cos\theta)\gamma_l$$

Equation 6

$$W_{ad} = 2\sqrt{\gamma_S \gamma_l}$$

Equation 7

The surface energy of a solid by contact angle measurements with different liquids on this solid can be calculated by combining the equations 5 and 6 (Young-Dupre` equation).

$$(1 + \cos\theta)\gamma_l = 2\sqrt{\gamma_S \gamma_l}$$

Equation 8

There are several models known for calculating the surface energy of solids with the help of contact angle data. For example, there are the Acid-Base model of van Oss and Good, the WORK (Owens-Wendt-Rabel-Kaelble) model, the method of Zisman, the equation of state theory, and the Wu-harmonic mean model⁷⁵⁻⁷⁷.

2.7 Spectroscopic methods

2.7.1 Absorption and Fluorescence

Luminescence is light emitted from substances in electronically excited states. A photon gets absorbed from a photoactive substance. The absorbed energy of the photon results in an excitation of electrons (change from the energy ground level S_0 to an excited state S_1). When the electron drops back to the ground state, the absorbed energy is released. This energy release can occur due to oscillation, rotation, or the emission of an electromagnetic wave (photon). In case of luminescence, the major part of the absorbed energy is released by the emission of a photon. There are two main categories of luminescence: phosphorescence and fluorescence. They differ in their nature of the excited states. The processes of fluorescence and phosphorescence are illustrated in the Jabłoński diagram (**Figure 23**).

2.7.2 Fluorescence

In case of fluorescence, electrons get excited from the ground state S_0 to an excited state S_1 , when a photon hits a photoactive substance.

The main part of the absorbed energy is released by the immediate emission of light (10^{-9} sec), when the electron gets back from the lowest vibrational level of the excited state S_1 to the ground state S_0 . The emitted light has less energy and therefore a larger wavelength, compared to the excitation light. This phenomenon is known as the Stokes' shift. After excitation, the electrons lose energy in a non-radiative manner (vibration, rotation, etc.), until they reach the lowest vibrational level of the excited state S_1 (Internal crossover). When the electron falls back in the ground state S_0 , the energy of the emitted photon is therefore lower, compared to the energy of the absorbed photon. Because of that, the emission spectrum is a so-called mirror image of the absorption spectrum.

2.7.3 Phosphorescence

In case of phosphorescence, the electron changes its spin and changes from the excited singlet state S_1 to the excited triplet state T_1 (intersystem crossing). The relaxation from the excited triplet state T_1 to the ground singlet state S_0 is spin forbidden. Therefore, in case of phosphorescence, remarkably longer live times (milliseconds) are observed, compared to fluorescence.

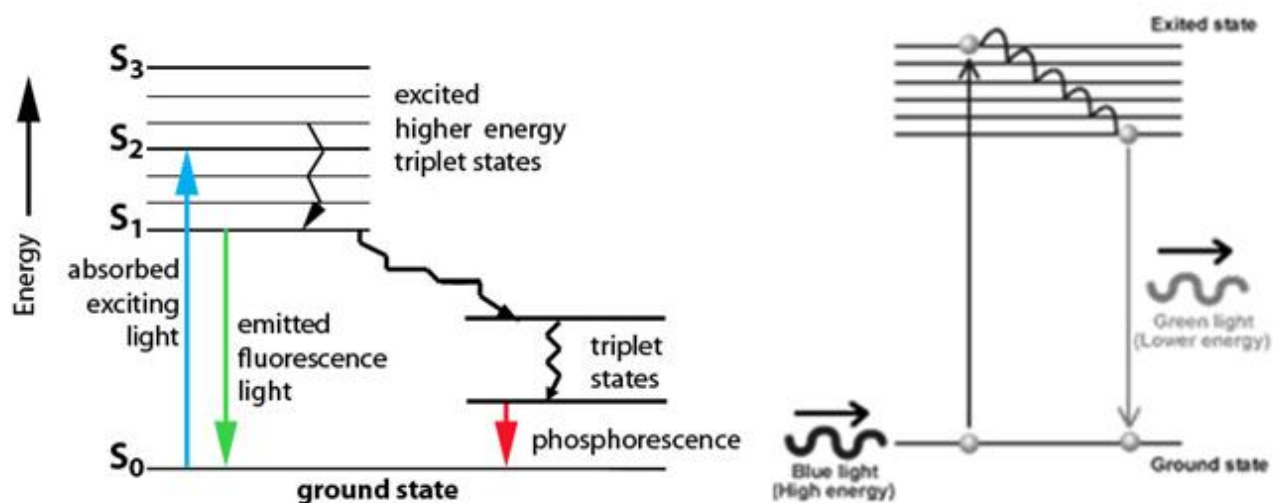


Figure 24: Jabłonski energy diagrams^{78, 79}.

$$\lg\left(\frac{I}{I_0}\right) = -\varepsilon[J]l$$

Equation 9

I_0 Intensity of the incident beam of a definite wavenumber

I Intensity after the covered distance

$[J]$ concentration of the absorbing particle

ε molar absorption coefficient (extinction coefficient)

The molar absorption coefficient is addicted by the frequency of the incoming radiation. The absorption is increasing with an increasing ε . The dimension is written as length multiplied with concentration. (L / (mol*cm)). The dimensionless product $A = \varepsilon*[J]*l$ which is called “absorption”. Other nomenclatures for the absorption are extinction, optical density, or absorption. The ratio I/I_0 is the transmission. Both dimensions are connected together with the equation $\lg T = -A$. The radiation intensity before and after the sample must be determined, before measuring the absorption. Through the negatively logarithm, the ratio of both intensities can be calculated.

2.7.4 Fluorescence spectroscopy

It is a common steady-state spectroscopic technique for measuring and quantifying fluorescence spectra and intensities. A short description of this method is given in **Figure 25**. Light is directed through a sample solution in a cuvette with four transparent sides. The incoming light goes through the sample solution in a linear way. The out coming fluorescence light is emitted in every direction. The detector (i.e. a photomultiplier, PM) is placed in a 90° angle to the lamp. Therefore only the emitted light reaches the detector, which reduces the background and increases the sensitivity. A monochromator (M_2) is used to separate certain wavelengths. The fluorescence spectrum is obtained by scanning through a broad wavelength range. A monochromator (M_1) can also be placed between the sample and the lamp (L). So an excitation spectrum can be measured. The output is converted in graphical form which can be stored digitally⁸⁰.

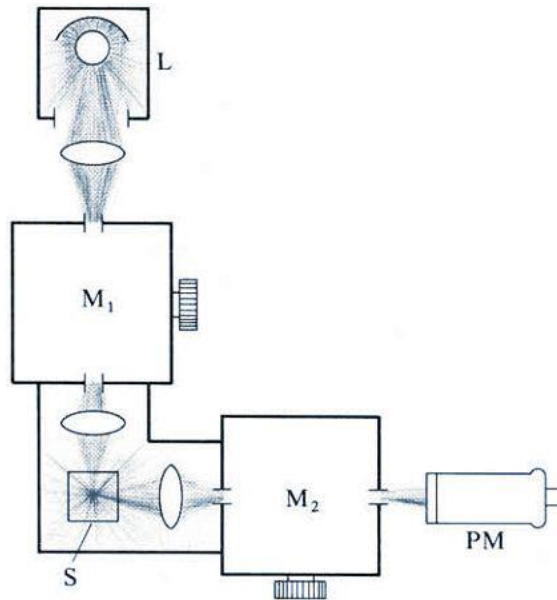


Figure 25: Spectralfluorometer⁸⁰.

2.8 Biotechnological processing

2.8.1 Horseradish peroxidase (HRP)

The plant horseradish which is also called *Armoracia rusticana* is cultivated in temperate regions worldwide. The most important part of this plant are the roots which are taken for the culinary use. These roots also contain highly versatile enzymes. One class of these enzymes are horseradish peroxidases (HRPs)⁸¹.

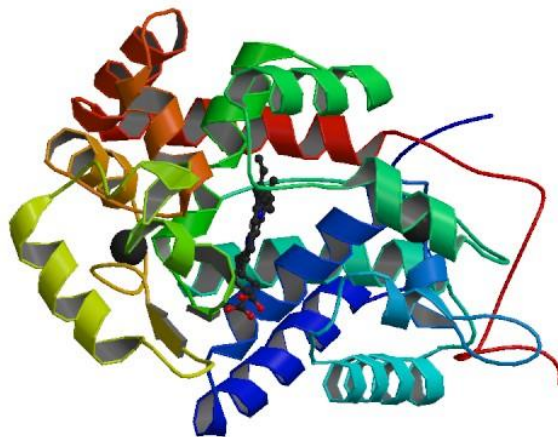


Figure 26: *Arabidopsis thaliana* peroxidase⁸².

In general, peroxidase enzymes vary very strongly in their structural properties, amino acid and/or genomic sequences, and catalytic characteristics. According to their active centre, one distinguishes between non-heme containing peroxidases and heme-containing peroxidases. These groups are further divided in super-families. The heme-containing peroxidases include 6 super-families; the non-heme containing peroxidases comprise 5 super-families⁸³. HRP belongs to the heme-containing peroxidases⁸⁴. Heme-containing peroxidases comprise a ferriprotoporphyrin IX prosthetic group. This is the catalytic key residue of the active site. Moreover, the active site includes a salt-bridge consisting of two calcium-binding sites and four cystein bridges. These enzymes are able to catalyze various oxidation reactions, and typically require H₂O₂ as electron acceptor. HRPs are classified according to their IEP. HRP A2 isoenzymes have acidic IEPs, HRP B and C isoenzymes have neutral or slightly basic IEPs, and HRP D and E isoenzymes have basic IEPs. One very important HRP C isoenzyme is the HRP C1A. It is frequently used as diagnostic tool in bio- and live science and medical applications, for example in ELISA Kits, and for sensors⁵⁷. The Institute of Biotechnology (IMBT) at the TU Graz is working on the design and improvement of novel HRP isoenzymes. Main goals are the improvement of catalytic properties (activity under certain conditions), increased stability against environmental impacts, the implementation of specific binding sites for immobilization, and the simplification of the enzyme purification process by changing the IEP and surface properties (i.e. degree of glycosilation). Novel isoenzymes are designed in a specific manner by introducing artificial and/or modified gene sequences into the expression system (*Pichia pastoris*).

2.8.2 Recombinant protein expression using Pichia pastoris

The disadvantages of extracting HRP out of *Armoracia rusticana* are manifold. On the one hand the purification of enzymes from plants is time consuming and laborious. On the other hand, the enzyme content in the plant varies a lot because of environmental influences on the plant growth (i.e. temperature, humidity, and soil). Therefore, an efficient biotechnological process is desired for producing this important enzyme. The most widely used expression system at the moment is the prokaryote *Escherichia coli*. The limitations of these microorganisms for producing biomacromolecules are the formation of inclusion bodies (aggregation of desired proteins), and a lack of efficiency (i.e. low yields). In order to overcome these problems, biotechnologists are working on establishing new, more efficient expression systems. One very promising candidate are yeast strains, i.e. *Saccharomyces cerevisiae*, or *Pichia pastoris*⁸⁵. For the expression of HRP, *Pichia pastoris* is used. *Pichia pastoris* takes

advantage of secreting the recombinant proteins directly into the cellular surrounding. This can be seen as a first “purification” step, because cell disruption (release of various different biomacromolecules) is not required. *Pichia pastoris* is generally recognized as safe (GRAS status), and does not contain or produce oncogenic/endotoxic by-products. Because *Pichia pastoris* is a eukaryotic microorganism, it is able to perform posttranslational modifications of the produced biomacromolecules, for example correct folding, processing of signal sequences, the formation of disulfide bridges, and O- as well as N-linked glycosylations⁸⁶.

Compared to other yeast species, *Pichia pastoris* does not produce large amounts of toxic ethanol. *Pichia pastoris* is able to grow with methanol, which is a cheap and easy available energy and carbon source. Therefore MeOH is used as the inducer in the fermentation process.

To be able to grow on methanol, *Pichia pastoris* requires specific metabolic enzymes. The most important enzymes for the methanol conversion are the alcohol oxidases 1 and 2 (AOX1 and AOX2), and the dihydroxyacetone synthase (DHAS). Moreover AOX1 is responsible for the expression of foreign DNA (heterologous gene expression).

The protein expression of AOX1, AOX2 and DHAS is controlled at the transcriptional level of their genes *AOX1*, *AOX2* and *DAS*. The wild-type genome of *Pichia pastoris* includes two copies of *AOX1* and *AOX2*. The *AOX1* promoter is more active, and regulates 85% of the alcohol oxidase production. The *AOX1* is inserted into the yeast using the *AOX1* promoter-Gene X expression cassette. For successful insertion, the expression cassette has to include the histidinol dehydrogenase gene (*HIS4*). The inserted expression cassette also includes an antibiotic resistance gene (which codes for the antibiotic “Zeocin”). The simultaneous introduction of an antibiotic resistance gene is needed for distinguishing between genetically successfully modified and non-modified cells. Non-modified cells die in the presence of Zeocin.

Three different mutants can be formed in this process. When inserting the expression cassette into the *AOX1* or *HIS4* locus via single crossover integration, the highly efficient MeOH converting Mut⁺ strain is created. The slow methanol converting strain Mut^S is obtained, when the expression cassette is inserted in the *AOX1* locus via double crossing over integration (Inactivation of *AOX1*). The Mut^S strain is also formed when the insertion of other genes inactivates *AOX1*. The third strain type which can be formed is called Mut⁻. This strain is not able to convert MeOH, because both, *AOX1* and *AOX2* are disrupted. Since *AOX1* is also responsible for the expression of inserted foreign DNA, an efficient MeOH consumption goes hand in hand with the desired expression of novel, specifically designed HRP isoenzymes⁸⁷.

Table 1: Different *Pichia pastoris* strains.

<i>Strain</i>	<i>Properties</i>
Mut ⁺	Good MeOH conversion
Mut ^S	Moderate MeOH conversion
Mut ⁻	No MeOH conversion



Figure 27: *Pichia pastoris*⁸⁸.

2.8.3 Expression of novel Horseradish peroxidase isoenzymes

For the genetically engineering of HRP, the technique of directed evolution was used. The main focus of the ongoing research at the TU Graz is the shortening of the clean-up, the improvement of the production efficiency, and the introduction of specific binding sites.

2.8.4 Directed evolution

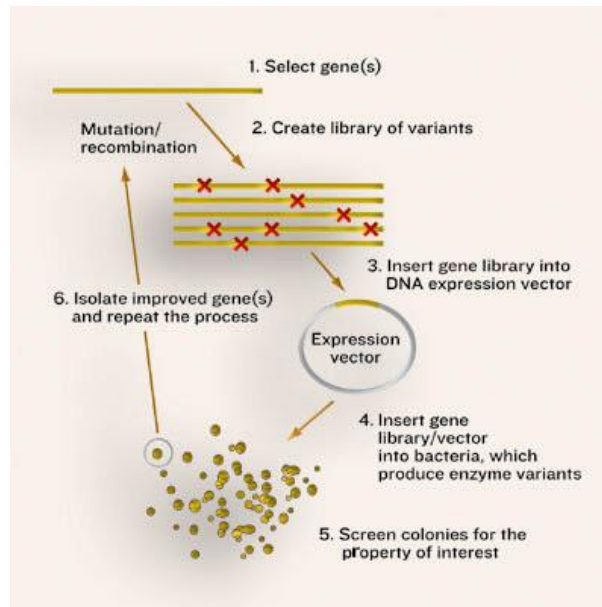


Figure 28: Directed evolution⁸⁹.

For producing new recombinant enzymes in biocatalysis and the white biotechnology, directed evolution is very important. Different macromolecules (proteins, enzymes, etc.) become modified and optimized for special purposes. In comparison to the rational protein design, where proteins get converted through introducing selective mutations, the directed evolution is a screening of coincidental occurring new mutations. For rational protein design, a good knowledge about the structures, forming mechanisms, and modi of action of the desired protein, is required. The coincidental mutagenesis for directed evolution is typically performed though error prone PCR. Error prone PCR is the amplification of genes or parts of genes, where defects are inserted intentionally into the DNA. This is because one is aiming for generating a large number of gene variations. The idea is that one of these variations may code for the desired and improved properties. Here, it often turns out that the enzyme activity is influenced by unexpected properties⁹⁰.

2.8.5 Fermentation

The process of fermentation is known as the chemical conversion of substances with the help of biological systems. These biological systems can be microorganisms (bacteria, fungi like yeasts), cell cultures, or active biomacromolecules (enzymes). In earlier times, fermentation processes were only performed under anaerobic conditions (i.e. beer production). Already the ancient Egyptians were using fermentation processes in their food preparation⁹¹. Louis Pasteur defined the fermentation process as

a process “c'est la vie sans l'air”, which means “a live without air”. Today every technical bioreactor is called “fermenter”⁸⁷. Many medical, pharmaceutical and food-technological products are prepared in a fermentation reaction. The major problems in biotechnology are the scale-up and microbial contamination. Therefore a lot of technical understanding and know-how is necessary for applying a profitable fermentation process. The most important factors to be optimized are: the genetically improvement of the microorganism strain (growing capacity, nutrients, growing factors, production efficiency, side products, inhibition, etc.), and the optimization of the culture medium (pH value, homogenization, O₂ concentration, temperature, nutrient composition, salt content etc.). The best operative mode has to be selected, in order to achieve highest production efficiency and easiest product purification after fermentation. The influence of the mentioned factors is evaluated by measuring rheological properties, the pH value, the gas content (i.e. O₂, CO₂) the temperature, and the nutrient content, for example⁸⁷.

2.8.6 Fermenting *Pichia pastoris*



Figure 29: *Pichia pastoris* strains for fermentation processes.

Both *Pichia pastoris* strains (Mut⁺ and Mut^S as described previously) can be used for fermentation processes like Fed-Batch fermentation techniques, or continuous stirred tank reactor (CSTR) fermentation techniques. The fermentation of *Pichia pastoris* strains is consisting of glycerol batch, glycerol fed-batch, transition, and methanol fed-batch/mixed feed. The whole fermentation process of *Pichia pastoris* strains is based on glycerol and methanol consumption models. Parameters have to be designed for this process, like broth volume, substrate feed rate, cell density and length of each process step. Recombinant proteins can be produced through the expression in *Pichia pastoris*. *Pichia pastoris* has the advantages of the very strong alcohol oxidase I (AOXI) promoter, growing in very simple defined media and in high cell densities. A stable integration of the expression plasmids into the genome of *Pichia pastoris* is possible. The expression plasmids can be purchased as a kit from Invitrogen Co. (San Diego, CA, USA). The advantages of *Pichia pastoris* are the relatively easy scale-up,

high-level expression, inexpensive growth, and effective protein folding. Fermentation protocols for both strains are purchased from Invitrogen Co. The substrate feed rate has to be maximized in terms of protein and cell growth productivity in the fed-batch process. For *Pichia pastoris*, the methanol feed rate is the most important one. It has an effect of the specific growth rate in the product formation.

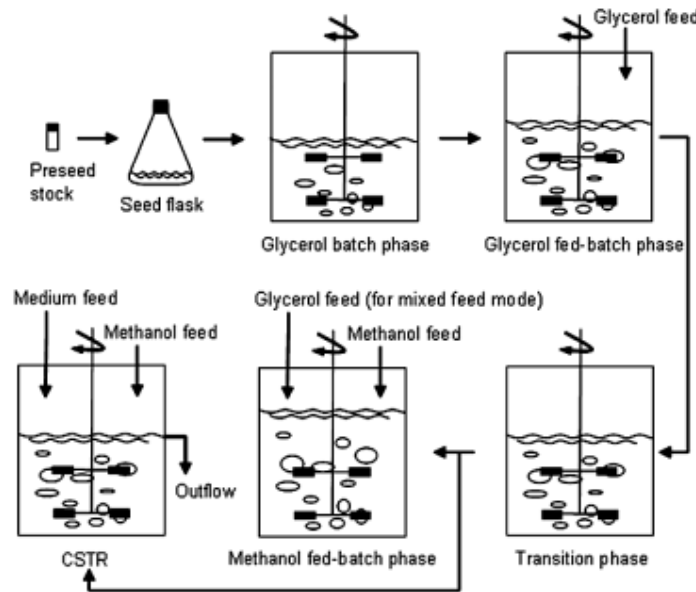


Figure 30: CSTR or Fed-Batch Fermentation Process.

The yeast cells which were kindly provided by the Institute of Biotechnology (IMBT) are used as inoculum in the seed flasks for the fermentation process. The glycerol batch and the fed-batch phases are acting as growth phases where yeast cells only get reproduced and no recombinant protein production arises. After an about 3 hours period the yeast cells acclimatize to methanol. Afterwards the methanol feed phase can start. There are two running modes for the recombinant protein production, which are the CSTR phase and the methanol fed-batch phase. In this work, the methanol fed-batch phase was performed (**Figure 30**).



Figure 31: Fermenter.

2.8.7 Purification of HRP

The purification of biomacromolecules (proteins, enzymes, etc.) after a fermentation process is very important to gain the molecule of interest. In case of HRP the purification is complicated, because lots of other enzymes, proteins, sugars, fatty acids, cells, etc. are present in the fermentation bulk. Therefore a good and also quick purification process has to be developed. At the moment HRP can get purified (reaching a Rz-value of about 3.5) through a cascade of different purification and concentrating steps including sedimentation, filtration, membrane separation, and chromatography. The main problem is, that the enzyme structure, ieP, activity, etc. must be known for optimizing separation steps. But the investigation of these parameters is very difficult when pure enzymes are not available. Chromatography is often the method of choice when aiming for separating biomacromolecules of similar properties.

2.8.8 Fast Protein Liquid Chromatography (FPLC)

Chromatography principles

Chromatography is a technique for separating molecules using two different phases, a mobile and a stationary phase. Molecules are separated due to differences in their affinity to these phases. The retention time increases with increasing affinity to the stationary phase. For most separation purposes, the stationary phase (solid or liquid) is densely packed into a column, and the mobile phase (liquid or gas) passes through this column.

Table 2 gives a brief overview about frequently used liquid chromatography techniques in biotechnology, and their separation principles.

Table 2: Chromatographic principles.

Separation principle	Chromatographic technique
Size and shape	Gel permeation chromatography (GPC)
Net charge	Ion exchange chromatography
Isoelectric point	Chromatofocusing
Hydrophobicity	Reversed phase (RP) chromatography
Biological function	Affinity chromatography
Antigenicity	Immunoabsorption
Carbohydrate content	Lectin affinity chromatography
Content of free – SH	Chemisorption (“Covalent chromatography”)
Metal binding	Ion affinity chromatography
Miscellaneous	Dye affinity chromatography and hydroxyapatite chromatography

Fast Protein Liquid Chromatography (FPLC) principles

FPLC is used for the preparative separation (clean-up) of proteins and other biomacromolecules from complex mixtures. In this work, FPLC was used for the purification of horseradish peroxidase enzymes. FPLC is principally similar to high performance liquid chromatography (HPLC)⁹².



Figure 32: ÄKTA purifier system.

2.8.8.1 Superdex™ columns

HiLoad™ Superdex columns are already XK laboratory packed. The columns can be loaded with different stationary phases. Superdex shows a good separation possibility with a mean particle size of

34 mm and a narrow particle size distribution. High back pressure is not appearing while the process of a good separation. In this work, Superdex columns were used for all chromatography steps. For size exclusion chromatography, the Superdex is packed with Superdex™ prep grade gel filtration media. The Superdex™ prep grade is a composite of cross-linked agarose and dextran. The agarose is highly physically and chemically stable, and the dextran component provides a highly separation efficiency. The process can be scaled-up to production levels, shows high capacities (120-320 ml bed volume, and 5-13 ml sample volume), high flow rates (up to 50 cm/h), high-resolution (10,000 - 600,000 Daltons), linear flow rates of 10 – 50 cm/h, and applicable for a variety of chromatography systems (i.e. FPLC™, or ÄKTA™⁹³).



Figure 33: ÄKTA column⁹⁴.

2.8.8.2 Size exclusion chromatography and gel filtration chromatography

Size exclusion chromatography, also called gel filtration, or gel permeation chromatography (GPC) is used for separating analytes according to their size and/or shape. The stationary phase is a densely packed, highly porous gel. As larger the analyte, the easier these molecules are eluted. This is because larger molecules are not able to enter small pores of the stationary phase. Accordingly, the dwell time increases with decreasing size (**Figure 34**)⁹⁵. The HiLoad™ 16/60 Superdex™ 200 prep grade column, prepacked with 120 ml matrix material is used.

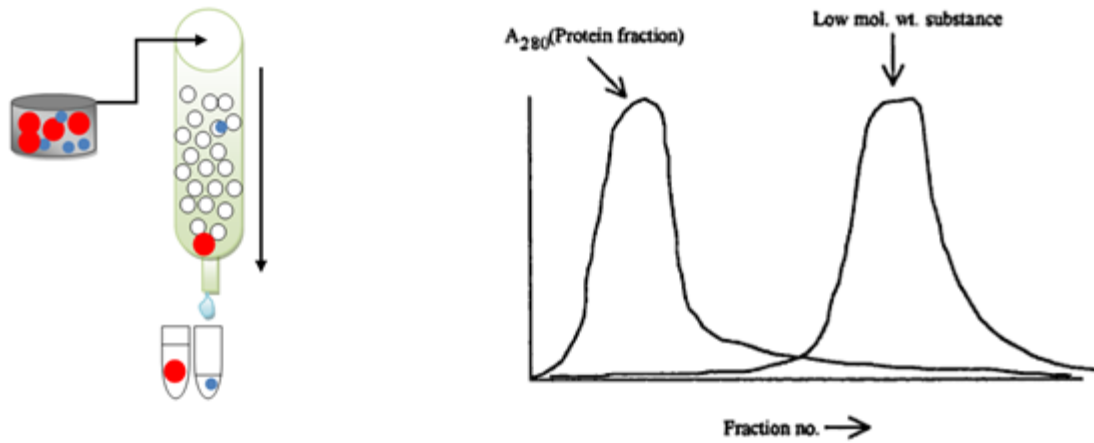


Figure 34: A: Size exclusion chromatography; larger molecules (red dots) eluting in the earlier fractions than the smaller ones (blue dots). **B:** Exemplary chromatogram⁹⁵.

2.8.8.3 Ion exchange chromatography (QFF → Q-Sepharose Fast Flow)

Ion exchange chromatography is a very powerful technique for purifying and separating proteins and other biomacromolecules. The driving force for separating analytes is electrostatic adsorption/desorption of molecules on a solid phase, which contains anionic or cationic functional groups (**Figure 35**). These interactions can be tuned in a very selective manner by adjusting the mobile phase pH or salt content. The analyte is retained when the analyte and the stationary phase, are oppositely charged. In particular, for binding the mobile phases' pH should lie between the acid dissociation constant (pKa) of the analyte and the charged functions of the solid phase. Bound analytes are eluted by varying the pH, and/or screening the electrostatic interactions by increasing the mobile phase's ionic strength. Linear as well as stepwise gradients can be used⁹⁶.

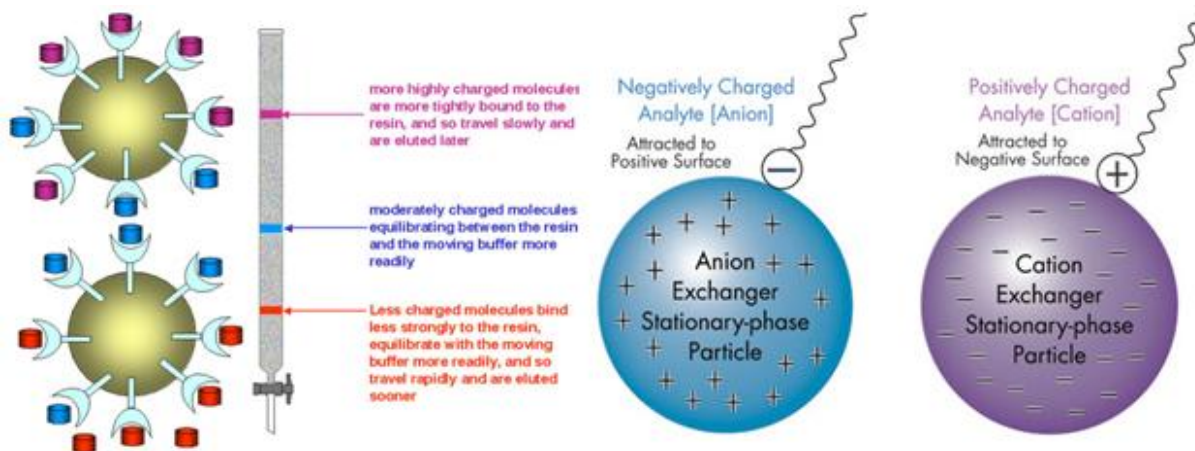


Figure 35: Ion exchange chromatography principles⁹⁷.

Hydrophobic interaction chromatography (HIC)

The stationary phase is modified with hydrophobic ligands. These hydrophobic molecules interact with hydrophobic moieties of the proteins of interest. In particular, the interaction of water molecules with the hydrophobic ligands on the column, and the hydrophobic regions of a protein is energetically not favoured. Therefore, water molecules do not interact, but form a highly ordered cage-like shell around the hydrophobic domains. The entropy is the driving force for the interaction of these hydrophobic domains according to **Equation 10**.

$$\Delta G = \Delta H - T\Delta S$$

Equation 10

When lipophilic domains interact and get in contact, parts of the water molecules are released, which yields an increase of entropy (decrease of order). HRP has an isoelectric point of 9.5. At the pH 7, the HRP is charged and hydrated. Therefore, no interactions occur and therefore no separation is achieved when the pH of the column buffer is 7. When the pH value is switched to 9.5, the HRP is uncharged and the hydrophobic interactions occur in a selective manner. Thus, the different compounds are separated according to their isoelectric points. The used stationary phase material is called Phenyl Sepharose® 6 Fast Flow (packed in a XK26/20 column). For concentration each sample and for buffer changing, Vivaflow 50 system (30,000 MWCO cut-off), and Sartorius Vivaspin 20 system (3,000 MWCO cut-off) were used.

2.9 Solid phase extraction (SPE)

The Solid phase extraction (SPE) is used for separating and concentrating substances out of complex mixtures. The compound of interest is separated due to its affinity to the stationary phase. The matrix is washed out of the column. The selective elution of the compound of interest is performed through washing with a specifically composed mobile phase⁹⁸.

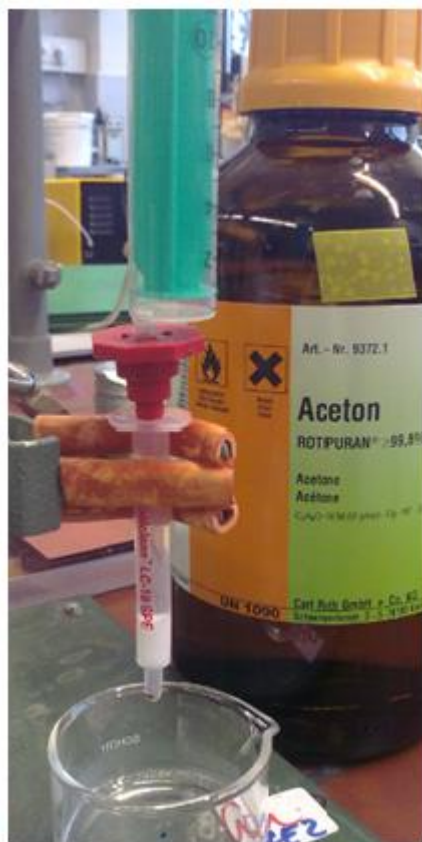


Figure 36: SPE tube.

2.9.1 Supelco LC-18 SPE tubes (1ml)

Supelco LC-18 SPE tubes (1ml) were used for SPE. The matrix of these LC-18 SPE cartridges consists of silica gel based material with irregular shape. The active groups on the matrix are substituted octadecyl groups. The matrix's particles size is 45 μm and the pore volume is 0.8 cm^3/g which a pore size of 60 \AA . The surface area is 475 m^2/g ⁹⁸.

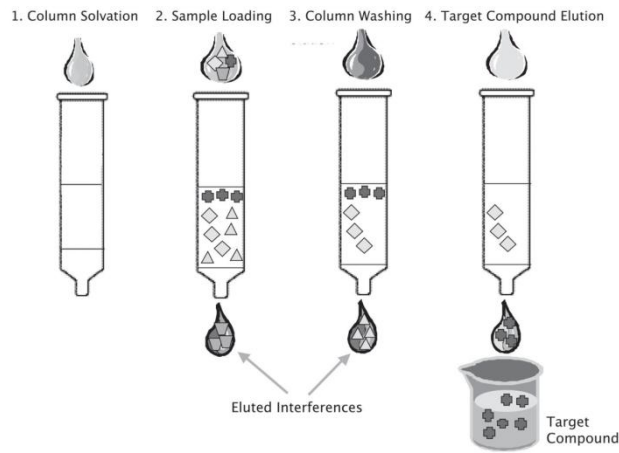


Figure 37: Schema of solid phase extraction procedure⁹⁸.

2.10 The electrical double layer and the Zeta-Potential

Surfaces in solutions show electrical potentials, this is because ions of the bulk solution adsorb, and/or charged functional groups are present. The first layer of adsorbed ions is called the inner Helmholtz plane. Oppositely charged ions bind to the inner Helmholtz plane due to electrostatic interactions. This layer is called outer Helmholtz plane. Next to the outer Helmholtz plane, ions are arranged in the diffuse layer. The electrostatic attraction decreases with increasing distance from the surface. Within the inner Helmholtz plane the potential increases linearly. Within the outer Helmholtz plane the potential decreases linearly. In the diffuse layer one can observe an exponential decrease of the potential⁹⁹.

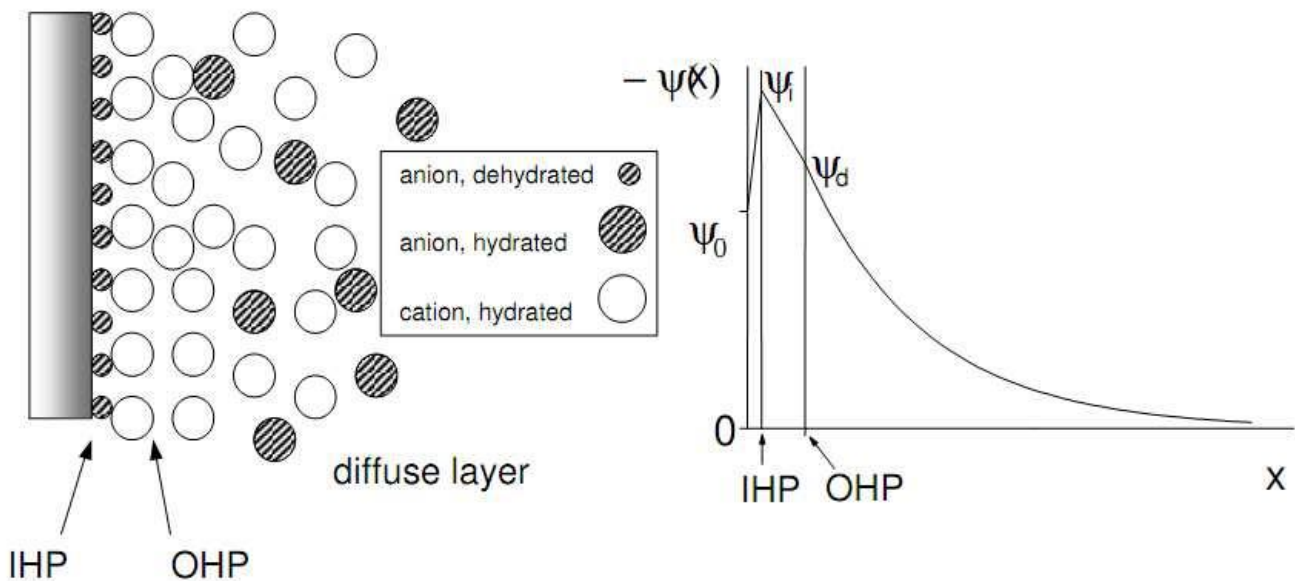


Figure 38: Stern model for a negatively charged surface.

IHP: inner Helmholtz plane, OHP: outer Helmholtz plane¹⁰⁰.

2.10.1 ζ -potential

According to the Gouy-Chapman Model, electrical neutrality is given in steady state, because ions from the bulk solution compensate the surface charges. When moving the surface relative to the liquid, a so called shear plane is formed. The shear plane is the boundary between the closer part of the diffuse layer which moves with the surface due to electrostatic attraction, and the outer part which does not move. Because electrical neutrality is not given anymore, a measurable potential is formed. This potential is called the zeta-potential (ζ -potential).

2.10.2 Electrophoretic light scattering (ELS) – micro-electrophoresis

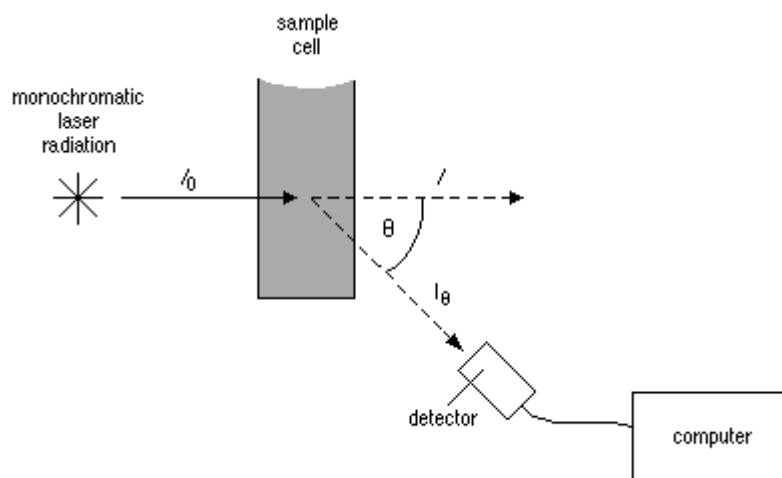


Figure 39: Electrophoretic light scattering principles¹⁰¹.

The electrophoretic mobility of colloids is measured using electrophoretic light scattering technique (ELS). Small particles in solution are moved due to an applied external electrical field. Coherent light is directed through the sample, and the moving particles cause a Doppler shift of the frequency. The particle velocity in the sample can be determined through the measured frequency shift and shift distribution. The electrophoretic mobility is calculated through this particle velocity when consideration the Brownian motion (**Equation 11**). From the electrophoretic mobility, the Zeta-potential (ζ -potential) can be calculated using the Smoluchowski equation (**Equation 12**).

$$ve = \mu e \cdot E$$

Equation 11

The electric field is E , the velocity is v_e , the electrophoretic mobility is determined as μ_e , the particle dimensions is determined as α , the double layer thickness determined as κ^{-1} (Debye-Hückel parameter). The electrophoretic mobility is μ_e , η is the viscosity of the medium, ζ is the zeta-potential, and $\epsilon\epsilon_0$ is the permittivity¹⁰².

$$\mu_e = \frac{\epsilon\epsilon_0\zeta}{\eta}$$

Equation 12

2.10.3 Dynamic light scattering (DLS)

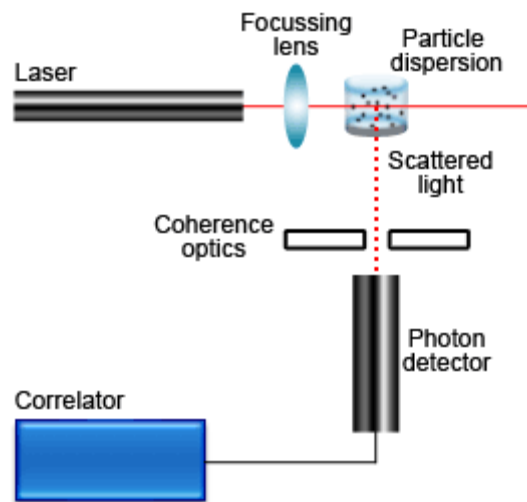


Figure 1: Schematic diagram of a conventional, 90° dynamic light scattering instrument.

Figure 40: Dynamic light scattering principles¹⁰³.

The dynamic light scattering is also known as photon correlation spectroscopy, or quasi-elastic light scattering. It is frequently used for measuring the size and size distribution of colloids in a suspension. Particles are scattering light when they are small, compared to the wavelength of the incoming light. The time-dependence of the scattered light at a fixed angle is monitored in DLS. Fluctuations in the scattering field and in the scattering intensity are caused due to the Brownian motion of the particles. The particles show a random motion which is depending on their diffusion coefficient, which can be calculated by the transducing signal $I(t)$ in its autocorrelation function (ACF). The intensities are monitored at two different times t and $t+\tau$. Close to $I(t)$ the signal $I(t+\tau)$ is measured when the delay

times τ are short. This is because the particles have no chance to move a great distance away. For short values of τ the function is correlated and the correlation is decreasing to zero with longer delay times. The ACF consist of a superposition of decay curves which a large number and forms an exponential function.

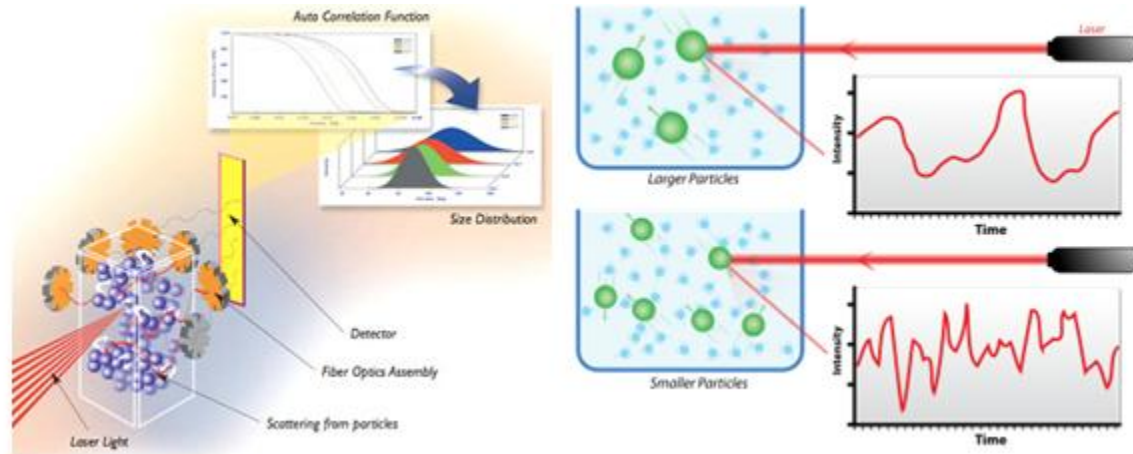


Figure 41: Principles of dynamic light scattering¹⁰⁵.

2.11 Real time polymerase chain reaction (RT-PCR)

The real time polymerase chain reaction (RT-PCR) is a method for DNA amplification which can be monitored in real time. The RT-PCR is used to quantify the amount of DNA in a sample. This can be performed through fluorescence measurements (through fluorescence-labelled nucleoside triphosphates / dNTP's), in the reaction solution. The fluorescence increases proportional to the amount of PCR products. The compounds which are necessary for performing a RT-PCR experiment are template DNA (from the desired sample), primers (ssDNA, or ssRNA), buffer, polymerase, dNTP's and a special fluorescent dye³⁸.

3. Materials

3.1 Chemicals

All analytical grade chemicals were used as obtained. Acetone, methanol, ethanol, 2-propanol, isopropanol, dimethyl sulfoxide (DMSO), diethyl ether, toluene, dichloromethane, butyl methyl ether, petrol ether, n-hexane, and dimethylformamide (DMF), sodium chloride (NaCl), potassium chloride (KCl), monopotassium phosphate (KH_2PO_4), hydrochloric acid (HCl, 37 wt.% aqueous solution), potassium diphosphate (KH_2PO_4), dipotassium phosphate (K_2HPO_4), potassium sulphate (K_2SO_4), calciumsulfat-dihydrat (CaSO_4), magnesium sulfate ($\text{MgSO}_4 \cdot 7\text{H}_2\text{O}$), phosphoric acid (H_3PO_4), potassium hydroxide (KOH), concentrated ammonium hydroxide, zinc chloride (ZnCl_2), mangan sulphate ($\text{MnSO}_4 \cdot \text{H}_2\text{O}$), copper sulphate ($\text{CuSO}_4 \cdot 5\text{H}_2\text{O}$), sodium iodide (NaI), boric acid (H_3BO_3), sodium molybdate ($\text{Na}_2\text{MoO}_4 \cdot 2\text{H}_2\text{O}$), cobalt(II) chloride (CoCl_2) iron sulphate ($\text{FeSO}_4 \cdot 7\text{H}_2\text{O}$), sulphuric acid (H_2SO_4), 2',2'-azino-bis(3-ethylbenzthiazoline-6sulphonic acid) (ABTS), ammonia sulfate ($(\text{NH}_4)_2\text{SO}_4$), tris(hydroxymethyl)aminomethane (Tris), calcium chloride (CaCl_2), and ammonium hydroxide (NH_4OH), glucose, sodium dihydrogenphosphate dihydrate ($\text{NaH}_2\text{PO}_4 \times 2 \text{H}_2\text{O}$), potassium dihydrogenphosphate (KH_2PO_4), potassium chloride, sodium chloride (NaCl), magnesium sulfate (MgSO_4) ammonium chloride (NH_4Cl), thiamine, and casamino, disodium hydrogen phosphate (Na_2HPO_4), hydrochloric acid ((HCl) 37 wt.% aqueous solution) and sodium hydroxide (NaOH), acetic acid glacial (CH_3COOH , ROTIPURAN® = 100%), 1, 4-Dioxane (M=88.11 g/mol, $\rho=1.039$, ROTIPURAN® = 99.5%), hydrogen peroxide (H_2O_2), (M=34.02 g/mol, $\rho=1.139$, ROTIPURAN® = 35%, ROTH), and Sulphuric acid, (H_2SO_4), (M=98.08 g/mol, $\rho=1.849$, ROTIPURAN® = 95%-98%) were purchased from Roth (Karlsruhe, Germany). Anhydrous ethanol was purchased from Ethanol Handels GmbH (Spielfeld, Austria). Tetrahydrofuran (THF) HPLC grade was purchased from Merck (Darmstadt, Germany). 1,4-dioxane was purchased from Merck (Darmstadt, Germany). Cellulose acetate DS 2.5, M_w 54,000 was kindly provided by Norit Membrane Technology (Enschede, Netherlands). Cellulose acetate 39.8 %w/w acetyl content (DS 2.5) M_n 50,000, and cellulose acetate 39.8 %w/w acetyl content (DS 2.5). Aminocellulose and CMC Avicel 1 (AV1) were kindly provided by FSU Jena (Jena, Germany). Hydrolyzed Chitosan M_w 12,000 - 15,000 was kindly provided by CePoL Central Polymer Lab, NAWI Graz (Graz, Austria). Low molecular weight chitosan was prepared according to the method of Fasl et al. Spectra/Por CE dialysis tubings 100 kDa MWCO, 10 mm flat width, were purchased from Spectrum Laboratories Inc. (Breda, Netherlands). A three blade stirrer R 1381 (diameter: 45 mm, ID-Nr.: 1296000 were purchased from IKA –Werke GMBH & CO. KG Staufen

(Germany). Hydroxyethyl cellulose (HEC, viscosity of a 1 wt. % solution in H₂O at 20°C: 145 mPa.s) was purchased from Fluka (Buchs, Switzerland). Albumin from bovine serum (BSA), (purity ≥96%), glycerol (for molecular biology, ≥ 99 %), 17 α Ethinylestradiol, δ-ALA (δ-Aminolevulinic acid) and biotin (≥ 99 %) were purchased from Sigma Aldrich (Steinheim, Germany). Silicon Wafers (100 nm SiO₂-layer) were purchased from Silchem. Surfs (SiO₂-surfaces for Sarfus measurements) were purchased from nanoLANE. Deionized sterile water, purchased from Fresenius Kabi (Graz, Austria). Agar was purchased from Becton and Dickinson Company (Heidelberg, Germany). *Pichia pastoris* strains (A2_{syn} and A2_{mut}), and horseradish peroxidase (HRP) isoenzymes sequences A2 and C1A were kindly provided by the institute of Biotechnology (IMB) at the Technical University of Graz (Graz, Austria). WY, USA. Bacto™ yeast extract, yeast nitrogen base (YNB), and Bacto™ peptone were purchased from BD Bioscience (Schwechat, Austria).

3.2 Instruments

3.2.1 Atomic force microscope

A Veeco Nanoscope V Multimode AFM was used for characterizing surface morphologies and structures. The polymeric surfaces were analyzed using tapping mode (Veeco TESP7 cantilever). The radius of the tip was 8 nm, the resonant frequency was 320 kHz, and the average spring constant was 40 N/m. Data analysis was performed using WSXA software¹⁰⁶.

3.2.2 Contact angle instrument

The evaluation of the surfaces water affinities was performed with the Dataphysics OCA15+ contact angle measurement system. Milli-Q (>18 mΩ cm) water was used for these experiments. The samples were measured in triplicates and were repeated five times for each sample. All contact angle measurements were performed under room temperature conditions.

3.2.3 Dynamic and electrophoretic light scattering (DLS, ELS)

A Brookhaven ZetaPlus zeta-potential Analyzer (wavelength: 674 nm, scattering angle: 90°) was used for measuring the composite-nanoparticles effective zeta-potential, polydispersity indices (Pdl), and

mean hydrodynamic diameter. The nanoparticle samples were diluted with bidistilled water (10×10^{-3} wt. % particle content). The effective zeta-potential of the nanoparticles was measured using electrophoretic light scattering (ELS). For that purpose, the ZetaPlus zeta-potential Analyzer in PALS mode (wavelength: 674 nm) was used. The effective zeta-potential was calculated with the Smoluchowski equation assuming log normal size distribution. The measurements were repeated 5 times each.

The nanoparticles mean hydrodynamic diameter and polydispersity indices (PDI) were determined using dynamic light scattering (DLS). A Brookhaven Instruments ZetaPlus zeta-potential Analyzer at a wavelength of 674 nm at a scattering angle of 90° was used for this purpose. The samples were diluted with bidistilled water to a concentration of 5×10^{-3} wt%. Mean particle diameter were approximated as the effective (z-average) diameter and the width of the distribution as the PDI which was achieved by the cumulates method presuming spherical particle shape and Log-normal size distribution.

3.2.4 SarfusTM

The Sarfus technique was used for measuring thickness and roughness of model films and polysaccharide coatings. For the Sarfus measurements, the optical microscope LEICA DM2500 M with Sarfusoft software (*nanoLANE*)¹⁰⁶. was used. Each sample was probed on at least five spots and the magnification was 20 fold. The absolute film thickness of each sample was determined by using a step-height standard (std. no. 04005-02-C06) for calibration. Every sample was measured in duplicate for five times. Surfs are used for preparing the polymeric model surfaces. These Surfs can be use for preparing model films with the help of spincoating and dip coating. Also spray coating or knife coating would be possible⁷³.

3.2.5 Scanning electron microscopy (SEM)

A Digital Zeiss DSM 982 Gemini instrument was used for producing SEM pictures and measurements. The samples were measured in a SE (secondary electron) detection mode (detection mode of 10 kV voltages).

3.2.6 Spin coater

A Polos spin coater MCD-200-NPP was used for preparing model surfaces. The acceleration was 2500 rpm*sec, the spinning speed was 4000 rpm, and the spinning time was 60 seconds.

3.2.7 Death/Live fluorescence staining assay

All steps were performed under sterile conditions. The staining tests were performed using the L 7007 Live/death *Baclight*TM bacterial viability KIT for microscopy, purchased from LifeTech (Vienna, Austria). The test includes two fluorescent dyes. SYTO[®] 9 colours all bacteria (λ_{ex} : 480 nm, λ_{em} : 500 nm). Propidium iodide colours solely death bacteria (λ_{ex} : 490 nm, λ_{em} : 635 nm). Due to the FRET effect the intensity of propidium iodide gets intensified and the intensity SYTO[®] 9 gets suppressed, when both dyes are present in one microorganism. In particular, the samples were incubated with the aqueous colouring solution, containing each dye solution. After that, the samples were washed with PBS buffer, and dried. Finally, the samples were then analyzed using fluorescence microscopy. The data analysis was performed using MetaMorph Microscopy Automation and Image Analysis Software, purchased from Molecular Devices (Ismaning, Germany). All experiments were performed in duplicate.

3.2.8 Real-time polymerase chain reaction (RT-PCR)

All steps were performed under sterile conditions. First, the samples were transferred into centrifugation tubes containing PBS buffer, and the bacteria were detached from the surface, and sedimented via centrifugation. After removing the supernatant, the pellet was redispersed in PBS buffer. The cells were then disrupted by thermal treatment. Next, the DNA was extracted, and cell fragments were sedimented. The supernatant containing the DNA (Matrix DNA) was further analyzed by RT-PCR. The primers were kindly provided by the Institute of Molecular Biosciences, Karl-Franzens-University of Graz. The master mix solution (primer solution) consisted of 22 μl forward primer solution, 22 μl reverse primer solution, and 71 μl H₂O. The RT-PCR reaction mixture consisted of 2 μl matrix DNA solution, 10 μl master mix solution, and 12 μl Sybergreen KIT mix solution (kindly provided by the Institute of Molecular Biosciences, Karl-Franzens-University of Graz).

3.2.9 BIOSTAT CT fermenter

BIOSTAT CT fermenter was used for the *Pichia pastoris* fermentations.

3.2.10 FPLC ÄKTA purifier system

Fast liquid protein chromatography (FPLC) for purifying biomacromolecules was used. Therefore the ÄKTA purifier system was used. The system was controlled using UNICORN™ software.

3.2.11 Spectramax Plus 384 spectrophotometer

Spectramax Plus 384 spectrophotometer at 405 nm (ϵ of oxidized ABTS is 34,700 M⁻¹ cm⁻¹) was used for determining absorption values.

4. Surface modification of cellulosic model films

4.1 Methods

4.1.1 Hollow fibre membrane production process (X-Flow)

For producing hollow fibre membranes following substances are used. The solvent is N-Methyl-2-pyrrolidone (NMP), the non-solvent is glycerine and cellulose acetate butyrate (CAB-171-15) or cellulose acetate (CA-398-30) is used as the polymer.

The NMP is heated in a vessel with a double wall. The polymer is added when the NMP is on temperature and the mixture is stirred for several hours till the polymer is dissolved in the NMP. The solution is kept warm and the non-solvent is added to the mixture under continuous stirring. When this process is finished, vacuum is applied in order to remove the air in this so called "dope" solution.

The membrane is processed through pumping the viscous, air-free polymer solution through a filter and afterwards directed to a spinneret. In the spinneret, the membrane is formed. Here the dope solution is mixed with a so called "bore" liquid (which is mostly a non-solvent like water). The bore liquid is pumped through the inner tube of the spinneret (**Figure 42/1**). Then the membrane passes through controlled atmosphere (chimney with steam). Water vapour in the chimney enters the fibre

and moves the composition closer to the direction of the bimodal (**Figure 42/2**). The fibre is immersed in the following coagulation bath containing water (**Figure 42/3**). Then the membrane is collected in a container with water to wash out the rest of the solvent and non-solvent. For the post treatment the membranes need some wash steps to remove the solvent completely. Finally the membranes get dried in an oven.

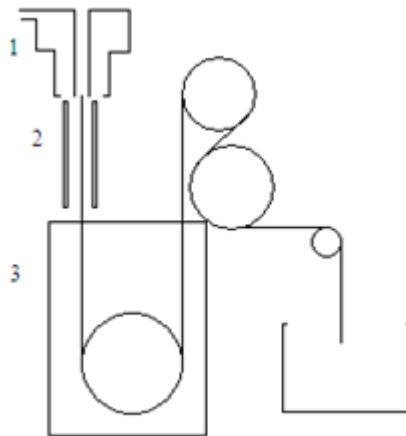


Figure 42: Schematic picture of the membrane process. **1:** Inner tube of the spinneret, **2:** bimodal, and **3:** coagulation bath filled with water.

4.1.2 Synthesis of CA nanoparticles

20 mg CA (M_n 30,000 DS 2.5) was dissolved in 10 ml THF. 60 ml of the non-solvent (water/THF 80/20_{v/v}) is placed in the ultrasonic bath and gets stirred continuously with a stainless steel three blade stirrer while the solvent solution is added dropwise to his non-solvent (**Figure 43**). The velocity of the stirrer is 350 rpm. To remove larger coagulates, the CA nanoparticle suspension after the precipitation is filtered through a 5 μm PTFE syringe filter.

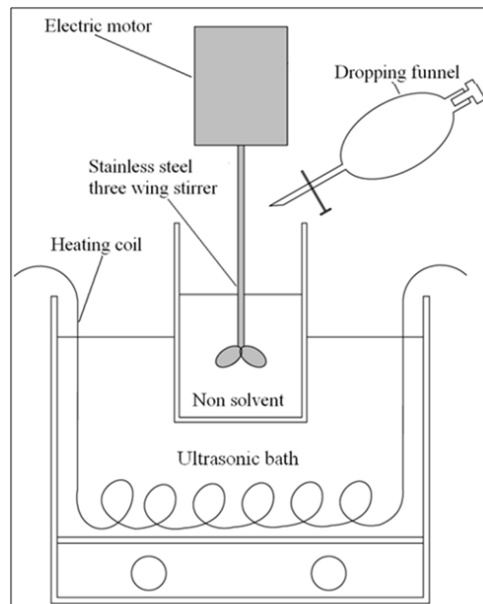


Figure 43: CA nanoparticle precipitation setup including sonication and stirring with a stainless steel agitator¹⁰⁷.

Synthesis of composite nanoparticles from CA and a variable hydrophilic polysaccharide (CANPs)

The same precipitation method is used for forming composite nanoparticles from CA and a variable hydrophilic polysaccharide (CANPs). The difference to the afore mentioned process is that a hydrophilic polysaccharide (amino cellulose AC, carboxymethyl cellulose CMC, low molecular weight chitosan L-CHI, or hydroxyethyl cellulose HEC) is added to the non-solvent (15×10^{-4} wt.%). The non-solvent is placed in the ultrasonic bath and gets stirred continuously with a stainless steel three blade stirrer (350 rpm) while the polymer solution is added dropwise to his non-solvent (**Figure 43, Figure 44**). To remove larger coagulates, the CA nanoparticle suspension after the precipitation is filtered through a 5 μm PTFE syringe filter.

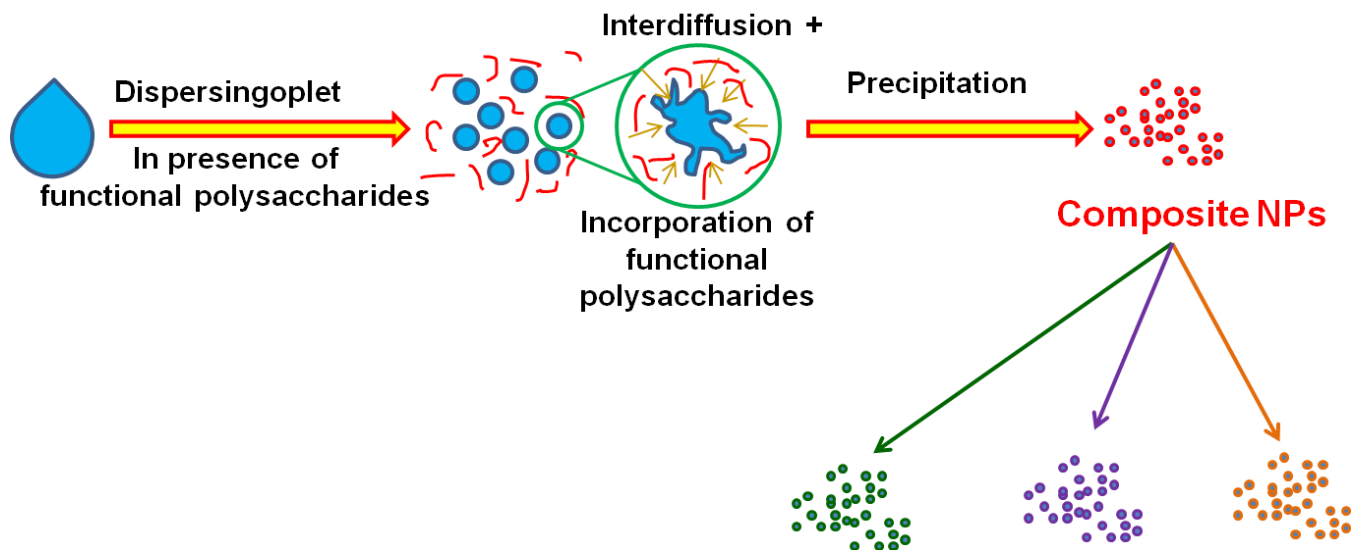


Figure 44: Polysaccharide composite nanoparticles from CA.

4.1.3 Preparation and activation of CA model films (CAA)

Silicium oxide surfaces (so called SiO_x wafers) were cut into small pieces (1cmx1cm). First they got washed with bidistilled water, acetone, or ethanol and bidistilled water. Then the SiO_x wafer were put in a fresh prepared piranha solution for 10 minutes. Afterwards the wafer had to be washed with bidistilled water again. Then they got dried in a nitrogen stream. After washing the solid surfaces, CA (1.0 wt.%) was solved in 1,4-dioxane. This solution was taken for spincoating the SiO_x wafer. 100 µl of CA solution was placed onto the SiO_x wafer, which was fixed on the spinning plate (Spin coater). Then the spin coating procedure was started. So prepared CA thin films were tempered at 60°C over night. In order to make the CA surface more accessible for the adsorption of polysaccharides, the surface has to be activated by dipping into a 0.1 M potassium hydroxide solution for 15 minutes. Afterwards, the model surfaces were rinsed with bidistilled water for 5 minutes twice. Then the surfaces were dried in the N₂ gas stream.

Polysaccharide coatings of activated cellulose acetate (CAA) model films (Figure 45)

Polysaccharide monolayers were applied as following onto CAA or precoated CAA. The coated wafers were put in a solution of the desired polysaccharide (0.1 wt.%) for 30 minutes. The procedure was followed by washing for 5 minutes two times. In this way, CAA model films were decorated with one, two, or three layer of different polysaccharides. Finally, the decorated surfaces were dried in a N₂ gas stream. Such precoated CAA model films were coated with polysaccharide composite CA nanoparticles

via dipping them into the 1:3 diluted nanoparticle suspensions, followed by washing two times for 5 minutes and drying with N₂.



Figure 45: Layer by layer with polysaccharides and C.A. nanoparticles. The first block is a model surface without any coated substances, the second block contains the polymers which are introduced on the surface by LbL-technique, and the third block shows the polymer coatings with adsorbed active compounds like enzymes on it.

4.2 Results and discussion

4.2.1 Polysaccharide composite nanoparticles

The composite nanoparticles were prepared through the nanoprecipitation of CA in aqueous solutions of different hydrophilic polysaccharides (**Figure 46**). In order to optimize the process (smallest particles, good size distribution, satisfying yields), the hydrophilic polysaccharide content, and the pH value were varied. The size of the composite CA nanoparticles and the Pdl were not affected by varying the dispersive media with a polysaccharide content between 15×10^{-4} - 10×10^{-3} wt.%. Therefore the concentration was fixed at 15×10^{-4} wt.% in order to avoid the presence of unbound hydrophilic polysaccharide in the nanoparticle (NP) dispersion. Contrary, the dispersive media pH value influences the NP formation to a high extent. At acidic pH values, only large aggregates were formed. Small CA/CMC and CA/HEC nanoparticles could be generated at neutral and alkaline pH. Smallest CA/AC nanoparticles were generated at a pH value of 6.5. The smallest CA/L-CHI nanoparticles were generated at a pH value of 9.0. Therefore, the CA/AC, CA/CMC, and CA/HEC nanoparticles were generated at a pH value of 6.5. CA/L-CHI were generated at a pH value of 9.0. The large particles obtained at low pH values can be explained when considering that unmodified CA nanoparticles are not stable and tend to coagulate under acidic conditions²⁷. The composite nanoparticles were analyzed using: SEM (size, shape), ELS (effective zeta-potential), DLS (Pdl, size), and by determining the composite nanoparticle yields.

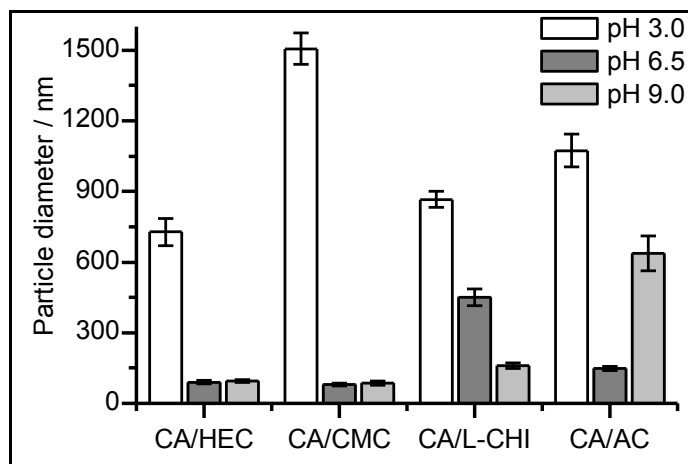


Figure 46: Mean composite nanoparticle diameters as a function of pH values and dispersive media

Table 3: Composite nanoparticle properties.

Composite nanoparticle	Diameter [nm]	STD [nm]	PdI [nm]	Zeta- potential [mV]	Yield [%]	STD [%]
CA	120	18	0.21	-37	87	12
CA/HEC	89	7	0.18	-21	82	9
CA/CMC	95	6	0.16	-27	87	12
CA/L-CHI	159	12	0.18	-19	69	11
CA/AC	148	9	0.12	+24	71	14

The mean particle diameters were significantly influenced by the hydrophilic polysaccharides. CMC and HEC reduced the particle size (by 30 nm), and AC and L-CHI increased the particle size (by 35 nm), in comparison to non-functionalized CA nanoparticles. These data are supported by SEM measurements which show spherical NPs of similar size compared to DLS data (**Figure 47**). All polydispersity indices (PdI) of the composite nanoparticles (below 0.19) indicate for a narrow size distribution. The nanoparticle yields were high and nearly the same for all kinds of composite nanoparticles. These data show that the hydrophilic polysaccharide influence the particle formation process and does not only adsorb onto the surface of freshly prepared CA NPs.

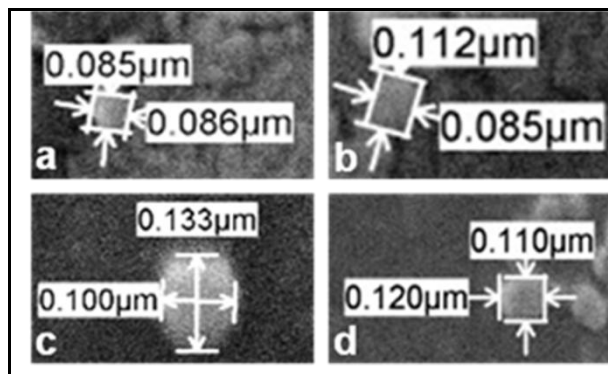


Figure 47: SEM images of different in-situ composite CA nanoparticles. **a:** CA/HEC **b:** CA/CMC **c:** CA/L-CHI. **d:** CA/AC.

The effective zeta-potential was also strongly influenced by the hydrophilic polysaccharide (shifts from 10 to 61 mV). L-CHI, CMC, and HEC decreased the effective zeta-potential in the order CMC < HEC ≤ L-CHI. CA/AC nanoparticles provided positive zeta-potentials but the potentials were in absolute values lower than that of unfunctionalized CA nanoparticles.

The composite CA nanoparticles show spherical shapes and their diameters increase in the order of HEC ~ CMC < L-CHI ~ AC (**Table 3, Figure 47**). These data show clearly that the hydrophilic polysaccharides are present at the NP surface and influence their surface properties.

4.2.2 Effective zeta potential

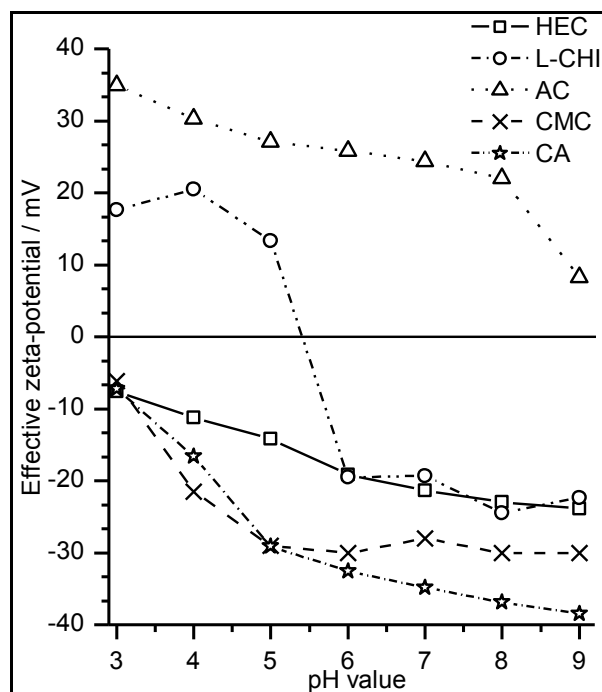


Figure 48: pH value depended effective zeta-potential of composite CA nanoparticles.

The effective zeta-potential was measured at varying pH values ranging from 3.0 to 9.0 (**Figure 48**). The effective zeta-potential of CA/CMC nanoparticles stayed constant from a pH value of 5.0 to 9.0 (-28 mV). At lower pH values it decreased linearly. Although CMC comprises negative charge at moderate and alkali pH values, the zeta-potential of the composite NPs in this region is lower compared to unmodified CA NPs. This is because the modification with CMC increases the NPs surface hydrophilicity yielding lower zeta-potentials¹⁰⁸.

Under neutral and alkaline conditions, CA/L-CHI nanoparticles comprised negative effective zeta-potentials, which decreased (by 10 mV) towards lower pH values. From pH value 6.0 to 5.0, the zeta-potentials turned to positive values (+20 mV), which remained constant at acidic pH. This is because the majority of the amino functions of chitosan gets positively charged below its $pK_a=6.5$ ²⁷. CA/AC nanoparticles showed positive zeta-potentials over the pH value range from 3.0 to 8.0, and it dropped from pH values of 8.0 to 9.0 (by 14 mV). This can be explained by the positive charges of the primary and secondary amino functions of AC.

The zeta-potential - pH value curve obtained for CA/HEC NPs decreases linearly with decreasing pH value. This is typical for hydrophilic, uncharged surfaces.

Summing up the zeta-potential - pH values curves are characteristic for the different hydrophilic polysaccharides used for preparing composite NPs. This shows clearly that CA NPs were successfully functionalized with HEC, CMC, L-CHI, and AC, and that these hydrophilic polysaccharides dominate the NP surface characteristics.

4.2.3 Stability of composite CA nanoparticles

The stability of composite CA nanoparticles during storage and against mechanical stress like centrifugation, and redispersion reflects the nanoparticles' surface properties. The stability tests were performed by my college Martin Kulterer¹⁰⁷.

Conclusions, problems, difficulties

Spherical functional composite nanoparticles of narrow size distribution from hydrophobic and hydrophilic polysaccharides were successfully prepared. The developed technique allows modifying the nanoparticle surface properties very specifically by varying the hydrophilic polysaccharide. This was shown through different surface characterization methods. The nanoparticles' stability was improved significantly through the modification with hydrophilic polysaccharides. It was not required to chemically modify the materials.

4.2.4 Modification of CA surfaces

CA model films

Model films of CA are required in order to analyze the adsorption and surface modification processes in more detail using techniques like AFM, Sarfus, water contact angle, QCM-D, etc..

Model films from CA were prepared on SiO_x wafer. These substrates provide very smooth and well defined surfaces. Nanometer thin films of CA were applied to these substrates via spin coating. The spincoating conditions (solvent, CA concentration, spinning time, etc.) were optimized by Martin Kulterer. Under optimal conditions, smooth (roughness of 2.98 nm) homogenous films of (film thickness of 70 nm) were obtained, as can be seen in **Figure 49**. The contact angle measurements of CA surfaces showed contact angles of 58°.

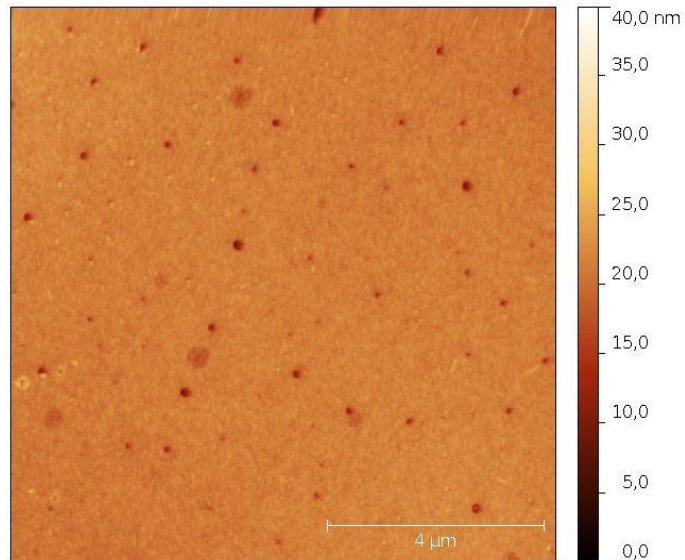


Figure 49: Cellulose acetate (CA) surface (AFM picture).

4.2.5 Activation of CA surfaces

In order to introduce functionalities (antimicrobial action) or specific binding sites (e.g. carboxyl- or amino- functions), the aim was for coating CA surfaces either with functional polysaccharides or polysaccharide nanoparticles.

Neither CMC, HEC, L-CHI, AC, nor polysaccharide NPs adsorbed onto plain CA surfaces, regardless which conditions (pH, salt, salt content, polysaccharide content, etc.) were chosen. Therefore, it was required to find a method for making the CA surface more "active" for binding polysaccharides or NPs. Different activation techniques were tested by Martin Kulterer. Best results were obtained by dipping the model films into a 0.1 M KOH solution for 15 min. Through this activation process ester bounds are cleaved, and the surface becomes more cellulosic (**Figure 50**). The film thicknesses decreased to 60 nm, while the roughness did not change significantly. The contact angles decreased to contact angles of 35°. This surface is more accessible for adsorption, compared to CA, because more OH- groups are accessible for forming H- bonds. Moreover, more ions are able to adsorb onto the surface, and adsorbents like charged polysaccharides can therefore bind through electrostatic interactions. Additionally, a more cellulosic surface comprises a higher structural affinity to charged polysaccharides with cellulosic backbones (e.g. CMC).

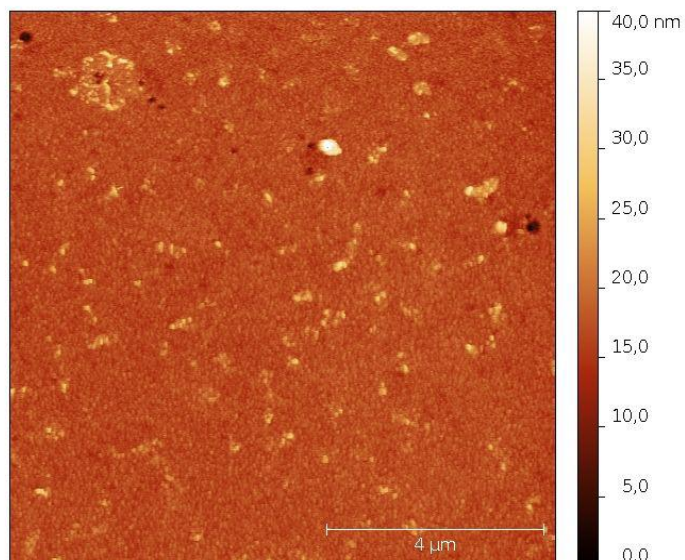


Figure 50: Activated cellulose acetate (CAA) surface (AFM picture).

4.2.6 Polysaccharide coating

L-CHI, and CMC were successfully adsorbed onto activated CA (CAA) surfaces. The adsorption processes were optimized by testing different salt additives (KCl, CaCl₂), salt concentrations (50 – 200 mM), and pH values (pH 5 – 7) by Martin Kulterer. The addition of salt is required in order to shield charged functional groups. This reduces electrostatic repulsion, changes the polysaccharides conformation, decreases its solubility, and therefore increases its tendency to adsorb on a surface. Similarly, changing the pH-value changes the charge density of weak polyelectrolytes, and can therefore be used for adjusting the adsorption process. The adsorption process was analyzed using SARFUS and water contact angle.

Best results were obtained at a pH value of 5.5, 150 mM KCl, and 0.1 wt% polysaccharide content. The adsorption of L-CHI and CMC increased the layer thickness by three nm, compared to unmodified CAA. Accordingly, coating with L-CHI increased the water contact angle by 10° (more hydrophobic), whereas adsorption of CMC resulted in more hydrophilic surfaces (decrease of 7°). However, HEC did not adsorb on CAA, and the CMC monolayer turned out to be unstable.

In order to overcome these limitations, we designed bi- and tri-layer, with the desired polysaccharides on the top. CMC adsorbed nicely on L-CHI precoated CAA surfaces. The water contact angle dropped by 11°, when strongly hydrophilic CMC was applied onto the L-CHI layer. The decrease of the layer

thickness can be explained by a compression of the layer caused by the compensation of positive charges of L-CHI with negative charges of CMC. Also HEC was successfully adsorbed onto L-CHI precoated CAA. The layer thickness increased by 2 nm, whereas the water contact angle decreased by 7° because of an increased surface hydrophilicity.

These data were approved by QCM-D measurements, which were performed by Martin Kulterer.

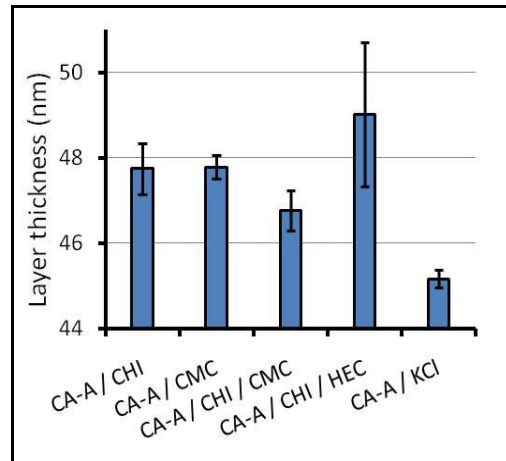


Figure 51: Layer thickness of the polysaccharide coated CA-A surfaces

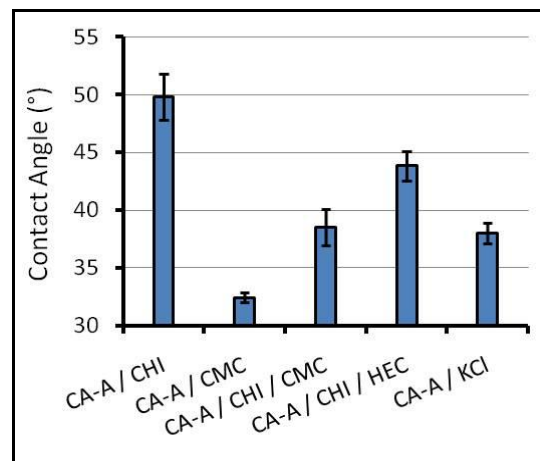


Figure 52: Water contact angle of the polysaccharide coated CA-A surfaces

4.2.7 Coating with polysaccharide composite nanoparticles

The prepared polysaccharide composite nanoparticle did not adsorb onto CAA. Therefore, a precoating with different functional polysaccharides was required.

The prepared composite NPs were applied to precoated CAA, with HEC, CMC, and L-CHI as top-coating. After applying CA/L-CHI, CA/AC, CA/CMC, or CA/HEC, and nanoparticles to the different surfaces, the samples were analyzed using SEM (**Figure 53**).

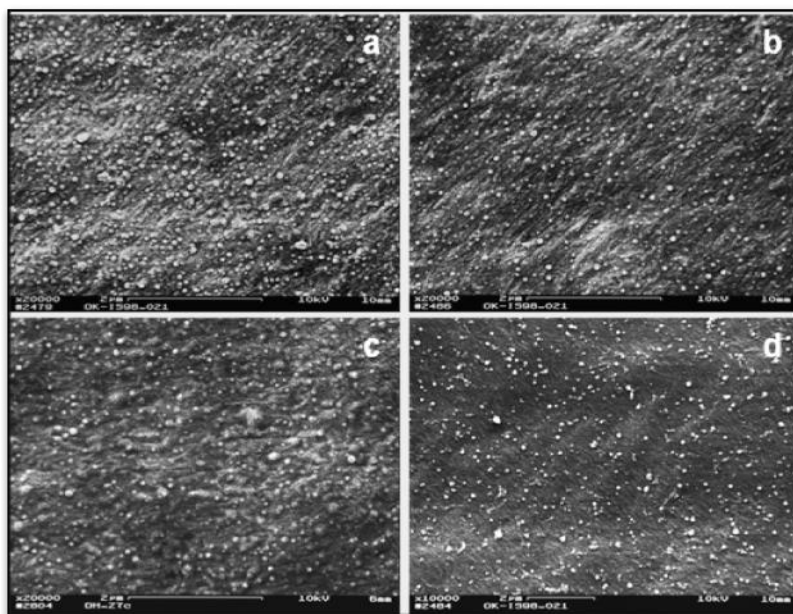


Figure 53: a: CA/CMC NPs onto L-CHI surface, b: CA/HEC NPs onto L-CHI surface, c: CA/L-CHI NPs onto HEC surface, d: CA/AC NPs onto CMC surface

The composite nanoparticles showed very specific adsorption behaviour. In particular CA/L-CHI nanoparticles adsorbed only on HEC, CA/AC nanoparticles adsorbed only on CMC, and CA/HEC and CA/CMC nanoparticles adsorbed only on L-CHI. If successfully adsorbed, the particles formed a monolayer of individualized nanoparticles of evenly size distribution. Moreover, they did not cover the surface completely. Therefore, this approach allows introducing specific functional groups, but having the underlying surface still accessible for selective chemical modifications.

4.3 Conclusions, problems, difficulties

Functional nanostructures on CA surfaces were successfully designed in a very specific manner. CA surfaces turned out to be very inert against physiochemical modifications via adsorption. Therefore, a proper surface activation, followed by applying desired polysaccharide precoatings in one, two, or three steps, was required in order to coat the surface with polysaccharide composite nanoparticles in the final step. Polysaccharide precoatings take advantage of high affinities to CA-A and nanoparticles

due to their similar chemical structures. Moreover, the nanoparticle-surface-interactions can be tuned in a very specific manner by varying the polysaccharide top coating. This procedure, compared to plain polysaccharide coatings, take advantage of on the one hand providing larger surface areas, and on the one hand having functional groups of the underlying layer still accessible for chemical modifications.

5. Novel and versatile approach for testing bacterial growth on solid supports

5.1 Methods

5.1.2 Preparation of media, buffer, and bacteria suspensions

A Systec U-150 autoclave was used for sterilizing the prepared media and buffer solutions by autoclaving (121°C). M9 minimal media was used for growing the bacteria. 100 ml M9 minimal media consist of 10 ml of 1/10 diluted M9 stock solution, 1 ml 20 wt.% glucose solution, 0.2 ml thiamine, 0.1 g MgSO₄, 0.3 g casamino acids, and 90 ml bidistilled water. The M9 stock solution was prepared by adding to 1 l of bidistilled water 30 g KH₂PO₄, 128 g NaH₂PO₄ × 2 H₂O, 10 g NH₄Cl and 85 g NaCl. The test set-up was evaluated with the *E.coli* strain MG1655 [R1-16]. Bacteria stock solutions were prepared by dispersing cells, which were taken directly from the strain bank, in 30 ml of M9 minimal media, and incubating the cell solution at 37 °C over night under continuous shaking (Over night culture ONC, OD₆₀₀: 0.8 – 1.2). The phosphate buffer system (1xPBS buffer) was prepared by adding to 1 l of bidistilled 8.0 g NaCl, 0.2 g KCl, 1.4 g NaH₂PO₄ × 2 H₂O and 0.2g KH₂PO₄. The 3xPBS buffer was prepared, using a three times higher salt concentration.

5.1.3 Sample surface preparation

Silicium oxide platelets (1 cm x 1 cm) were decorated with a CA model film as described. CA model films were decorated with L-CHI or CMC according to the method described above. The surface analysis was performed using water contact angle and Sarfus as described above (data not shown explicitly). For each antimicrobial test 9 samples, three replicates for each test method, were

prepared. Additionally, textile fibres and hollow fibre membranes were used directly without any pretreatment.

5.1.4 Incubation procedure

All steps were performed under sterile conditions. First, the substrates were sterilized and dried. The samples were then fixed on the bottom of well- plates. The ONC was diluted with M9 minimal media to an OD_{600} of 0.03. The samples were incubated with 2 ml of this bacteria solution over night and continuous shaking. Next, the bacteria suspension was removed. In order to determine the amount of bacteria growing in solution, the optical density was measured at 600 nm (OD_{600}), using a Hitachi Metrohm U-5100 spectrophotometer. Loosely bound bacteria on the surface were removed by rinsing with 1xPBS buffer. Finally, the samples were analyzed after rinsing with 1xPBS buffer.

5.2 Results and Discussion

5.2.1 Incubation and cultivation procedure

The preparation of CA model films and the procedure for coating a film with CHI and/or CMC is described above. These model films were used for the set-up of the antimicrobial test. Antimicrobial CHI coated CA was used as negative control; whereas CMC coated CA films were used as positive control.

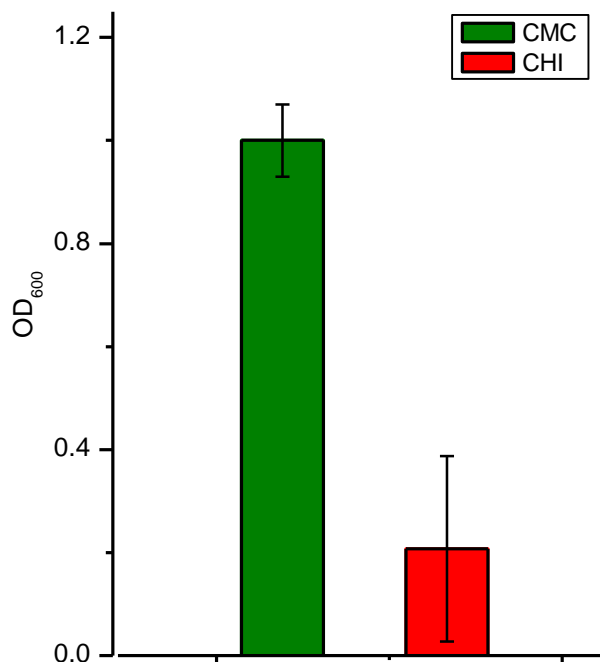


Figure 54: OD_{600} of bacteria suspensions (*E. coli* MG 1655 [R1-16]) after incubation for 12 h.

The model films were first incubated in a bacterial solution over night, in order to allow the microorganisms to attach to the surface. The amount of bacteria in solution after incubation was determined (OD_{600}) in order to evaluate the influence of the surface coating on the bacteria in its surrounding (**Figure 54**). The data show clearly that the coating with antimicrobial CHI reduced the amount of bacteria in solution significantly, compared to CMC. Unbound and loosely bound bacteria were then removed, and only surface bound bacteria were further cultivated over night (biofilm formation). The bacteria on the surfaces were then analyzed using afore mentioned techniques.

5.2.2 Live/Death fluorescence staining technique

After removal of loosely attached microorganism, the bacteria on the surfaces were stained with SYTO[®] 9 and propidium iodide. The green SYTO[®] 9 stains all bacteria, whereas propidium iodide binds solely to death bacteria. The images obtained for each dye are matched together in order to visualize death and alive bacteria in one picture.

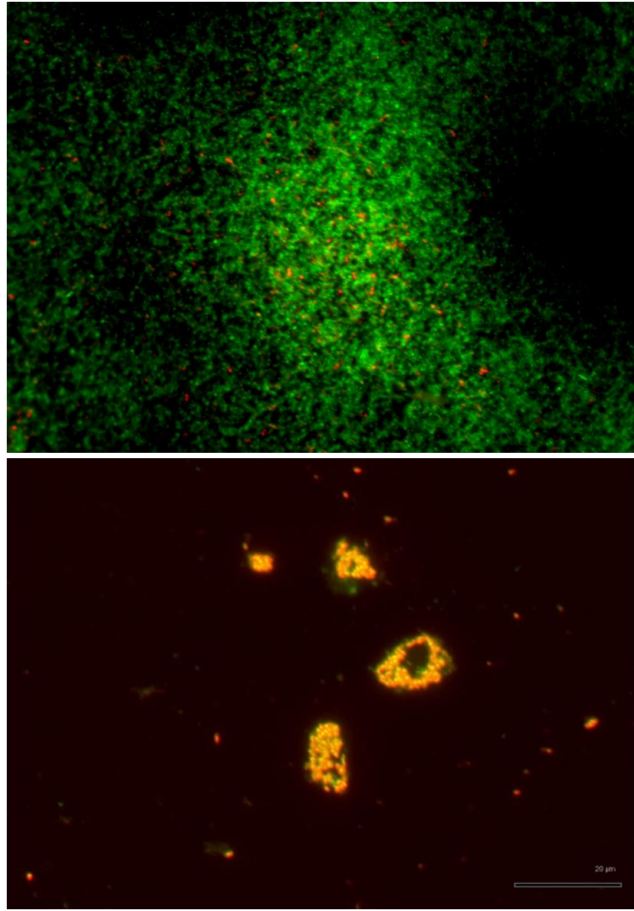


Figure 55: Fluorescence microscopy results. The images obtained for SYTO[®] 9 (green) and propidium iodide (red) are matched together. Upper picture: CMC coated CA surface. Lower picture: CHI coated CA surface.

The upper image (**Figure 55**) show that, on CMC coated CA surfaces, bacteria grow nicely (green) in form of a thick layer (biofilm). Only few death bacteria were found on these surfaces (red). In comparison, no living bacteria were found on antimicrobial CHI coated CA surfaces (**Figure 55**, lower image).

5.2.3 Real Time (RT) PCR

For quantifying the total amount of bacteria on the surface, the amount of DNA was determined using RT-PCR. The system was calibrated by measuring bacteria suspensions at concentrations ranging from 10^9 to 10^3 bacteria per ml (**Figure 56**). The number of bacteria in solution correlates linearly over 6 magnitudes with the number of RT-PCR cycles after which the fluorescence signals starts to increase rapidly (**Figure 57**).

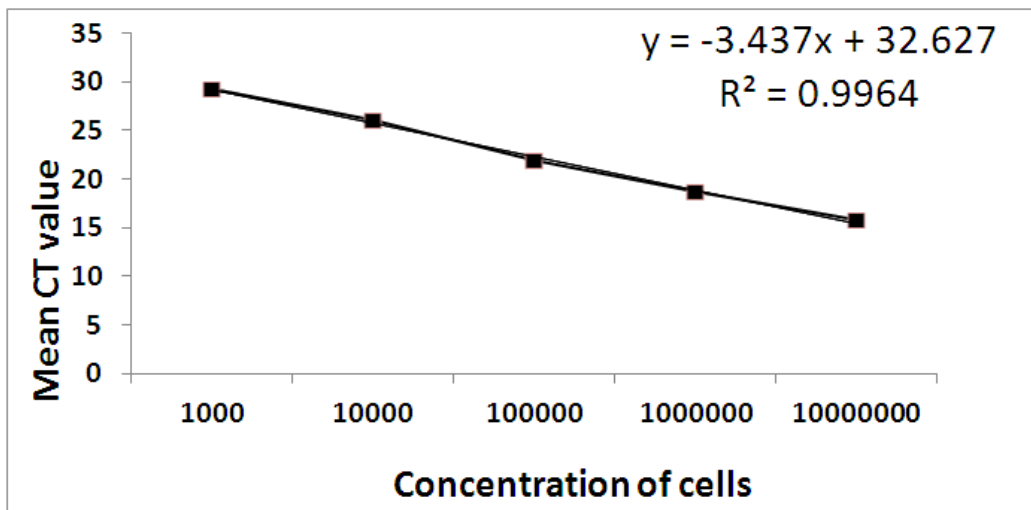


Figure 56: Calibration curve of RT-PCR.

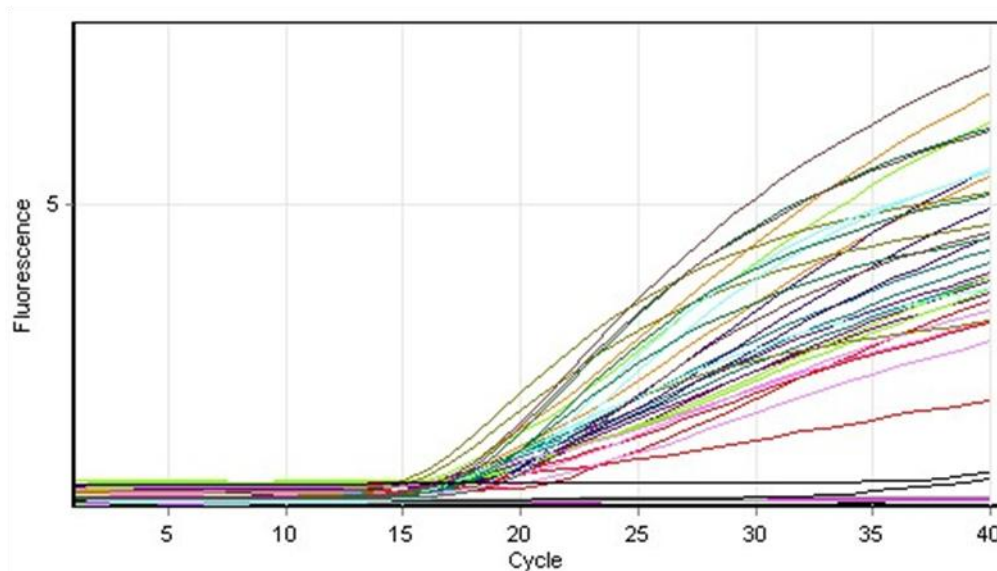


Figure 57: Fluorescence intensity with respected of the RT-PCR cycles.

The most critical step of the RT-PCR procedure is the disruption of the bacteria and the extraction of the DNA from the surface. In order to evaluate the efficiency of the disruption/extraction process, the samples were loaded with a defined number of death bacteria. This was performed by putting a suspension containing death bacteria on the surface, followed by drying. The results of this test showed clearly that the DNA was very efficiently extracted. The results correspond well with the values obtained for bacterial solutions of the same concentration. Moreover, the different surface functionalities did not affect the results. Therefore our test assembly can be used for analyzing bacteria on polysaccharide surfaces. 10 times less bacteria were found at the CHI coated CA surface, compared to the CMC coated CA surface (**Figure 58**).

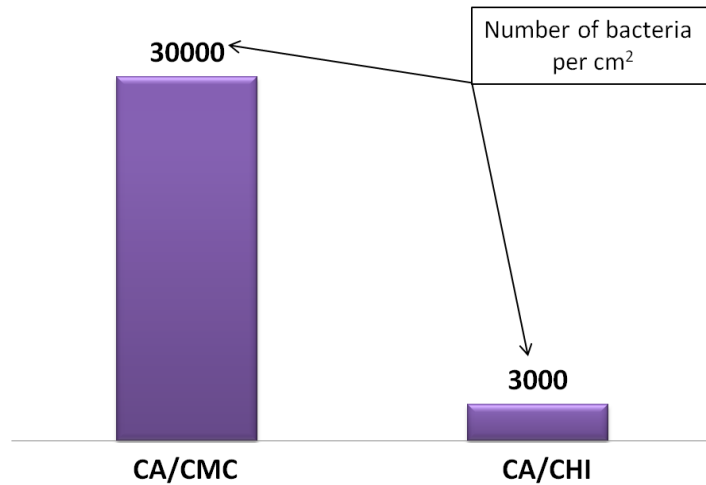


Figure 58: Number of bacteria found on 1 cm² coated CA surface.

Taking into consideration the results from Live/Death fluorescence staining experiments, one can nicely explain the obtained differences in the number of bacteria on the surface. The high number of bacteria detected on CMC coated surfaces origin from a thick biofilm, which mostly contains living bacteria. In contrast, the relative few bacteria detected on CHI surfaces were death, and no biofilm was formed (**Figure 59**).

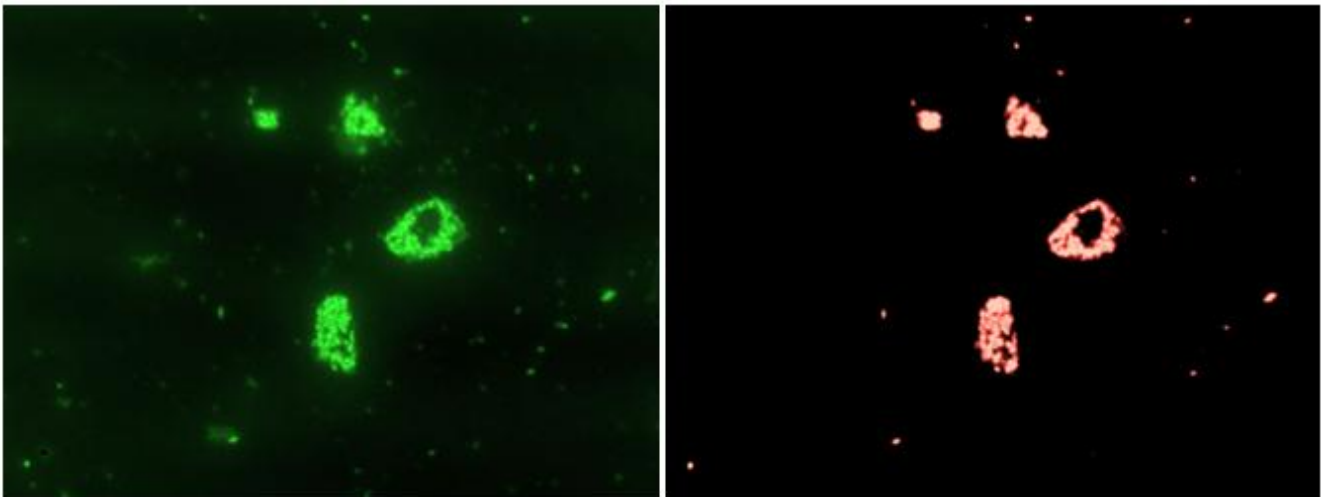


Figure 59: Fluorescence microscopy results. The images obtained for SYTO[®] 9 (green) and propidium iodide (red) are matched together. CHI coated CA surface.

5.2.4 Scanning electron microscopy (SEM)

The obtained results were validated by visualizing the bacterial growth on the surfaces directly using SEM. The main drawback of this method, besides the expensive instrumentation, is that no quantitative data are obtained. SEM images show clearly bacteria forming a biofilm in early state on CA/CMC surfaces (**Figure 60**). Contrary, only few individualized, strongly distorted bacteria were found on CA/CHI surfaces (**Figure 60**). The bacteria are surrounded by a flower-like structure, which can be interpreted as cytoplasm secreting out of the death bacteria. These results support the data obtained with Live/Death fluorescence staining and RT-PCR. This shows that the presented approach based on a combination of staining techniques and RT-PCR allows investigating the bacterial growth in qualitative and quantitative way.

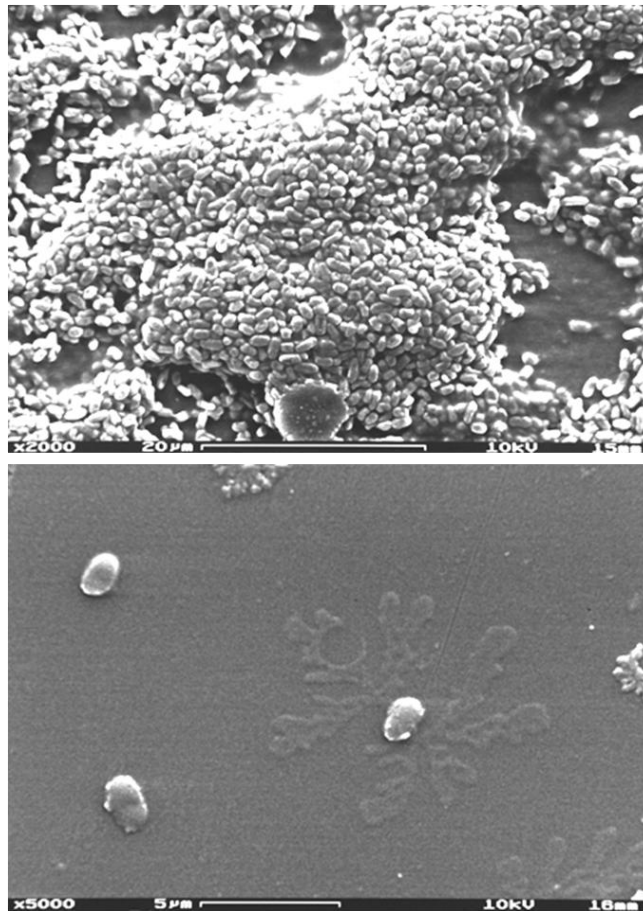


Figure 60: Upper picture: Bacteria on CMC coated CA surface. Lower picture: Bacteria on CHI coated CA surface.

5.3 Conclusions, problems, difficulties

The developed approach, which bases on standard instrumentation in microbiology, can be used for investigating bacteria attachment and biofilm formation reproducible and in very short time. The test was already performed with other antimicrobial samples, for example silver nanoparticles coated fibres and yarns.

6. Enzymatic hormone degradation →

Hormone & enzyme incubation

6.1 Methods

6.1.1 Preparation of 17 α Ethinylestradiol solution

The saturation concentration of 17 α Ethinylestradiol (EE2, **Figure 61**) in water is 11.3 mg/l. However, it was not possible to prepare aqueous solutions of satisfying concentration directly. Therefore, solutions of 10 mg/l EE2 content had to be prepared as following: First, 1 mg/ml solution was prepared using a water miscible organic solvent (MeOH, DMSO, DMF, EtOH, THF, and ISO were tested). Ethanol was chosen as the best one. Next, 1 ml of this solution was added to 99 ml of bidistilled water, or 10 mM CaCl₂.

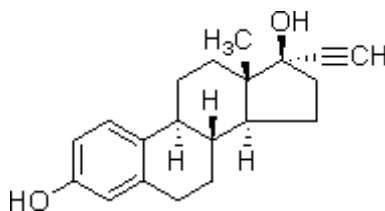


Figure 61: 17 α Ethinylestradiol (C₂₀H₂₄O₂).

6.1.2 Enzyme and hormone incubation procedure

150 μ l of enzyme solution (fermentation bulk solution, or purified enzyme solution) was added to 1.4 ml of an aqueous 10 mM CaCl₂ hormone solution (10 mg/l). Next, the mixture was incubated for 10 -

120 min under continuous shaking at room temperature. Following this procedure, the activity of four different HRP isoenzymes against EE2, (C1A 11/2, C1A 263, C1A 4/4, and A2) was tested.

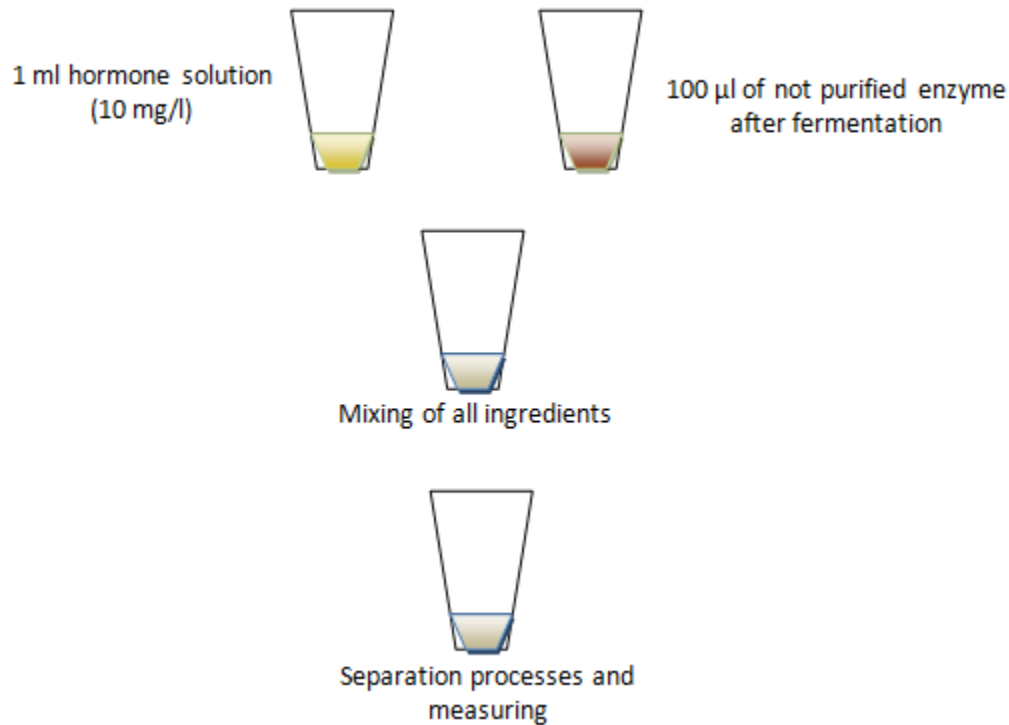


Figure 62: Enzyme and hormone incubation procedure.

6.1.3 Determination of the enzyme activity

Activity test

The first activity tests with the isoenzymes C1A and A2 were performed using fermentation bulk with an average overall protein content of 0.8 µg/ml. The activity test with ultra pure HRP A2 was performed using a 34.2 µg/ml solution (Rz: 1). For testing the enzyme activity, 150 µl of the enzyme solution was added to 2.95 ml of EE2 (10 µg/ml) dissolved in 10 mM CaCl₂ (see above). The reaction mixture was incubated under continuous shaking (10 min – 120 min) in the dark. After extractive separation of the analyte from the reaction mixture, the activity was determined using fluorescence spectroscopy.

Fluorescence spectroscopy measurements

In order to analyze the degradation process by spectroscopy, EE2 and its degradation products had to be separated from the enzymes. This was necessary because these substances exhibit very similar, overlapping absorption as well as fluorescence emission and spectra.

In order to find specific, intensity signals, the emission spectra were recorded at excitation wavelengths ranging from 220 nm to 380 nm. Moreover, hormone and enzyme were measured in bidistilled water, in bidistilled water + H₂O₂, and in aqueous 10 mM CaCl₂ solutions in order to investigate the influence of solutes on the intrinsic fluorescence.

Liquid-Liquid extraction procedures

Following organic solvents and solvent mixtures were tested to extract EE2 out of the reaction mixture: Toluene, diethyl ether, hexane, ethyl acetate, dichloromethane, butylmethylether/petrol (30/70). The ratio organic phase / aqueous phase was altered from 5 to 7.5, and the extraction times were varied from 20 – 60 min. A laboratory shaker was used for 20 minutes at room temperature (20°C-25°C). In case of butylmethylether/petrol (30/70), also phase separation via freezing out was evaluated. In particular, the two phase system was freezer cooled to -25°C, and the still liquid supernatant was taken off. Finally, the organic phases were concentrated to dry using N₂ gas, and the residue was taken up in 400 µl MeOH in order to avoid influences of the organic solvents on the EE2 spectra. The analysis was performed using UV-VIS absorption spectroscopy and fluorescence emission spectroscopy.

Solid phase extraction (SPE)

SPE was performed using TC 18 reversed phase cartridges, which were purchased from Sigma Aldrich (Steinheim, Germany). The SPE was prepared as mentioned in the manufacturers' protocol⁹⁸.

Tube washing

First the tubes were washed with in order to remove impurities which are origin form the production process. Therefore the tubes were washed with 1 ml n-hexane (three times), following by 1 ml acetone (two times), 1 ml methanol (three times), and 1 ml bidistilled water (pH value of 3, three times).

Washing and elution procedure

The tube is loaded with 2 ml of the sample. Rinsing with 3 ml of bidistilled H₂O (pH value of 3), and 3 ml of methanol/ bidistilled H₂O 40/60 (pH value of 3) is followed. Finally, the sample gets eluted after one drying step (2 minutes N₂ incubation) with 2x2 ml of methanol/ bidistilled H₂O 80/20.

6.2 Results and discussion

6.2.1 EE2 analysis

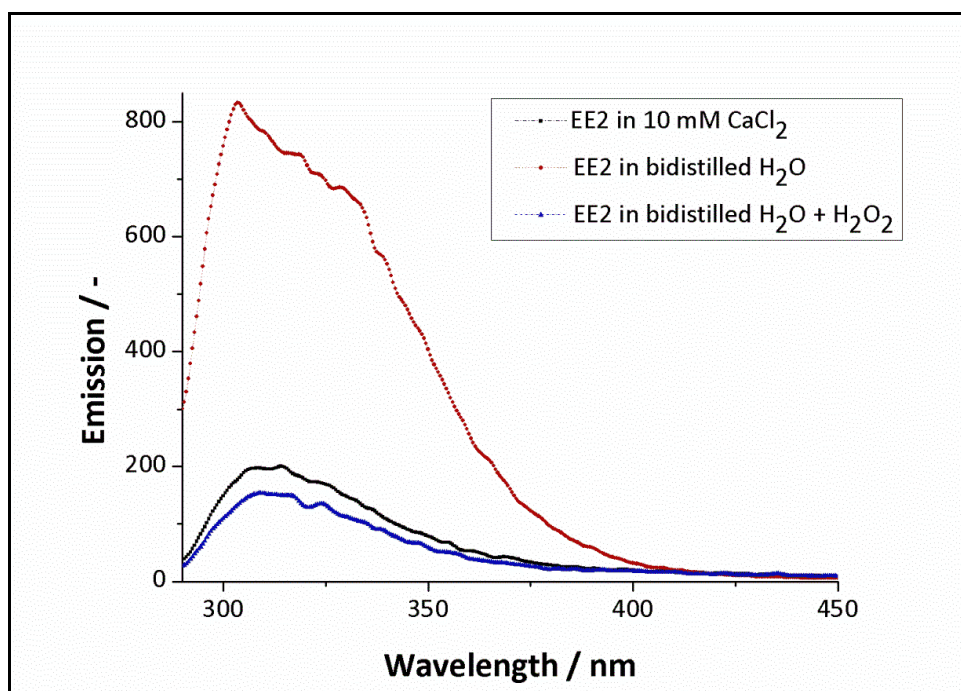


Figure 63: Emission spectra (Excitation: 280 nm) of EE2 (10 mg/ml)

To prepare an aqueous solution of 17 α Ethinylestradiol (10 mg/ml), the hormone has to be solved first in a water mixable solvent (1 mg/ml), followed by adding 1 ml of this solution to 99 ml aqueous solution (pure water, 10 mM CaCl₂, and 0.085 wt.% H₂O₂). CaCl₂ and H₂O₂ solutions were tested, because these chemicals are usually required for the enzyme to be active. For this procedure, we tested MeOH, DMSO, DMF, EtOH, THF, and ISO as organic solvents. The procedure was only successful with EtOH. In all other cases the hormone precipitated.

Next, the fluorescence emission spectra (290 nm – 450 nm) of this solution were measured. The best signals were obtained. The results for the tested solutions are depicted in **(Figure 63)**. The hormone

spectra in the bidistilled water and 0.085 wt.% H₂O₂ are very similar. The slightly smaller intensity found in the H₂O₂ solution can be explained by the fact that H₂O₂ may also oxidize EE2. The intensity found in the CaCl₂ solution is four times higher than the signal found in pure water.

6.2.2 Sample clean up

Unfortunately, the fluorescence emission spectra of EE2 and HRP are overlapping, and the signals could not be separated by screening the excitation wavelength. Hence, for evaluating the enzyme activity one has to find a procedure for separating the hormone from the enzyme.

Several extraction processes were tested.

6.2.3 Liquid-liquid extraction (LLe)

Liquid-liquid extraction was used for separating compounds due to their different affinities to two immiscible liquids. The compounds are extracted from one liquid phase into the other liquid phase (Figure 64).

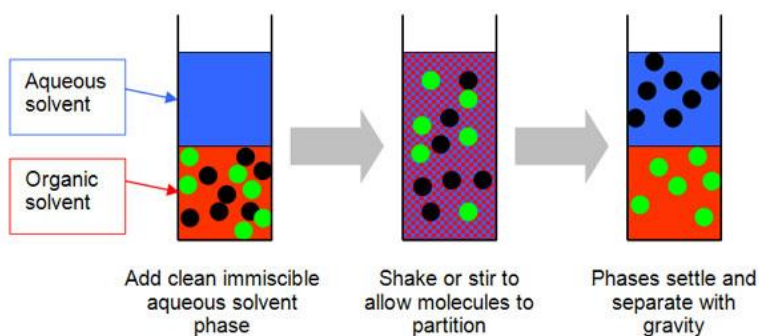


Figure 64: Liquid-liquid extraction

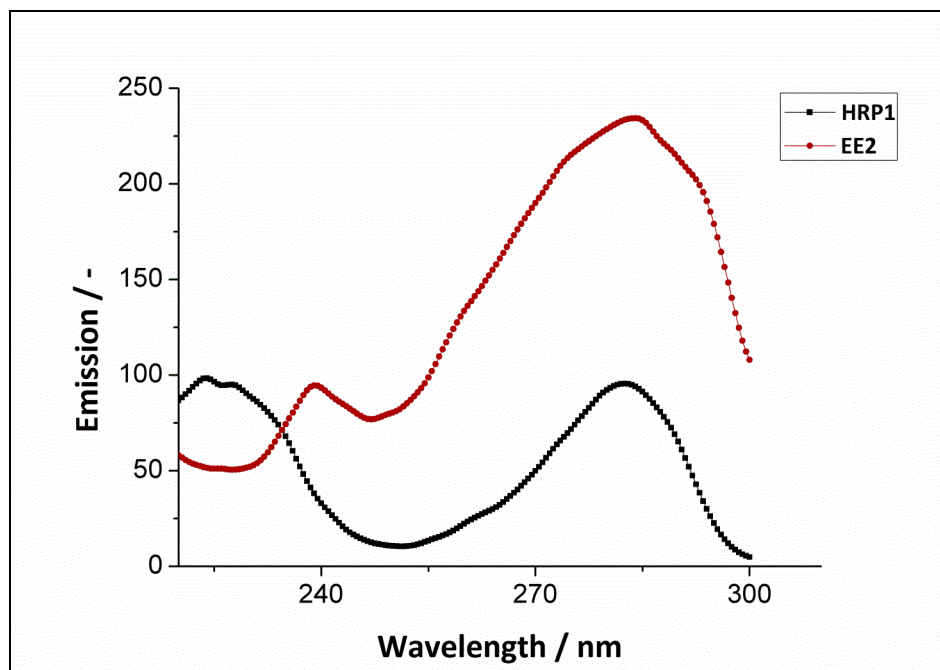


Figure 65: Exemplary fluorescence spectrum obtained from extracts of pure HRP fermentation bulk and EE2 solutions. Dark blue line: HRP spectrum, red line: hormone spectrum.

The LLE was not successful for separating enzymes and hormones. In all cases disturbing impurities, which origin from the fermentation bulk solution, where co-extracted. This can be seen clearly when comparing the fluorescence spectra of extracts from pure fermentation bulk and EE2 solutions (**Figure 65**). Therefore it was not possible to analyze the hormone in a reproducible manner.

6.2.4 Solid phase extraction (SPE)

To overcome this problem a separation process was introduced. The separation is based on differences in the affinity of analytes and impurities to the stationary and mobile phase. First, the cartridges were washed with different organic solvents and water in order to remove impurities origin from the production process (conditioning). The SPE procedure consists of 1 sampling step, 2 washing steps, and 1 elution step. After applying the sample the column was first rinsed with water (pH value of 3) in order to remove hydrophilic compounds (proteins like HRP). Next, for removing more hydrophobic compounds without eluting EE2, the column was washed with a water/organic solvent mixture. After drying the cartridge, the analytes were finally eluted with a hydrophobic solvent mixture.

In order to optimize this procedure, several solvent mixtures were tested for washing, and eluting EE2. The first washing step with water was not changed. Based on a method description obtained from a hormone analyzing kit, we used a 80/20_{v/v} mixture of 10 mM CaCl₂/MeOH (pH value of 8.5) for washing the column followed by eluting with acetone. With this procedure, it was not possible to remove all disturbing compounds. Next, we applied a procedure consisting of washing with 50/50 bidistilled water/MeOH, followed by rinsing with acetone. Here, EE2 was already eluted during the washing procedure. Next, we changed the washing solvent composition to 40/60 methanol/distilled water, and eluted with acetone. Also here clean fractions could not be obtained. Finally, clean EE2 fractions could be obtained when eluting with 80/20 MeOH/water instead of acetone. The affectivity of the washing procedure is depicted in **Figure 66**.

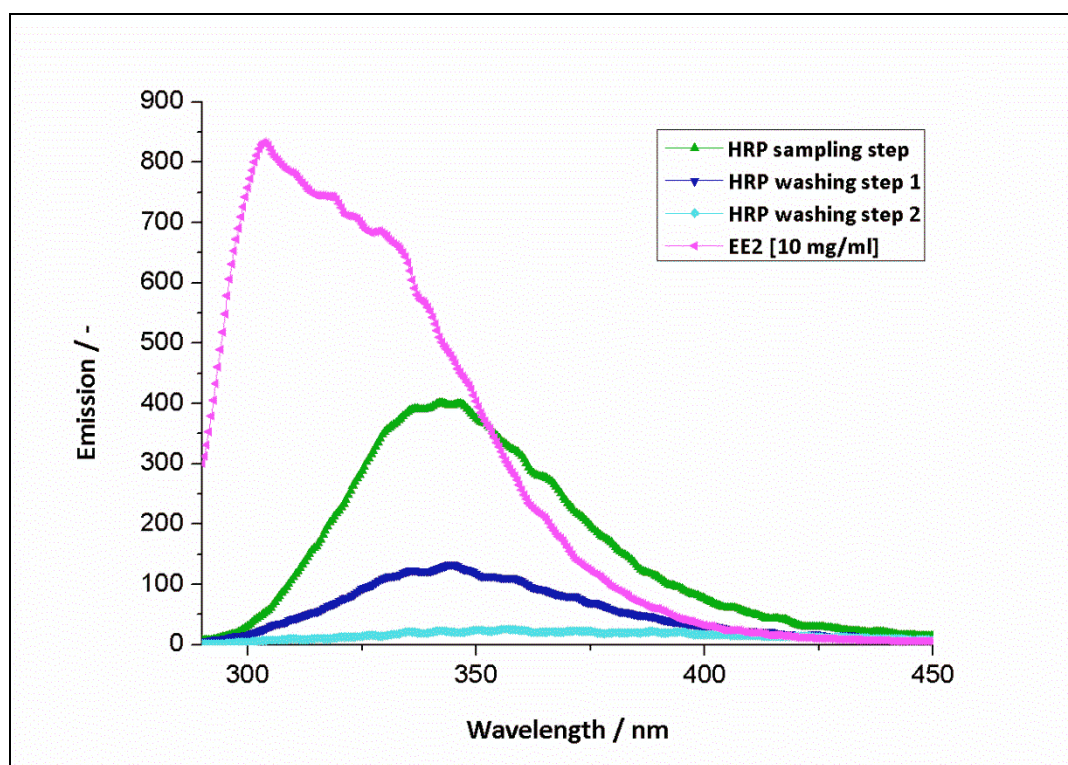


Figure 66: Emission spectra (Excitation: 280 nm) of different fractions from the optimized SPE procedure. Pink line: hormone before enzyme incubation, green line: HRP sampling step after SPE, dark blue line: HRP washing step 1 after SPE, light blue line: HRP washing step 2 after SPE.

6.2.5 Evaluation of the enzyme activity

After setting up a convenient method for analyzing the enzyme activity against EE2, we tested the activity of different HRP isoenzymes, and investigated the dependence of the enzyme activity on the

presence of the cofactors CaCl_2 and H_2O_2 . First, the activity of the two isoenzymes (C1A and A2) was evaluated using fermentation solutions in the presence of both co-factors. Both enzymes degraded EE2 efficiently (**Figure 67**), which results in a strong decrease of the fluorescence signal for EE2. Differences in the enzyme activity could not be observed. The use of HRP C1A would take advantage of the fact that this enzyme provides only one primary amino function at the surface. Therefore, this functional group could be used for the selective chemical immobilization of the enzyme. Moreover, this amino function is oriented oppositely to the active centre. Hence, after immobilization, the enzyme would be oriented in a sterically most favourable position on the surface. However, the main disadvantage of this enzyme is its high degree of glycosylation. Because of this, HRP C1A does not show highly specific interactions with surfaces. Hence, the purification via chromatography of this enzyme turned out to be very complicated. Taking this into consideration, HRP A2 was chosen, because the fermentation and clean up processes are well developed.

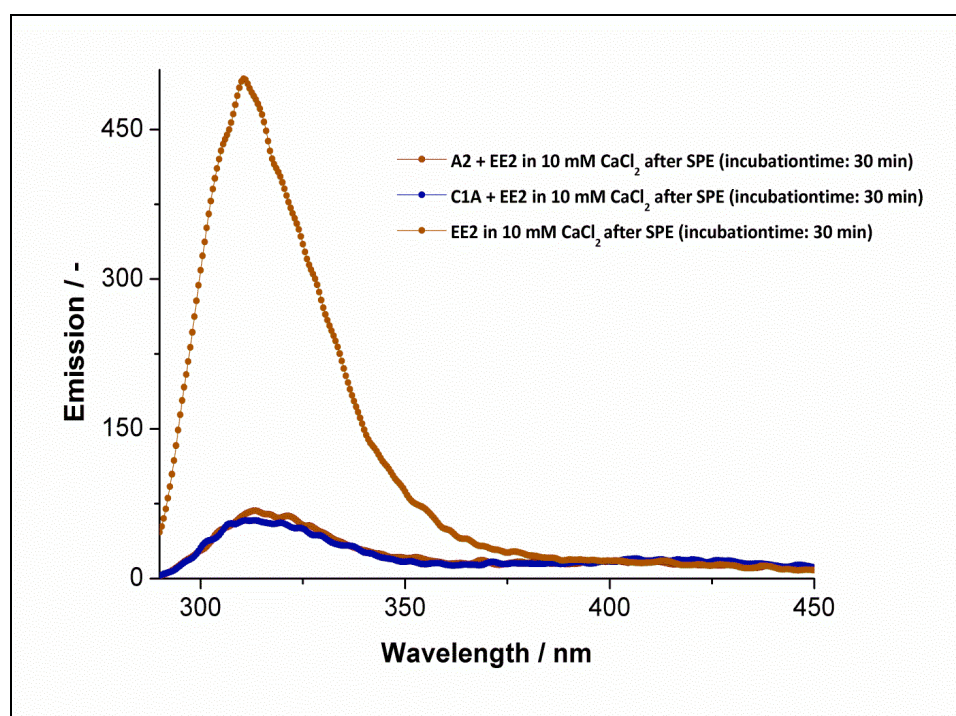


Figure 67: Emission spectra (Excitation: 280 nm) of EE2 (10 mg/ml) and EE2 with enzymatic incubation.

Orange line: A2+EE2 incubation for 30 min after SPE, dark blue line: C1A+EE2 incubation for 30 min after SPE, brown line: EE2 without enzyme incubation after SPE.

Next, we investigated the influence of the co-factors on the reaction. The absence of H_2O_2 did not affect the enzyme activity. In the reaction cycle (Figure 67), H_2O_2 acts as electron acceptor.

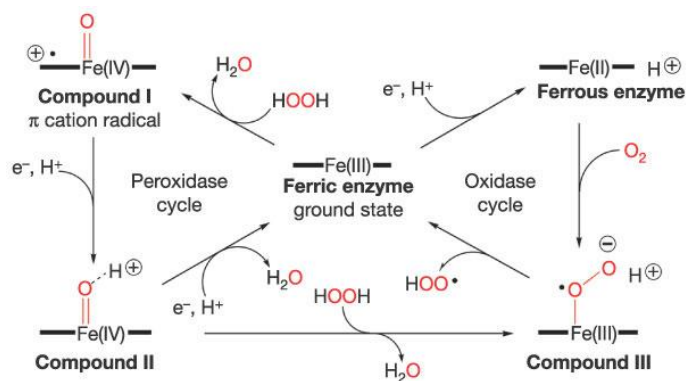


Figure 68: Ferric enzyme reaction mechanisms¹⁰⁹.

Here, H₂O₂ is not required, most probably because O₂ may act as electron acceptor. In contrast, the absence of CaCl₂ leads to inactivation of the enzymes.

6.3 Conclusions, problems, difficulties

We set up an analytical method which allows analyzing the enzyme activity using fluorescence spectroscopy. Using this method, we successfully showed that HRP isoenzymes can be used to degrade EE2. Moreover, we demonstrated that the presence of the usually required co-factor H₂O₂ is not necessary. This shows that the catalytic cycle most probably includes O₂ as electron donor, instead of H₂O₂.

7. Fermentation and purification of horseradish peroxidase

7.1 Methods

7.1.2 Media and buffer solutions

Buffered glycerol-complex medium (BMGY)

All solutions were sterilized at 121°C.

BMGY medium is used for culturing *Pichia pastoris* cells. For creating 1 l BMGY medium, 20 g peptone and 10 g yeast extract were dissolved in 698 ml bidistilled water. To this solution, 100 ml of 1M potassium phosphate buffer (pH 6.0), 100 ml yeast nitrogen base (YNB) solution (134 g/l), 2 ml biotin solution (200 mg/l), and 100 ml glycerol solution (100 g/l) were added.

Basal salt medium (BSM)

BSM medium was used for the fermentation process. For preparing 1 l, 18.2 g K_2SO_4 , 0.9 g $CaSO_4$, 14.9 g $MgSO_4 \cdot 7H_2O$, 26.7 ml 85 wt.% H_3PO_4 , 40.0 g glycerol, and 4.1 g KOH were dissolved in bidistilled water. The medium pH was adjusted to 5.0 using 28 wt.% ammonia solution. Finally, the medium was sterilized at 121°C.

Trace salts solution (PTM1)

3.00 g $MnSO_4 \cdot H_2O$, 6.00 g $CuSO_4 \cdot 5H_2O$, 0.08 g NaI, 0.02 g H_3BO_3 , 0.20 g $Na_2MoO_4 \cdot 2H_2O$, 20.00 g $ZnCl_2$, 0,50 g $CoCl_2$, 0,20 g biotin, 65.00 g $FeSO_4 \cdot 7H_2O$ and 5.00 ml H_2SO_4 were dissolved in 1l bidistilled water. The solution was sterilized at 121°C.

Glycerol feed solution

630 g glycerol was dissolved in 1 l bidistilled water. After autoclaving (121°C), 12 ml PTM1 solution were added.

100% Methanol feed solution

12 ml PTM1 were added to 1 l MeOH.

Pre-cultures

To start the fermentation process, 500 ml of cell suspension with sufficient cell density had to be prepared. This step contains the cultivation of one over night culture, followed by the cultivation of two precultures.

Overnight culture (ONC)

One colony of *Pichia pastoris* was dispersed in 50 ml BMGY medium. The cells were cultivated over night at 28°C, and continuous shaking at 110 rpm.



Figure 69: ONC's and precultures for the fermentation process.

Preculture 1

50 ml of the ONC were added to 100 ml BMGY solution, and the cells were cultivated over night at 28°C, and continuous shaking at 110 rpm.

Preculture 2

An aliquot of the preculture 1 (OD_{600} : ~20) was diluted with BMGY medium to an OD_{600} of 2. This cell solution was further cultivated at 28°C and continuous shaking (110 rpm) until an OD_{600} of 9 was reached.

7.1.3 Fermentation process

The fermentation procedure consisted of three steps. First, the cells were adapted to the fermentation conditions, followed by the cultivation of cells in the fermenter (glycerol feed). Finally, the production of HRP was induced (methanol feed).

7.1.4 Fermenter

For the fermentation process, a 5000 ml BIOSTAT CT fermenter was used. The device allows controlling the temperature, pH value, and stirring speed (500 rpm). The system is equipped with sensor devices for measuring the solution's pH, and dissolved oxygen amounts. The pH was automatically adjusted to a pH value of 5.0 using 28 wt.% ammonia solution and 30 wt.% H₂SO₄. Air is continuously injected in the fermentation mixture (minimum of dissolved oxygen of 30%). The stirring speed was automatically varied in order to keep the oxygen content if the dissolved oxygen went below 30%. The temperature was held constant at 28°C¹¹⁰.

7.1.5 Fermentation procedure

The following procedure was performed for both cell strains.

Starting feed:

After autoclaving (121°C), the basin was filled with 3500 ml BSM media and 500 ml preculture 2 (OD₆₀₀ ~ 10). The cells were then cultivated for 12 hours. This so called batch phase was run until the whole nutrients in the starting medium were used by the *pichia pastoris* cells. This was indicated by the "starvation peak" in the oxygen levels.

FedBatch phase/glycerol feed:

The cultures grown to high cell densities due to a glycerol feed medium flow (5.0 mL/h per reactor). This step took about 6 hours.

Induction phase/methanol feed:

The expression of HRP was induced by adding MeOH with a flow rate of 3.0 ml/min. This step took about 90 hours.

7.1.6 Measuring the enzyme activity

The enzyme activity was determined using ABTS assay.

The 2',2'-azino-bis(3-ethylbenzthiazoline-6-sulphonic acid) (ABTS) assay is a standard test in biotechnology for analyzing enzymatic activities of peroxidases. For testing the enzyme activity of horseradish peroxidases (HRPs), the assay was performed according to Morawski *et al*, 2000¹¹¹. In

particular, 140 μl 50 mM NaOAc buffer solution containing 1 mM ABTS (pH value of 4.5) is mixed with 15 μl of the supernatant from fermentation cultures, or solution of purified enzymes. Next, the conversion was started by adding 1.75 μl of a 30 wt. % aqueous H_2O_2 to 20 ml of the ABTS solution. The conversion of ABTS is indicated by changing the solution's colour from colourless to blue. Hence, the absorption intensity at 405 nm measured using a Spectramax Plus 384 spectrophotometer (ϵ of oxidized ABTS is $34,700 \text{ M}^{-1} \text{ cm}^{-1}$).

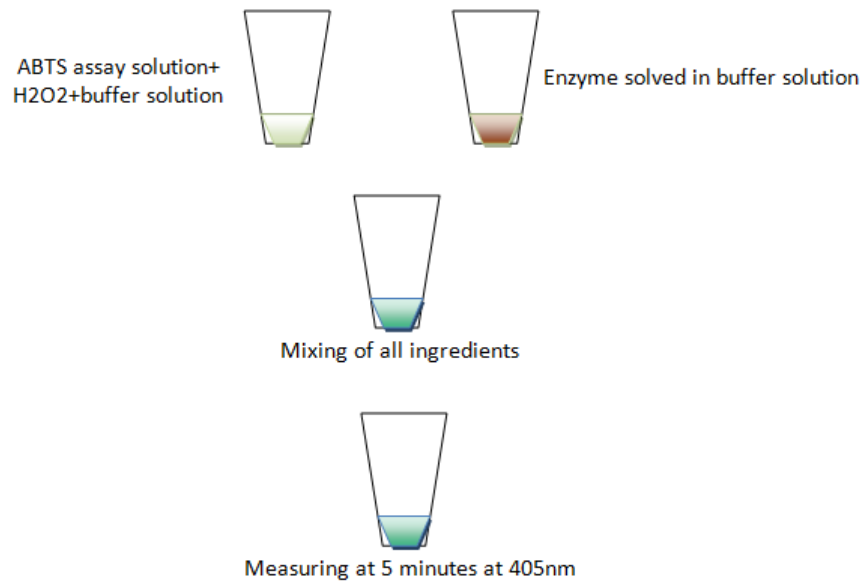


Figure 70: ABTS assay protocol¹¹¹.



Figure 71: ABTS assay¹¹¹.

7.1.7 Harvesting process

First, the fermentation mixture was centrifuged at 4,000 rpm in order to separate the cells from the liquid phase without disrupting them. The supernatant, which contains the HRP, was taken up and centrifuged a second time at 10,000 rpm on order to remove smaller colloids. Next, the supernatant

was filtered in three steps using filters of decreasing pore sizes (0.8 µm, 0.45 µm and 0.2 µm). Finally, the product solution was concentrated using a 10kD cross flow membrane.

7.1.8 Enzyme purification

The enzymes were purified using fast protein liquid chromatography (FPLC). This was performed using an ÄKTA™ purifier FPLC-system (Amersham). The system was controlled using UNICORN™ software. The purification was performed in a three step chromatographic process using hydrophobic interaction chromatography (HIC column), followed by anion exchange chromatography (QFF column), and size exclusion chromatography (Superdex column). The conductivity and the absorption at 404 nm and 280 nm were recorded in all cases. The HRP activity was evaluated by taking fractions, and analyzing them using ABTS approach. Between the chromatographic procedures, the product mixture had to be concentrated, and buffer systems had to be changed. Depending on the sample volume, this was performed using the Sartorius Vivaspin 20 system (3,000 MWCO cut-off, small volumes), or the Sartorius Vivaflow 50 system (30,000 MWCO cut-off, larger volumes).

Hydrophobic interaction chromatography (HIC)

As stationary phase, phenyl sepharose® 6 Fast Flow packed in a XK26/20 column was used. It was done as recommended by the manufacturer. First, the column was equilibrated with buffer HIC-A (1 M (NH₄)₂SO₄ + 20mM Tris, pH 7). After applying the product mixture, the column was rinsed with HIC-A buffer. Next the mobile phase was changed gradually from 100 % HIC-A which was replaced to 100 % HIC-B (20mM Tris, pH 7) in a linear gradient from 0% HIC-B to 100% HIC-B over 23x column volumes (CV), and with a flow rate of 15 ml/min.

Anion exchange chromatography (QFF)

As stationary phase, about 20 ml Q Sepharose® Fast Flow material packed in a XK26/20 column was used. First, the system was rinsed using QFF-A (50mM Tris, pH 9.5) buffer, as recommended by the manufacturer. Next, the product mixture was applied. Elution was performed by changing the mobile phase in a stepwise gradient from QFF-A to QFF-B (50mM Tris + 1M NaCl, pH 9.5) buffer. After 2x CV, 0% QFF-B was added, after 4x CV, 5% QFF-B was added, after 4x CV, 10% QFF-B was added, after 4x CV, 20% QFF-B was added and after 4x CV, 100% QFF-B was added for the elution of the bound proteins.

Size exclusion chromatography (Superdex)

As stationary phase a HiLoad™ 16/60 Superdex™ 200 prep grade column, pre-packed with 120 mL matrix material, was used. It was equilibrated according to the manufacturer. An aqueous 10mM CaCl₂ solution (pH 6.5) was used as mobile phase. After rinsing the system, the product mixture (50 ml) was applied. Elution was performed at a flow rate of 0.3 ml/min over 2 column volumes.

For size exclusion chromatography, the Superdex buffer (3.5 mM citrate, 32,9 mM Na₂HPO₄, pH 7.0) was used.

7.2 Results and discussion

7.2.1 Preculturing

The preculturing process was followed by measuring the OD₆₀₀. The factor changes linearly with the cell density. An OD₆₀₀ of 1 corresponds to 10⁹ cells per ml.

Two different *Pichia pastoris* strains were used. Both strains are genetically optimized for metabolizing MeOH. However, although the genes coding the MeOH converting enzymes (in this case AOX1) are coupled with the HRP expression system, the strains differ in their ability for producing HRP. Moreover, differences may occur in producing disturbing impurities. In contrast to A2 mut, the *Pichia pastoris* strain A2 syn includes a new recombinant synPDI HRP expression system. PDI genes are supports for the correct disulfide bridge formation and folding of the recombinantly expressed HRP. The team of the Research Centre Applied Biocatalysis, Graz, isolated the PDI704 gene from gDNA of *P. Pastoris* CBS7435. The synthetic gene synPDI based on the sequence of a *P. Pastoris* X-33 PDI. The synthetic gene synPDI N314H is a mutant of the synthetic gene synPDI with a N314H spontaneous mutation.

This system is encoded by a nucleic acid comprising a sequence of SEQ ID NO:52, which was developed by the Institute of Biotechnology (IMBT).

In order to ensure an optimal cell concentration at the beginning of the fermentation process, cells were cultivated in three steps: First, an ONC was cultivated form a single cell culture. The ONC was then taken and further cultivated in order to increase the number of cells to a defined OD₆₀₀ (volume: 150 ml, OD₆₀₀: ~26, see **Table 4**). In particular, the OD₆₀₀ was increased by a factor of 1.6, whereas the

cell suspension's volume was increased by a factor of 3, compared to the ONC (volume: 50 ml, OD₆₀₀: ~16). For the fermentation, the preculture was diluted to 500 ml (preculture 2, OD₆₀₀: ~9). The purpose of the preculture 1 and the preculture 2 was to deliver enough fresh cells to get an approximately batch starting OD₆₀₀ of ~1.5 to 2.0 at a planned time point for inoculation, adjusted to the carbon source to be used in batch and fedbatch.

Table 4: Cell content of the ONC. OD₆₀₀ was back calculated from the diluted solution.

Sample	Dilution	OD ₆₀₀ after dilution	OD ₆₀₀
ONC from A2 syn 1	1/30	0.5609	16.8
ONC from A2 syn 2	1/30	0.5906	17.7
ONC from A2 mut 1	1/30	0.4165	12.5
ONC from A2 mut 2	1/30	0.5591	16.8

7.2.2 Fermentation process

The fermentation process was evaluated measuring the temperature, the pO₂, and the OD₆₀₀. The process was controlled by changing the stirring speed, and the feed flow rates (**Table 5**).

Table 4: Fermentation procedure.

Day	Temperature / °C	Velocity / rpm	pH value / -	pO ₂ / %	OD ₆₀₀ / -	Flow rate / ml/min	Feed / samples
1	28	500	5.72	99.3	9	2.0	Starting culture
2	28	500	5.26	91.1	25 - 200	2.0	Start of glycerol feed
3 a.m.	28	618	4.93	29.3	-	2.0	End of glycerol feed, 3.5 ml δ-ALA (Sample No. 1)
3 p.m.	28	633	4.92	29.6	-	2.0	Start of MeOH feed, (Sample No. 2)
4 a.m.	28	625	4.92	29.6	-	2.0	1.75 ml δ-ALA (Sample No. 3)
4 p.m.	28	653	4.95	29.5	-	2.0	Sample No.4
5	28	680	4.94	29.5	-	2.0	End of MeOH feed

The fermentation temperature is held constant at 28°C over the whole fermentation process. This is because *Pichia pastoris* cells are having their growing optimum at this temperature. The stirrer velocity was adapted continuously to the state of fermentation, in order to ensure constant oxygen supply.

Therefore, the stirrer velocity is coupled with the pO_2 sensing system. When cells are growing, by-products like proteins and polysaccharides are formed. This increases the solution's viscosity, hampers the oxygen transport, and therefore changes the pO_2 . The pH value was set to 5.0. Through the production of different organic acids during the fermentation process solutions pH turns to acidic values. This effect is more pronounced when MeOH is consumed, compared to glycerol. One of the main reasons is that more MeOH has to be consumed for gaining the same amount of energy, compared to glycerol. Therefore, the pH has to be adapted continuously during the fermentation process. The fermentation process consisted of 3 phases: The starting culture, the glycerol feed, and the MeOH feed. First, the diluted preculture was added to the fermentation media (overall volume: 4000 ml). Then the mixture was stirred over night in order to allow the cells to adapt themselves to the fermentation conditions (mechanical stress, etc.). The cell cultivation process (glycerol feed) was then started by continuously adding a glycerol solution to the fermentation bulk. Overnight in the fermenter, the cells grow very slowly (OD_{600} of about 25). The problem was that the concentration of the glycerol solution at the beginning was 10 times too small. However, after changing to the optimal glycerol content, the OD_{600} increased to 200 within 7.0 hours. This demonstrated that low glycerol content reduced the growing rate, but did not lead to cell death. Therefore, the fermentation process was continued. The OD_{600} was not further measured. During fed batch, a total of 462.2 g glycerol was added to the fermenter. Next, MeOH was added continuously to the fermenter (MeOH feed). The change from glycerol to MeOH as carbon- and energy source induces the expression of HRP. Additionally, δ -ALA is added two times, after 3 and after 4 days, to the fermentation bulk. δ -ALA is a precursor for heme, the key complex of the HRP's active centre. Therefore, the addition of δ -ALA shall increase the amount of expressed heme containing enzymes (HRP). The MeOH feed was stopped after 5 days. Finally, 349.5 g MeOH were consumed.

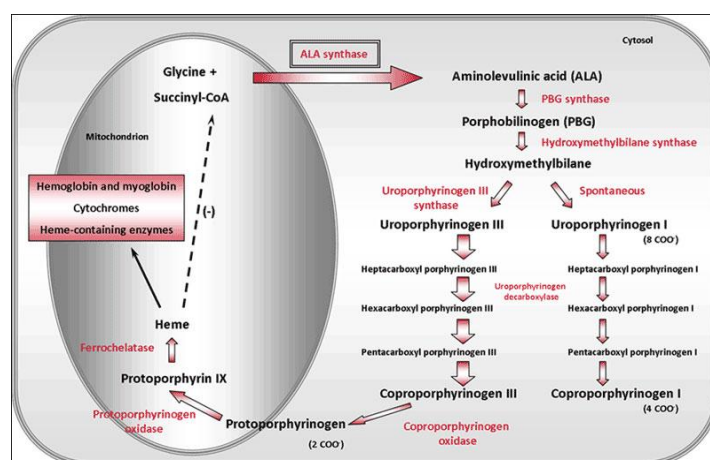


Figure 72: Heme pathway including δ -ALA¹¹².

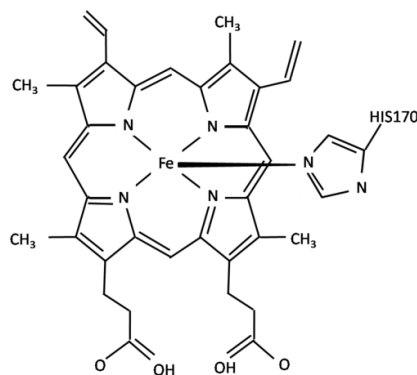


Figure 73: Structure of ion heme group in horseradish peroxidase.

7.2.3 Harvesting process

After finished fermentation procedure, the cells were separated from the supernatant via centrifugation. The supernatant contains the HRP, because *Pichia pastoris* secretes the enzyme into its surrounding. Therefore, cell disruption is not required. This makes the purification process much easier, because the separation of a very complex mixture consisting of the cell content and membrane components is not necessary.

After separating the cells, the supernatant was again centrifuged at higher speed in order to separate small colloids and remaining cells from the supernatant. After sedimentation, the supernatant was filtrated in a three step process, and finally concentrated in cross flow devices.

7.2.4 Purification

After harvesting, the concentrate was purified using chromatography. This was performed in a three step process, using hydrophobic interaction, anionic exchange, and finally gel permeation chromatography.

Hydrophobic interaction chromatography (HIC)

Figure 72 shows the chromatogram of the HIC. The green line is the activity (measured separately using ABTS assay), the blue line is the absorption at 280 nm (where proteins are absorbing), and the red line is the absorption at 404 nm (where heme, which is a component of the HRP's active site, is absorbing). The violet line shows the different fractions and the grey line is the conductivity.

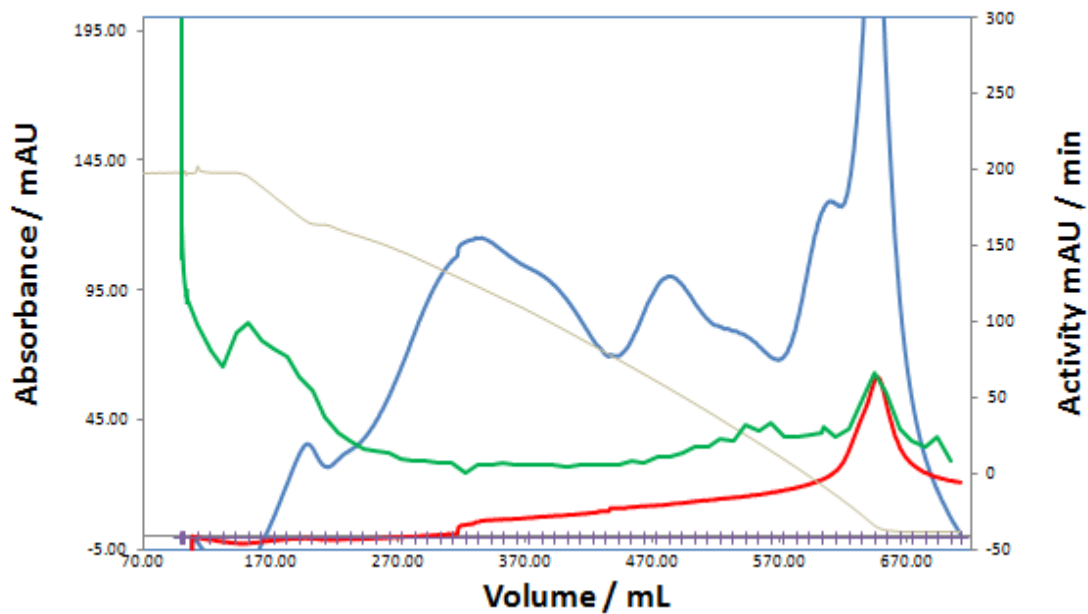


Figure 74: Hydrophobic interaction chromatography (HIC).

The HIC was not very successful. The column was overloaded very fast, and the majority of HRP did not interact with the stationary phase. Therefore, the HRP was washed out of the column, and nearly all the enzymatic activity of the HRP was collected in the flow through fractions. So, the column loading volume was too big and due to this fact, the HRP was washed out of the column. This indicates that the HRP content in the sample was surprisingly high. Because of this, we repeated this procedure with lower amounts of sample. However, it was not possible to obtain satisfying results. Unfortunately, large amounts of the A2 syn fermentation product were lost during these trials. Therefore, we mixed together the remaining fermentation product fractions, and went for the next chromatographic purification step.

Anionexchange chromatography (QFF)

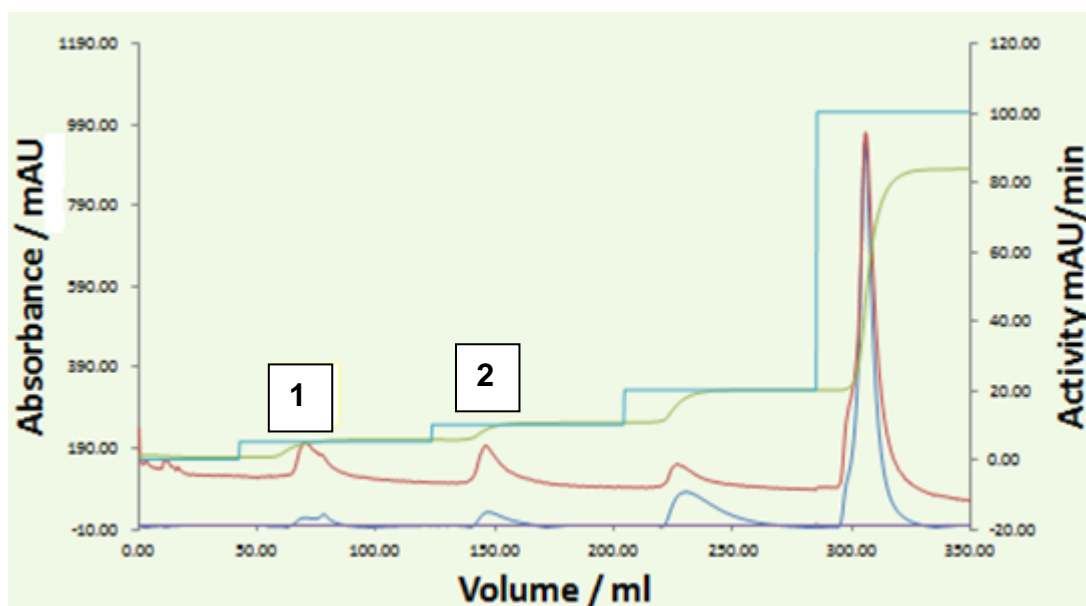


Figure 75: Anionexchange chromatography (QFF).

The QFF was working well; even through problems with the columns occurred. Several QFF columns had to be tested, until one with satisfying separation efficiency was found. Therefore, considerably amounts of the protein mixture were lost. **Figure 75** shows the chromatogram of the QFF with the best separation efficiency. The blue line is the absorption at 280 nm (where proteins are absorbing), the red line is the absorption at 404 nm (where heme, which is a component of HRP, is absorbing), the violet line shows the different fractions and the grey line is the conductivity. Three small peaks and one large peak were found in the chromatogram (absorption curves). The three smaller peaks (peak 1-3) correlated well with the enzyme activity (measured using ABTS test, not shown in the chromatogram). The large peak at the end of the chromatogram originates either from by-products, or from impurities. This peak increases, when Δ -Ala is added to the bulk solution during the fermentation (not shown explicitly). Therefore, this fraction most probably includes heme-containing proteins, but not HRP. This shows clearly, that the addition of δ -Ala boosts the production of by-products to a higher extent, compared to the production of HRP.

In contrast to our results, only one peak with activity occurs when the fermentation was performed without Δ -Ala. This may be because of the formation of larger protein complexes, but further investigations are required to clarify this result.

However, the fractions showing enzyme activity were collected, and further processed.

Size exclusion chromatography (Superdex)

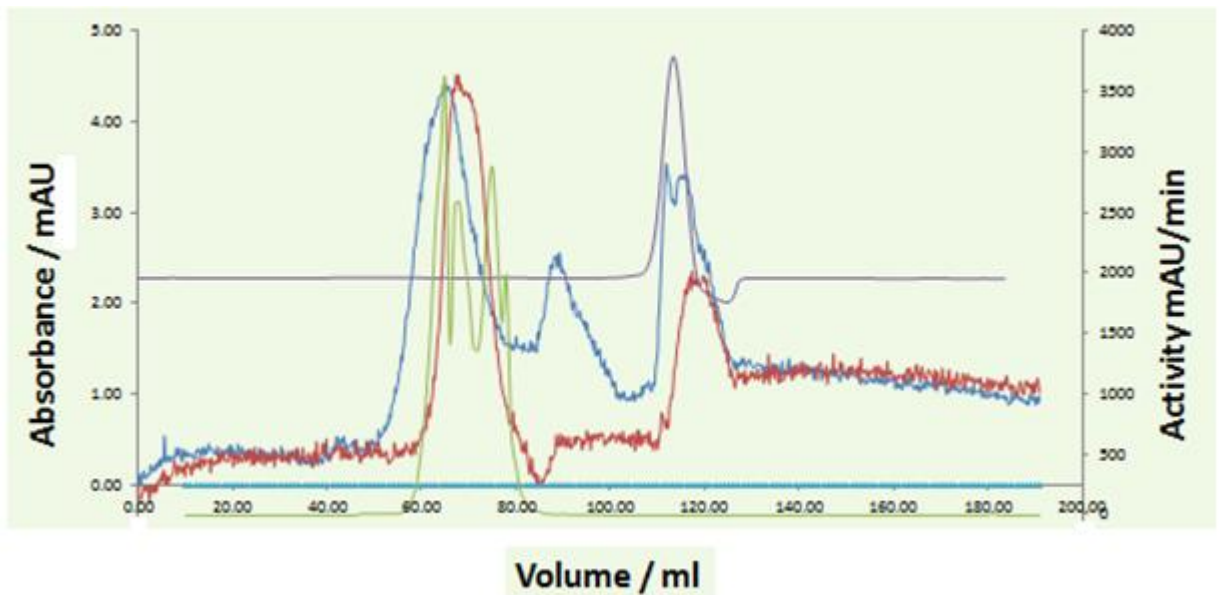


Figure 76: Size exclusion chromatography (Superdex).

The final purification was performed using size exclusion chromatography (**Figure 76**). The green line is the enzyme activity (measured separately with the ABTS assay), the blue line is the absorption at 280 nm (where proteins are absorbing), the red line is the absorption at 404 nm (where heme, which is a component of HRP, is absorbing), the violet line shows the different fractions and the grey line is the conductivity. The Superdex size exclusion chromatography was successful, but the separation efficiency was limited by the low concentration of the samples obtained from QFF. Even though the sample was loaded in small portions, their volume was too large, and the purification was not complete. The volume of 50 ml was applied onto the 120 ml column. A better variant would be about 5 ml onto the 120 ml column.

7.2.5 Characterization of the final product

Materials and Methods

BCA Protein Assay Kit was purchased from Thermo Scientific (Vienna, Austria). The BCA Protein Assay Kit was performed according to the company's protocol. The enzyme activity tests were performed according to chapter 6.

In order to quantify dissolved protein, I applied the microplate procedure protocol of the Pierce® BCA Protein Assay Kit (Thermo Scientific Fisher, Waltham, MA, USA). I used 250.0, 125.0, 50.0, 25.0, 5.0, 2.5 and 1.0 ng/μL BSA dilutions and 250.0, 120.0, 62.5, 31.25, 15.625 and 7.8125 ng/μL HRP VI-A dilutions for the generation of standard curves. I prolonged the suggested incubation time to 1 h at 37 °C prior to measuring the absorption at 562 nm.

Quantity and purity

The total amount of protein after chromatographic clean-up was determined through the BCA assay. Bovine serum albumin was used as calibration standard. A typical test assembly is depicted in **Figure 77**.

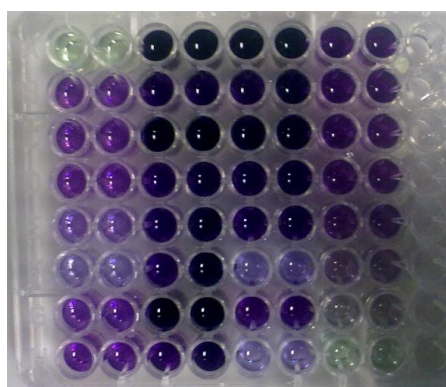


Figure 77: BCA assay

The calibration curve is depicted in **Figure 78**. After the size exclusion chromatography, all fractions which showed enzyme activity (12 ml) were combined. These combined fractions contained 34.2 μg/ml protein. From that, total protein content was calculated (437.8 μg).

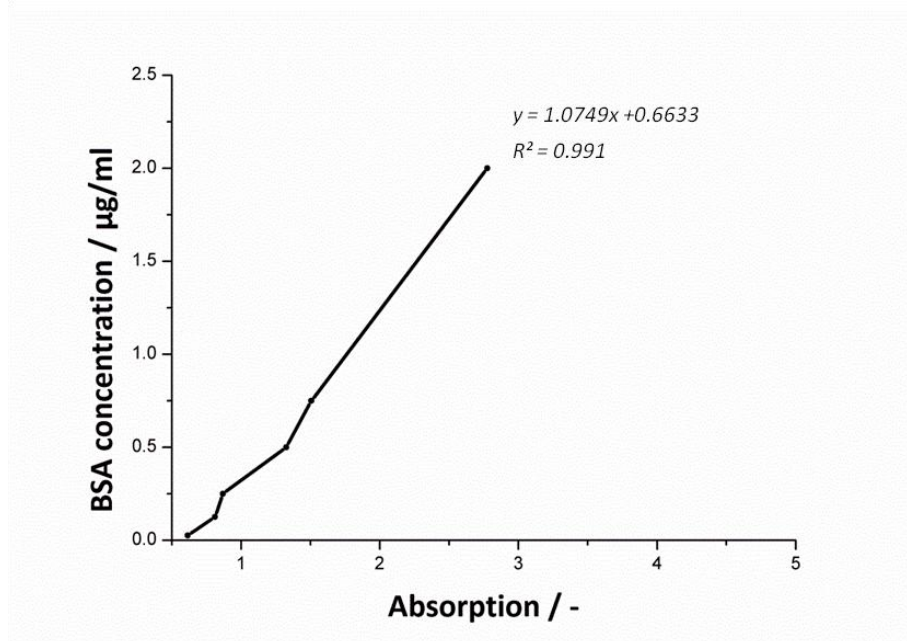


Figure 78: BSA calibration curve (BCA assay).

The purity of HRP in the final product solution was determined by calculating the Rz-values. The Rz-value is the relative intensity of the peaks (I_{404}/I_{280}) obtained at 280 nm (total protein content) and 404 nm (heme containing enzymes). For the final product, a Rz-value of 1 was obtained. This is relatively low, compared to Rz-values of 3 which were obtained from fermentations without Δ -Ala.

Activity

The activity of the final product against EE2 was determined using the approach described in chapter 6. In **Figure 79**, it can be seen, that the pure HRP A2 (3 µg/ml) degrades the hormone (10 µg/ml) very efficiently after a short incubation time (10 minutes). After longer incubation times, the hormone is totally degraded (30 minutes, data not shown explicitly).

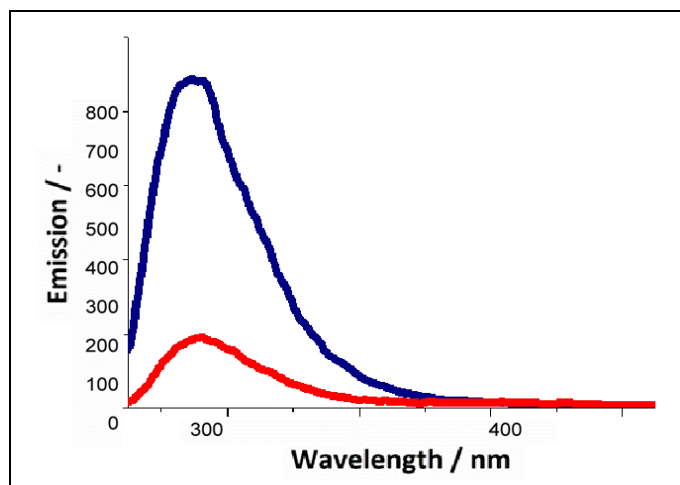


Figure 79: Fluorescence spectra (Excitation: 280 nm) of the enzymatic hormone incubation of HRP A2 (Rz-value of 1). Dark blue line: EE2 before enzymatic incubation, red line: EE2 after enzymatic incubation.

Therefore, we showed that pure HRP A2 is degrading EE2 very efficiently, and the activity observed in crude fermentation bulk solutions originates from HRP.

7.2.5 Conclusion, problems, difficulties

To sum up, the fermentation process was very successful, since large amounts of protein were produced. However, because of overloading, the large amount of protein in the crude product solution was the major problem during the chromatographic purification procedure. Therefore, large amounts of product solution were lost, especially during the HIC clean up. So, bigger columns are required in order to successfully and quantitatively process the bulk after fermentation in presence of δ -ALA.

Moreover, the addition of δ -ALA leads to significant changes of the elution pattern, especially during QFF. Further investigations are required for clarifying these observations.

So, the addition of δ -ALA leads to the production of larger amounts of protein, but causes significant problems during the clean up procedure. Therefore, the final product was of lower purity, compared to the product after fermentation. Finally, we demonstrated that the pure HRP A2 degrades EE2 very efficiently.

8. Summary

We demonstrated that novel, genetically engineered HRP isoenzymes can be used for the fast and efficient degradation of hormones (EE2). The enzymes were highly active under environmental conditions, addition of co-factors (hydrogen peroxide) was not required. The most promising HRP isoenzyme A2 was then produced and purified at a large scale via expression through the yeast *Pichia pastoris* in a modified fermentation process (addition of the heme precursor δ -ala). This process yielded larger amounts of heme containing proteins (like HRP), compared to the "classical" procedure. Nonetheless, it turned out that the clean-up of the fermentation process is much more complicated when δ -ala is added during the fermentation. Because of this, the final HRP A2 product was of lower purity, compared to the product after fermentation without δ -ala. However, the final purified product, containing about 90 % HRP (Rz value of 1), showed to be highly active against EE2.

In parallel to that, we successfully modified cellulose acetate thin film surfaces with polysaccharides and polysaccharide composite nanoparticles. This was performed in a three step procedure. First, cellulose acetate surfaces were activated by cleaving some of the ester bounds. This was performed in a reproducible manner by immersing in 0.1M KOH solutions. Next, different functional polysaccharides (carboxymethyl cellulose, hydroxyethyl cellulose, low molecular weight chitosan, and amino cellulose) were adsorbed onto activated cellulose acetate surfaces in form of mono- or bi-layer. These functionalized cellulose acetate surfaces were then decorated selectively with specifically designed polysaccharide composite nanoparticles. This nanoparticle coating on the one hand introduces specific binding sites to the surface which can be used for immobilizing HRP, and on the other hand increases the number of accessible binding sites by causing the surface area.

These nanoparticles were generated using nanoprecipitation technique, and characterized measuring their size and shape (DLS, SEM), their pH dependent zeta-potential (ELS), and by evaluating their stability.

In order to evaluate the antimicrobial growth on the modified and nanostructured cellulose acetate surfaces (anti-fouling properties), a novel analytical procedure, basing on RT-PCR and fluorescence staining, was developed. The test was set-up using low-molecular weight chitosan (antimicrobial) coated surfaces as positive control, and carboxymethyl cellulose surfaces as negative control. Using this test approach, we could demonstrate that coating cellulose acetate with a mono-layer of low molecular weight chitosan reduced the number of bacteria on the surface by more than a factor of 10.

9. List of tables

Table 1: Different Pichia pastoris strains..... 41

Table 2: Chromatographic principles..... 46

Table 3: Composite nanoparticle properties..... 64

Table 4: Cell content of the ONC. OD600 was back calculated from the diluted solution. 94

10. List of figures

Figure 1: Influence of hormones on fish fertilization rates ²⁸ .	15
Figure 2: Anti-baby pill ³¹ .	15
Figure 3: 17 α Ethinylestradiol ³¹ .	16
Figure 4: Reaction scheme of cellulose carboxymethylation in LiOH/urea aqueous solution. .	19
Figure 5: Chitosan ⁴⁸ .	20
Figure 6: Influence of salt. .	21
Figure 7: LbL technique: A negative charged polymer attaches on a positive charged surface, then a positive charged polymer can attach on this negative charged polymer. Double layer and bi-layer can be created ⁵⁵ .	22
Figure 8: Nanoparticle precipitation instruments in the laboratory scale .	23
Figure 9: Pentair X-Flow water treatment ¹⁸ .	24
Figure 10: Hollow fibre membrane and hollow fibre membrane modules connected together to form the Megablock ^{60, 61} .	25
Figure 11: Spincoating procedure and Spincoater ^{63, 64} .	25
Figure 12: Schematic drawing of working principle: Laser diode (A), cantilever (B), mirror (C), position-sensitive photo detector (D), electronic feedback system (E), sample (F) ⁶⁶ .	26
Figure 13: SEM image of an AFM tip ⁶⁷ .	27
Figure 14: Forces between tip and sample with respect to the distance from the surface ⁶⁶ .	27
Figure 15: Different AFM modi: Contact mode (1), non-contact mode (2), tapping mode (3). .	28
Figure 16: Column of SEM with major components ⁷¹ .	29
Figure 17: Modern, digital scanning electron microscope ⁷¹ .	30
Figure 18: SEM. .	30
Figure 19: Sarfus standard ⁷³ .	32
Figure 20: Optical polarizing microscope (1), Surf (2), Incident medium (3), Nanometric sample (4), $\Delta\theta$ (5), θ (6), Objective (7), Differential Interference contrast device (8), Polarizer (9), Non-polarized white light beam (10), Mirror (11), Crossed polarizer = analyzer (12) ⁷³ .	32
Figure 21: Different contact angle formations. .	33
Figure 22: Liquid drop with the contact angel Θ on a solid surface .	34
Figure 24: Jabłoński energy diagrams ^{78, 79} .	36

Figure 25: Spectralfluorometer ⁸⁰	38
Figure 26: <i>Arabidopsis thaliana</i> peroxidase ⁸²	38
Figure 27: <i>Pichia pastoris</i> ⁸⁸	41
Figure 28: Directed evolution ⁸⁹	42
Figure 29: <i>Pichia pastoris</i> strains for fermentation processes	43
Figure 30: CSTR or Fed-Batch Fermentation Process	44
Figure 31: Fermenter	45
Figure 32: ÄKTA purifier system	46
Figure 33: ÄKTA column ⁹⁴	47
Figure 34: A: Size exclusion chromatography; larger molecules (red dots) eluting in the earlier fractions than the smaller ones (blue dots). B: Exemplary chromatogram ⁹⁵	48
Figure 35: Ion exchange chromatography principles ⁹⁷	49
Figure 36: SPE tube	50
Figure 37: Schema of solid phase extraction procedure ⁹⁸	51
Figure 38: Stern model for a negatively charged surface	51
Figure 39: Electrophoretic light scattering principles ¹⁰¹	52
Figure 40: Dynamic light scattering principles ¹⁰³	53
Figure 41: Principles of dynamic light scattering ¹⁰⁵	54
Figure 42: Schematic picture of the membrane process. 1: Inner tube of the spinneret, 2: bimodal, and 3: coagulation bath filled with water.	60
Figure 43: CA nanoparticle precipitation setup including sonication and stirring with a stainless steel agitator ¹⁰⁷	61
Figure 44: Polysaccharide composite nanoparticles from CA	62
Figure 45: Layer by layer with polysaccharides and C.A. nanoparticles. The first block is a model surface without any coated substances, the second block contains the polymers which are introduced on the surface by LbL-technique, and the third block shows the polymer coatings with adsorbed active compounds like enzymes on it.	63
Figure 46: Mean composite nanoparticle diameters as a function of pH values and dispersive media .	64
Figure 47: SEM images of different in-situ composite CA nanoparticles. a: CA/HEC b: CA/CMC c: CA/L-CHI. d: CA/AC.	65
Figure 48: pH value depended effective zeta-potential of composite CA nanoparticles.	66
Figure 49: Cellulose acetate (CA) surface (AFM picture).....	68

Figure 50: Activated cellulose acetate (CAA) surface (AFM picture).	69
Figure 51: Layer thickness of the polysaccharide coated CA-A surfaces	70
Figure 52: Water contact angle of the polysaccharide coated CA-A surfaces	70
Figure 53: a: CA/CMC NPs onto L-CHI surface, b: CA/HEC NPs onto L-CHI surface, c: CA/L-CHI NPs onto HEC surface, d: CA/AC NPs onto CMC surface	71
Figure 54: OD600 of bacteria suspensions (<i>E. coli</i> MG 1655 [R1-16]) after incubation for 12 h.	73
Figure 55: Fluorescence microscopy results. The images obtained for SYTO® 9 (green) and propidium iodide (red) are matched together. Upper picture: CMC coated CA surface. Lower picture: CHI coated CA surface.	75
Figure 56: Calibration curve of RT-PCR.....	76
Figure 57: Fluorescence intensity with respected of the RT-PCR cycles.....	76
Figure 58: Number of bacteria found on 1 cm ² coated CA surface.	77
Figure 59: Fluorescence microscopy results. The images obtained for SYTO® 9 (green) and propidium iodide (red) are matched together. CHI coated CA surface.	77
Figure 60: Upper picture: Bacteria on CMC coated CA surface. Lower picture: Bacteria on CHI coated CA surface.	78
Figure 61: 17 α Ethinylestradiol (C ₂₀ H ₂₄ O ₂).	79
Figure 62: Enzyme and hormone incubation procedure.....	80
Figure 63: Emission spectra (Excitation: 280 nm) of EE2 (10 mg/ml)	82
Figure 64: Liquid-liquid extraction.....	83
Figure 65: Exemplary fluorescence spectrum obtained from extracts of pure HRP fermentation bulk and EE2 solutions. Dark blue line: HRP spectrum, red line: hormone spectrum.	84
Figure 66: Emission spectra (Excitation: 280 nm) of different fractions from the optimized SPE procedure. Pink line: hormone before enzyme incubation, green line: HRP sampling step after SPE, dark blue line: HRP washing step 1 after SPE, light blue line: HRP washing step 2 after SPE.	85
Figure 67: Emission spectra (Excitation: 280 nm) of EE2 (10 mg/ml) and EE2 with enzymatic incubation. Orange line: A2+EE2 incubation for 30 min after SPE, dark blue line: C1A+EE2 incubation for 30 min after SPE, brown line: EE2 without enzyme incubation after SPE.	86
Figure 68: Ferric enzyme reaction mechanisms ¹⁰⁹	87
Figure 69: ONC`s and precultures for the fermentation process.	89
Figure 70: ABTS assay protocol ¹¹¹	91
Figure 71: ABTS assay ¹¹¹	91

Figure 72: Heme pathway including δ -ALA ¹¹²	96
Figure 73: Structure of ion heme group in horseradish peroxidase.	96
Figure 74: Hydrophobic interaction chromatography (HIC).....	97
Figure 75: Anionexchange chromatography (QFF).....	98
Figure 76: Size exclusion chromatography (Superdex).	99
Figure 77: BCA assay	100
Figure 78: BSA calibration curve (BCA assay).	101
Figure 79: Fluorescence spectra (Excitation: 280 nm) of the enzymatic hormone incubation of HRP A2 (Rz-value of 1). Dark blue line: EE2 before enzymatic incubation, red line: EE2 after enzymatic incubation.	102

References

- (1) Vulliet, E.; Cren-Olive, C.; Grenier-Loustalot, M. Occurrence of Pharmaceuticals and Hormones in Drinking Water Treated from Surface Waters. *Environmental Chemistry Letters* **2011**, *9*, 103-114.
- (2) Salierno, J. D.; Kane, A. S. 17 Alpha-ETHINYLESTRADIOL ALTERS REPRODUCTIVE BEHAVIORS, CIRCULATING HORMONES, AND SEXUAL MORPHOLOGY IN MALE FATHEAD MINNOWS (PIMEPHALES PROMELAS). *Environmental Toxicology and Chemistry* **2009**, *28*, 953-961.
- (3) LUBBERT, H.; LEOROSSBERG, I.; HAMMERSTEIN, J. Effects of Ethinyl Estradiol on Semen Quality and various Hormonal Parameters in a Eugonadal Male. *Fertil. Steril.* **1992**, *58*, 603-608.
- (4) Combalbert, S.; Hernandez-Raquet, G. Occurrence, Fate, and Biodegradation of Estrogens in Sewage and Manure. *Appl. Microbiol. Biotechnol.* **2010**, *86*, 1671-1692.
- (5) Avbersek, M.; Soemen, J.; Heath, E. Dynamics of Steroid Estrogen Daily Concentrations in Hospital Effluent and Connected Waste Water Treatment Plant. *J. Environ. Monit.* **2011**, *13*, 2221-2226.
- (6) Chapman, H. Removal of Endocrine Disruptors by Tertiary Treatments and Constructed Wetlands in Subtropical Australia. *Water Sci. Technol.* **2003**, *47*, 151-156.
- (7) Joseph, L.; Zaib, Q.; Khan, I. A.; Berge, N. D.; Park, Y.; Saleh, N. B.; Yoon, Y. Removal of Bisphenol A and 17 Alpha-Ethinyl Estradiol from Landfill Leachate using Single-Walled Carbon Nanotubes. *Water Res.* **2011**, *45*, 4056-4068.
- (8) Cabana, H.; Jiwan, J. H.; Rozenberg, R.; Elisashvili, V.; Penninckx, M.; Agathos, S. N.; Jones, J. P. Elimination of Endocrine Disrupting Chemicals Nonylphenol and Bisphenol A and Personal Care Product Ingredient Triclosan using Enzyme Preparation from the White Rot Fungus *Coriopsis Polyzona*. *Chemosphere* **2007**, *67*, 770-778.
- (9) Zheng, W.; Colosi, L. M. Peroxidase-Mediated Removal of Endocrine Disrupting Compound Mixtures from Water. *Chemosphere* **2011**, *85*, 553-557.
- (10) Chiu, S.; Chung, T.; Giridhar, R.; Wu, W. Immobilization of β -Cyclodextrin in Chitosan Beads for Separation of Cholesterol from Egg Yolk. *Food Res. Int.* **2004**, *37*, 217-223.
- (11) Kirsch, C.; Woermeyer, K.; Zetzel, C.; Smirnova, I. Enzymatic Hydrolysis of Lignocellulose in a Fixed Bed Reactor. *Chem. Ing. Tech.* **2011**, *83*, 867-873.
- (12) Chiemchaisri, W.; Chiemchaisri, C.; Dumrongsukit, C.; Threedeach, S.; Huu Hao Ngo; Vigneswaran, S. Removal of Water-Borne Microorganisms in Floating Media Filter-Microfiltration System for Water Treatment. *Bioresour. Technol.* **2011**, *102*, 5438-5443.
- (13) Guo, H.; Hu, J. Y. Optimization Study of a Hybrid Alum Coagulation-Membrane Filtration System for Virus Removal. *Water Sci. Technol.* **2011**, *64*, 1843-1850.

- (14) Edzwald, J. K.; Haarhoff, J. Seawater Pretreatment for Reverse Osmosis: Chemistry, Contaminants, and Coagulation. *Water Res.* **2011**, *45*, 5428-5440.
- (15) Diogo, J. C.; Morao, A.; Lopes, A. Persistent Aromatic Pollutants Removal using a Combined Process of Electrochemical Treatment and Reverse Osmosis/Nanofiltration. *Environ. Prog. Sustain. Energy* **2011**, *30*, 399-408.
- (16) Zhao, S.; Zou, L. Effects of Working Temperature on Separation Performance, Membrane Scaling and Cleaning in Forward Osmosis Desalination. *Desalination* **2011**, *278*, 157-164.
- (17) Bodzek, M.; Dudziak, M. Elimination of Steroidal Sex Hormones by Conventional Water Treatment and Membrane Processes. *Desalination* **2006**, *198*, 24-32.
- (18) Anonymous Pentair X-Flow membrane products. <http://www.x-flow.com/products/> (accessed November/ 30.11.2011, .
- (19) Chen, X.; Chen, Z.; Zhu, J.; Xu, C.; Yan, W.; Yao, C. A Novel H₂O₂ Amperometric Biosensor Based on Gold nanoparticles/self-Doped Polyaniline Nanofibers. *Bioelectrochemistry* **2011**, *82*, 87-94.
- (20) Zhu, H.; Hu, Y.; Jiang, G.; Shen, G. Peroxidase-Like Activity of Aminopropyltriethoxysilane-Modified Iron Oxide Magnetic Nanoparticles and its Application to Clenbuterol Detection. *Eur. Food Res. Technol.* **2011**, *233*, 881-887.
- (21) Auriol, M.; Filali-Meknassi, Y.; Tyagi, R. D.; Adams, C. D. Oxidation of Natural and Synthetic Hormones by the Horseradish Peroxidase Enzyme in Wastewater. *Chemosphere* **2007**, *68*, 1830-1837.
- (22) François, B. Recombinant Protein Expression in Escherichia Coli. *Curr. Opin. Biotechnol.* **1999**, *10*, 411-421.
- (23) Weidner, M.; Taupp, M.; Hallam, S. J. Expression of Recombinant Proteins in the Methylotrophic Yeast *Pichia Pastoris*. *Journal of visualized experiments : JoVE* **2010**.
- (24) Kulterer, M. R.; Reischl, M.; Reichel, V. E.; Hribernik, S.; Wu, M.; Köstler, S.; Kargl, R.; Ribitsch, V. Nanoprecipitation of Cellulose Acetate using solvent/nonsolvent Mixtures as Dispersive Media. *Colloids Surf. A Physicochem. Eng. Asp.* **2011**, *375*, 23-29.
- (25) Banerjee, I.; Pangule, R. C.; Kane, R. S. Antifouling Coatings: Recent Developments in the Design of Surfaces that Prevent Fouling by Proteins, Bacteria, and Marine Organisms. *Adv Mater* **2011**, *23*, 690-718.
- (26) Chao, Y.; Zhang, T. Growth Behaviors of Bacteria in Biofouling Cake Layer in a Dead-End Microfiltration System RID C-6786-2008. *Bioresour. Technol.* **2011**, *102*, 1549-1555.
- (27) Kulterer, M. R.; Reichel, V. E.; Kargl, R.; Köstler, S.; Sarbova, V.; Heinze, T.; Stana-Kleinschek, K.; Ribitsch, V. Functional Polysaccharide Composite-Nanoparticles from Cellulose Acetate and Potential Applications. *Advanced functional Materials* **2011**, **under review**.
- (28) Anonymous Hormone influences in fish.
<http://www.google.com/imgres?q=17+%CE%B1+Ethinylestradiol&hl=de&biw=1280&bih=963&qbv=2&tbn=isch&tbnid=N7XvirYOODQWM:&imgrefurl=http://green.myninapple.com/%3Fp%3D1279&doc>

[id=zJltEvtD9JuvUM&imgurl=http://www.myninjaplease.com/green/http://green.myninjaplease.com/wp-content/uploads/2008/02/druggedfish.jpg&w=300&h=194&ei=5TjCTtuCLMOAhQeU4sWPDq&zoom=1&iact=rc&dur=266&sig=117264551103411711334&page=1&tbnh=119&tbnw=184&start=0&ndsp=28&ved=1t:429,r:17,s:0&tx=142&ty=83](http://www.myninjaplease.com/green/http://green.myninjaplease.com/wp-content/uploads/2008/02/druggedfish.jpg&w=300&h=194&ei=5TjCTtuCLMOAhQeU4sWPDq&zoom=1&iact=rc&dur=266&sig=117264551103411711334&page=1&tbnh=119&tbnw=184&start=0&ndsp=28&ved=1t:429,r:17,s:0&tx=142&ty=83) (accessed November/15.11.2011, .

- (29) Cooke, B. A.; King, R. J. B.; van der Molen, H. J. In *Hormones and their Actions Part I*; Elsevier Science Publishers B.V. (Biomedical Division), Ed.; The Netherlands, 1988; .
- (30) Lüllmann, H.; Mohr, K.; Hein, L. In *Pharmakologie und Toxikologie Arzneimittelwirkungen verstehen - Medikamente gezielt einsetzen*; Thieme Verlag: 2006; Vol. 16. Auflage.
- (31) Anonymous <http://www.google.at/imgres?q=17+%CE%B1+Ethinylestradiol&hl=de&biw=1138&bih=555&gbv=2&tbm=isch&tbnid=P9yqx4fAZR92xM:&imgrefurl=http://www.estratiser.de/de/project/summary.htm&docid=9qHnqzb6pDqCyM&imgurl=http://www.estratiser.de/images/ethylen.bmp&w=209&h=112&ei=NjzCTtXcKNC7hAeRz7XiDQ&zoom=1&iact=rc&dur=172&sig=101614880769573872947&page=1&tbnh=78&tbnw=146&start=0&ndsp=19&ved=1t:429,r:0,s:0&tx=71&ty=69> (accessed November/15.11.2011, .
- (32) Anonymous EE2. <http://www.env.gov.bc.ca/wat/wq/BCguidelines/PhACs-EE2/PhACs-EE2-tech.pdf> (accessed December/09.12.2011, .
- (33) Zeilinger, J.; Steger-Hartmann, T.; Maser, E.; Goller, S.; Vonk, R.; Laenge, R. Effects of Synthetic Gestagens on Fish Reproduction Rid B-1728-2010. *Environ. Toxicol. Chem.* **2009**, *28*, 2663-2670.
- (34) James, H.; Ghannoum, M.; Jurevic, R. The Story of Biofilms. *J. Invasive Fungal Infect.* **2011**, *5*, 37-42.
- (35) Kaplan, J. B. Antibiotic-Induced Biofilm Formation. *Int. J. Artif. Organs* **2011**, *34*, 737-751.
- (36) Anonymous Japanese Standard. <http://www.ats-labs.com/microbiology-lab-test-definitions/JISZ2801.htm> January, 08.01.2012).
- (37) Anonymous Live Dead Kit. <http://products.invitrogen.com/ivgn/product/L7007> January, 08.01.2012).
- (38) Tevik Dorak, M. In *Real-time PCR*; Bios Advanced Methods, Ed.; Taylor & Francis Group: New York, USA, 2007; .
- (39) Reimer Ludwig In *Scanning Electron Microscopy Physics of Image Formation and Microanalysis*; Optical Sciences, Ed.; Springer Verlag: Germany, 1998; Vol. 2, pp 533-533.
- (40) Anonymous OD600. [http://people.hofstra.edu/beverly_clendening/adv_molecular_biology/Protocols/Measuring Optical Dens.htm](http://people.hofstra.edu/beverly_clendening/adv_molecular_biology/Protocols/Measuring_Optical_Dens.htm) January, 08.01.2012).
- (41) Klemm, D.; Heublein, B.; Fink, H. P.; Bohn, A. Cellulose: Fascinating Biopolymer and Sustainable Raw Material. *Angewandte Chemie-International Edition* **2005**, *44*, 3358-3393.

- (42) Dieter Klemm, Bertram Philipp, Thomas Heinze, Ute Heinze, W. Wagenknecht, and D. Klemm In *Fundamentals and Analytical Methods, Volume 1, Comprehensive Cellulose Chemistry*. Wiley-VCH, Ed.; Wiley-VCH: 1998; .
- (43) AnonymousCellulose.
<http://www.google.at/imgres?q=cellulose+structure&num=10&hl=de&biw=1138&bih=555&tbnid=HMXcn5q8IBJ79M:&imgrefurl=http://www.afma.org/f-tutor/cellulose.htm&docid=D9NR0ASf1NSPSM&imgurl=http://www.afma.org/f-tutor/Images/Cell.GIF&w=390&h=375&ei=tpHeTtuDMsjk4QTFleGKBw&zoom=1&iact=rc&dur=240&sig=101614880769573872947&sqi=2&page=1&tbnh=106&tbnw=110&start=0&ndsp=21&ved=1t:429,r:2,s:0&tx=72&ty=42>December/09.12.2011).
- (44) Mark, C. P. In *Handbook of industrial membrane technology*; Noyes Publications, Ed.; US, New Jersey, 1990; .
- (45) AnonymousCA.
http://www.sigmaaldrich.com/catalog/ProductDetail.do?N4=180955|ALDRICH&N5=SEARCH_CONCAT_PNO|BRAND_KEY&F=SPEC (accessed December / 09.12.2011, .
- (46) Remington, J. P. In *The Science and Practice of Pharmacy*; University of Sciences in Philadelphia, Ed.; Berincott Williams & Wilkins: US, Baltimore, Maryland, 2006; .
- (47) Derek Horton, e. In *Advances in Carbohydrate Chemistry and Biochemistry, Vol. 51*; Academic Press, Ed.; Academic Press: 1995; Vol. 1st edition.
- (48) AnonymousCHI.
http://www.sigmaaldrich.com/catalog/ProductDetail.do?lang=de&N4=448869|ALDRICH&N5=SEARCH_CONCAT_PNO|BRAND_KEY&F=SPEC (accessed December / 09.12.2011, .
- (49) Rabea, E.; Badawy, M.; Stevens, C.; Smagghe, G.; Steurbaut, W. Chitosan as Antimicrobial Agent: Applications and Mode of Action. *Biomacromolecules* **2003**, *4*, 1457-1465.
- (50) Begin, A.; Van Calsteren, M. R. Antimicrobial Films Produced from Chitosan. *Int. J. Biol. Macromol.* **1999**, *26*, 63-67.
- (51) COMA, V.; DESCHAMPS, A.; MARTIAL-GROS, A. Bioactive Packaging Materials from Edible Chitosan Polymer?Antimicrobial Activity Assessment on Dairy-Related Contaminants. *J. Food Sci.* **2003**, *68*, 2788-2792.
- (52) Fleeer, G. J.; Cohen Stuart, M. A.; Scheutjens, J. M. H. M.; Cosgrove, T.; Vincent, B. In *Polymers at Interfaces*; Springer: 1993; Vol. 1st edition.
- (53) Joanny, J. F. In *Polyelectrolyte adsorption and charge inversion*; European Physical Journal B, Ed.; European Physical Journal B: 1999; .
- (54) Atkins, P. W. In *Physikalische Chemie*; Wiley-VCH Verlag GmbH: 1996; .

- (55) Decher, G.; Hong, J. D.; Schmitt, J. Buildup of Ultrathin Multilayer Films by a Self-Assembly Process: III. Consecutively Alternating Adsorption of Anionic and Cationic Polyelectrolytes on Charged Surfaces. *Thin Solid Films* **1992**, 210-211, Part 2, 831-835.
- (56) Decher, G.; Schlenhoff, J. B. In *Multilayer Thin Films: Sequential Assembly of Nanocomposite Materials*; Wiley-VCH: 2003; .
- (57) AnonymousSensors. <http://www.mdpi.com/journal/sensors> (accessed December/04.12.2011, .
- (58) Hashino, M.; Katagiri, T.; Kubota, N.; Ohmukai, Y.; Maruyama, T.; Matsuyama, H. Effect of Surface Roughness of Hollow Fiber Membranes with Gear-Shaped Structure on Membrane Fouling by Sodium Alginate. *J. Membr. Sci.* **2011**, 366, 389-397.
- (59) Whitford, W. G.; Cadwell, J. J. S. Interest in Hollow-Fiber Perfusion Bioreactors is Growing. *BioProcess International* **2009**, 7, 54-64.
- (60) AnonymousHollow fibre. http://www.google.at/imgres?q=hollow+fibres+membrane+Pentair&hl=de&biw=1138&bih=555&tbnid=isch&tbnid=wwlOwF4562Y4ZM:&imgrefurl=http://www.x-flow.com/applications/seawater%2520pre-treatment/&docid=iuBvffAQjYqZBM&imgurl=http://www.x-flow.com/import/assetmanager/3/8013/200/Seaguard_kl.png&w=200&h=135&ei=tC7OTvngCcXrsqa4qcmsDA&zoom=1&iact=hc&vpx=338&vpy=291&dur=32&hovh=108&hovw=160&tx=85&ty=31&sig=101614880769573872947&page=10&tbnh=108&tbnw=160&start=110&ndsp=10&ved=1t:429,r:1,s:110 (accessed 2011/ 30.11.2011, .
- (61) AnonymousMega Block. <http://www.google.at/imgres?q=Megablock+X-Flow&hl=de&biw=1138&bih=555&tbnid=isch&tbnid=b8cqeP637plekM:&imgrefurl=http://www.x-flow.com/news/new%2520aquaflex/&docid=x5ojcCqjOwn0QM&imgurl=http://www.x-flow.com/import/assetmanager/6/12606/300/Aquaflexskid.png&w=300&h=210&ei=qTDOTvSyOpDEsqbhivXzDA&zoom=1&iact=rc&dur=269&sig=101614880769573872947&page=1&tbnh=110&tbnw=157&start=0&ndsp=19&ved=1t:429,r:13,s:0&tx=116&ty=48> (accessed 2011/ 30.11.2011, .
- (62) Norrman, K.; Ghanbari-Siahkali, A.; Larsen, N. B. Studies of Spin-Coated Polymer Films. *Annu. Rep. Prog. Chem. , Sect. C: Phys. Chem* **2005**, 101, 174-201.
- (63) AnonymousSpincoating drop. http://www.google.at/imgres?q=spincoater&hl=de&sa=X&biw=1280&bih=737&tbnid=isch&prmd=imvns&tbnid=Jiv_yFrNpeQnyM:&imgrefurl=http://www.brewerscience.com/research/processing-theory/spin-coater-theory&docid=salLDzdvtgf6xM&imgurl=http://www.brewerscience.com/uploads/images/products/equipment/spin_theory/spinner.gif&w=200&h=156&ei=SNjDTumLE6aP4qT01LWTDQ&zoom=1&iact=rc&dur=165&sig=106994417291287727100&page=1&tbnh=124&tbnw=160&start=0&ndsp=15&ved=1t:429,r:1,s:0&tx=52&ty=16 November/18.11.2011).
- (64) AnonymousSpincoating 1. http://www.google.at/imgres?q=spincoater&hl=de&sa=X&biw=1280&bih=737&tbnid=isch&prmd=imvns&tbnid=Jiv_yFrNpeQnyM:&imgrefurl=http://www.brewerscience.com/research/processing-theory/spin-coater-theory&docid=salLDzdvtgf6xM&imgurl=http://www.brewerscience.com/uploads/images/products/equipment/spin_theory/spinner.gif&w=200&h=156&ei=SNjDTumLE6aP4qT01LWTDQ&zoom=1&iact=rc&

[dur=165&sig=106994417291287727100&page=1&tbnh=124&tbnw=160&start=0&ndsp=15&ved=1t:429,r:1,s:0&tx=52&ty=16](http://www.google.at/imgres?q=afm+tips&hl=de&sa=X&biw=1066&bih=802&tbnid=5vhHm0q9U1e7CM:&imgrefurl=http://courses.ee.nd.edu/87022/documents/AFM%26Milliped e.pptx&docid=10qL3-0XlMrS6M&w=1280&h=1024&ei=GEqMT06CDITysqbq1ZibAg&zoom=1&iact=rc&dur=140&page=2&tbnh=121&tbnw=151&start=20&ndsp=20&ved=1t:429,r:1,s:20&tx=76&ty=23)November/22.11.2011).

- (65) Bhushan, B., Ed. In *Springer Handbook of Nanotechnology*; Springer: Berlin, 2007; .
- (66) braga, P. C.; Ricci, D. In *Atomic Force Microscopy Biomedical Methods and Applications*; Human Press Inc.: New Jersey, 2004; Vol. Volume 242.
- (67) AFM tip
<http://www.google.at/imgres?q=afm+tips&hl=de&sa=X&biw=1066&bih=802&tbnid=5vhHm0q9U1e7CM:&imgrefurl=http://courses.ee.nd.edu/87022/documents/AFM%26Milliped e.pptx&docid=10qL3-0XlMrS6M&w=1280&h=1024&ei=GEqMT06CDITysqbq1ZibAg&zoom=1&iact=rc&dur=140&page=2&tbnh=121&tbnw=151&start=20&ndsp=20&ved=1t:429,r:1,s:20&tx=76&ty=23> (accessed 05.10.2011, .
- (68) Bushan In *Handbook of Nanotechnology*; Springer: 2004; .
- (69) Anonymous Non contact mode.
<http://www.chembio.uoquelpa.ca/educmat/chm729/afm/details.htm#noncontact> (accessed October/20.10.2011, .
- (70) Wasa, K.; Kitabatake, M.; Adachi, H. In *Thin films Materials Technology Sputtering of Compound Materials*; US, 2004; , pp 518.
- (71) Bozzola John J.; Russel Lonny D. In *Electron Microscopy: Principles and Techniques for Biologists*; Library of Congress Cataloging-in-Publication Data, Ed.; Jones and Bartlett Publishers: India, 1999; Vol. 2, pp 675-675.
- (72) Ausserre, D.; Valignat, M. -. Surface Enhanced Ellipsometric Contrast (SEEC) Basic Theory and $\lambda/4$ Multilayered Solutions. *Opt. Express* **2007**, *15*, 8329-8339.
- (73) Anonymous Sarfus techniques. <http://www.nano-lane.com/index.php> (accessed October/02.10.2011, .
- (74) Shin, J. Y.; Park, J. Y.; Liu, C. Y.; He, J. S.; Kim, S. C. Chemical Structure and Physical Properties of Cyclic Olefin Copolymers - (IUPAC Technical Report). *Pure and Applied Chemistry* **2005**, *77*, 801-814.
- (75) Manoj K., C. Interfacial Interaction between Low-Energy Surfaces. *Materials Science and Engineering: R: Reports* **1996**, *16*, 97-159.
- (76) Qing, S. In *Surface properties of cellulose and cellulose derivatives: A review*. In: Maren Roman, editor. *Model Cellulosic Surfaces*. American Chemical Society: Washington DC, 2009; , pp 259-89.
- (77) Anonymous Krüss contact angle measurements.
<http://www.kruss.de/de/theorie/messungen/kontaktwinkel/einfuehrung.html>November/22.11.2011).
- (78) Anonymous Fluor1.
<http://www.google.at/imgres?q=fluorescence&hl=de&biw=1138&bih=555&tbnid=6wWnr8sEt4wxIM:&imgrefurl=http://web.uvic.ca/ail/techniques/epi-fluorescence.html&docid=CE5K5mGy6SPLOM&imgurl=http://web.uvic.ca/ail/techniques/Jablonski.jpg&w=504&h=331&ei=HxagTriWMpT04QTx9o22BA&zoom=1&iact=rc&dur=102&sig=101614880769573>

[872947&page=1&tbnh=109&tbnw=166&start=0&ndsp=18&ved=1t:429,r:1,s:0&tx=75&ty=32](http://www.google.at/imgres?imgrefurl=http://www.rsc.org/chemistryworld/Issues/2004/July/rational.asp&h=400&w=400&sz=27&tbnid=6mJxp0SQKdz3iM:&tbnh=79&tbnw=79&prev=/search%3Fq%3Ddirected%2Bevolutio%26tbnid%3Disch%26tbo%3Du&zoom=1&q=directed+evolution&docid=qUhFVUHfMwS3xM&hl=de&sa=X&ei=31jPTtj8II7ktQbm1JHmDA&sqi=2&ved=0CHYQ9QEwCA&dur=485)October/20.10.2011).

(79) AnonymousFluo2.

http://www.google.at/imgres?q=fluorescence&hl=de&biw=1138&bih=555&tbnid=3Nd0UWxowD_NM:&imgrefurl=http://scienceblogs.com/purepedantry/2007/11/two_photon.php&docid=ULHQfWSsoNBFsM&imgurl=http://scienceblogs.com/purepedantry/fluorescence.gif&w=287&h=280&ei=HxaqTriWMPt04QTx9o22BA&zoom=1&iact=rc&dur=194&sig=101614880769573872947&page=1&tbnh=112&tbnw=115&start=0&ndsp=18&ved=1t:429,r:2,s:0&tx=59&ty=52October/20.10.2011).

(80) J. R. Lakowicz In *Principles of Fluorescence Spectroscopy*; Springer, Ed.; Springer: Baltimore, USA, 2010; Vol. Third Edition, pp 923.

(81) Veitch, N. C. Horseradish Peroxidase: A Modern View of a Classic Enzyme. *Phytochemistry* **2004**, *65*, 249-259.

(82) AnonymousHRP picture. <http://www.rcsb.org/pdb/explore/explore.do?structureId=1QO4> (accessed December/09.12.2011, .

(83) Passardi, F.; Theiler, G.; Zamocky, M.; Cosio, C.; Rouhier, N.; Teixeira, F.; Margis-Pinheiro, M.; Ioannidis, V.; Penel, C.; Falquet, L.; Dunand, C. PeroxiBase: The Peroxidase Database. *Phytochemistry* **2007**, *68*, 1605-1611.

(84) Hofrichter, M.; Ullrich, R.; Pecyna, M. J.; Liers, C.; Lundell, T. New and Classic Families of Secreted Fungal Heme Peroxidases. *Appl. Microbiol. Biotechnol.* **2010**, *87*, 871-897.

(85) Ruth, C.; Hartner, F. S.; Glieder, A. Synthetic Pichia Pastoris Promoters

(86) Cregg, J. M.; Cereghino, J. L.; Shi, J. Y.; Higgins, D. R. Recombinant Protein Expression in Pichia Pastoris. *Mol. Biotechnol.* **2000**, *16*, 23-52.

(87) Cregg, J. M. In *Methods in Molecular Biology*TM 389 *Pichia Protocols*; Humana Press, Ed.; Humana Press: United States, 2007; Vol. Second Edition, pp 269.

(88) AnonymousPichia pastoris picture.

<http://www.google.at/imgres?q=pichia+pastoris&hl=de&sa=X&biw=1639&bih=783&tbnid=7-4T15oG1UiydM:&imgrefurl=http://bioinformatics.psb.ugent.be/genomes/&docid=UEO0lvU3MEcgpM&imgurl=http://bioinformatics.psb.ugent.be/readwrite/research/pichia.jpg&w=244&h=292&ei=qM2mTpWGJIXj4QTrr73qDw&zoom=1&iact=rc&dur=205&sig=104243967130752705234&page=1&tbnh=126&tbnw=105&start=0&ndsp=37&ved=1t:429,r:2,s:0&tx=72&ty=38>.

(89) AnonymousMutagenesis.

http://www.google.at/imgres?imgurl=http://www.rsc.org/images/evolution_tcm18-33294.jpg&imgrefurl=http://www.rsc.org/chemistryworld/Issues/2004/July/rational.asp&h=400&w=400&sz=27&tbnid=6mJxp0SQKdz3iM:&tbnh=79&tbnw=79&prev=/search%3Fq%3Ddirected%2Bevolutio%26tbnid%3Disch%26tbo%3Du&zoom=1&q=directed+evolution&docid=qUhFVUHfMwS3xM&hl=de&sa=X&ei=31jPTtj8II7ktQbm1JHmDA&sqi=2&ved=0CHYQ9QEwCA&dur=485.

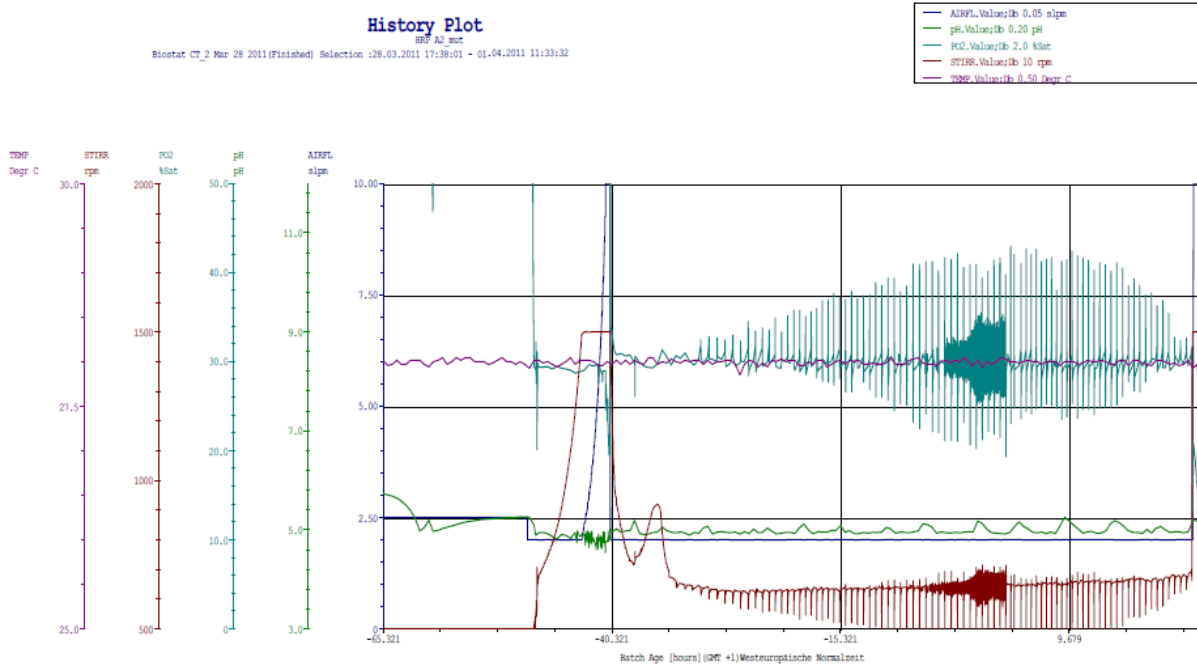
- (90) Esvelt, K. M.; Carlson, J. C.; Liu, D. R. A System for the Continuous Directed Evolution of Biomolecules. *Nature* **2011**, *472*, 499-U550.
- (91) Boulton, C.; Quain, D. In *Brewing Yeast and Fermentation*; Blackwell Science: USA, 2001; .
- (92) AnonymousHPLC. http://hiq.linde-gas.com/international/web/lq/spq/like35lqspq.nsf/docbyalias/anal_hplc (accessed October/24.10.2011, .
- (93) AnonymousÄKTA Purifier. http://www.gelifesciences.com/aptrix/upp01077.nsf/content/aktadesign_platform (accessed December/04.12.2011, .
- (94) AnonymousÄKTA pictures. http://www.google.at/imgres?q=superdex+column&hl=de&biw=1138&bih=555&tbm=isch&tbnid=YGOiC2LA7ovPJM:&imgrefurl=http://www.gelifesciences.com/aptrix/upp01077.nsf/Content/korea~product~consumables~korea_c_HiLoad%2BSuperdex%2BPrep%2BGrade%2BColumns%2Band%2BSuperdex%2BPrep%2BGrade%2BLab%2BPacks&docid=E1WdLoLo7d3gTM&imgurl=http://www.gelifesciences.com/aptrix/upp01077.nsf/4a0f132842ea4d354a25685d0011fa04/6c1bcf86a66709d5c12575a5000511b6/%2524FILE/p511_1.jpg&w=325&h=180&ei=8zLKTvmnEISftqbRqtmSDA&zoom=1&iact=rc&dur=158&sig=101614880769573872947&page=6&tbnh=131&tbnw=236&start=64&ndsp=12&ved=1t:429,r:8,s:64&tx=97&ty=17 (accessed December/04.12.2011, .
- (95) Walsh, G. In *Proteins Biochemistry and Biotechnology*; Jhon Wiley & Sons Ltd.: England, 2002; , pp 549.
- (96) AnonymousIon exchange chromatography. <http://www.separations.us.tosohbioscience.com/ServiceSupport/TechSupport/ResourceCenter/PrinciplesofChromatography/IonExchange> (accessed October/20.10.2011, .
- (97) AnonymousChromatography. <http://www.google.at/imgres?q=anionic+exchange+chromatography&hl=de&sa=G&biw=1366&bih=653&tbm=isch&tbnid=8UDF8q2qDq82FM:&imgrefurl=http://www.ucl.ac.uk/~ucbcdab/enzpur/ionX.htm&docid=KwEX8C4u8ITjWM&w=700&h=525&ei=U1yLTruxIsXAswbnkZmaAg&zoom=1> (accessed 05.10.2011, .
- (98) Gey, M. H. In *Instrumentelle Analytik und Bioanalytik*; Springer: 2008; .
- (99) Hunter, R. In *Foundations of Colloid Science*; Oxford University Press: Oxford, UK, 2001; .
- (100) Köstler, S. *Nanoparticle Dispersions of Organic Semiconductor Materials*, 2007.
- (101) AnonymousELS. <http://www.google.at/imgres?q=electrophoretic+light+scattering&hl=de&sa=X&biw=1138&bih=555&tbm=isch&prmd=imvns&tbnid=9ZzdImqV2QqYoM:&imgrefurl=http://www.currentprotocols.com/protocol/ps0708&docid=iJcH5bQyazz8M&imgurl=http://media.wiley.com/CurrentProtocols/PS/ps0708/ps0708-fig-0001-1-full.gif&w=403&h=245&ei=mszKTpmMlcfLswb08rDcDA&zoom=1&iact=hc&vpx=640&vpy=144&dur=66&hovh=175&hovw=288&tx=142&ty=97&sig=101614880769573872947&page=1&tbnh=88&tbnw=145&start=0&ndsp=21&ved=1t:429,r:4,s:0> (accessed December/04.12.2011, .

- (102) Ohshima, H.; Furusawa, K. In *Electrical phenomena at interfaces: fundamentals, measurements and applications*, Marcel Dekker Inc. New York, 1998; .
- (103) AnonymousDLS.
http://www.google.at/imgres?q=dynamic+light+scattering&hl=de&biw=1138&bih=555&tbm=isch&tbnid=yhA4WZchcUcVLM:&imgrefurl=http://www.malvern.com/LabEng/technology/dynamic_light_scattering/classical_90_degree_scattering.htm&docid=niWddrQ5qpUc_M&imgurl=http://www.malvern.com/labeng/technology/images/dynamic_light_scattering_beampath.gif&w=292&h=327&ei=H83KtW1N47BswbY45XIDA&zoom=1&iact=rc&dur=478&sig=101614880769573872947&page=1&tbnh=101&tbnw=90&start=0&ndsp=20&ved=1t:429,r:2,s:0&tx=32&ty=60 (accessed December/04.12.2011, .
- (104) Glatter, O. In *Scattering methods applied to soft condensed matter*; Elsevier: Amsterdam, 2007; .
- (105) Anonymoushttp://www.google.at/imgres?q=dynamic+light+scattering&hl=de&sa=X&biw=1066&bih=802&tbm=isch&prmd=ivnsb&tbnid=xqRb9WHL4A4dIM:&imgrefurl=http://ujkeb.com/facilities.html&docid=GMCFPtH2IY1shM&w=350&h=294&ei=VxpuTpLiLiXsqb_rJzWBA&zoom=1&iact=rc&dur=148&page=1&tbnh=149&tbnw=177&start=0&ndsp=16&ved=1t:429,r:4,s:0&tx=127&ty=123 (accessed October/03.10.2011, .
- (106) AnonymousnanoLANE Sarfus. <http://www.nano-lane.com/> (accessed December/09.12.2011, .
- (107) Kulterer, M. R.; Reischl, M.; Reichel, V. E.; Hribernik, S.; Wu, M.; Köstler, S.; Kargl, R.; Ribitsch, V. Nanoprecipitation of Cellulose Acetate using solvent/nonsolvent Mixtures as Dispersive Media. *Colloids Surf. Physicochem. Eng. Aspects* **2011**, 375, 23-29.
- (108) Müller, R. H. In *Zetapotential und Partikelladung in der Laborpraxis*; Paperback, Ed.; Wissenschaftliche Verlagsgesellschaft mbH Stuttgart: 1996; Vol. 37.
- (109) AnonymousHeme Pathway.
http://www.google.at/imgres?q=horseradish+peroxidase&hl=de&biw=1680&bih=901&tbm=isch&tbnid=DqVFdohM8wUxmM:&imgrefurl=http://www.nature.com/nature/journal/v417/n6887/fig_tab/417463a_F1.html&docid=nARi2icYnuJGJM&imgurl=http://www.nature.com/nature/journal/v417/n6887/images/417463a-f1.2.jpg&w=600&h=333&ei=3gniTr_jlInV4QSB2MT7BA&zoom=1&iact=rc&dur=146&sig=102809386527884128660&page=1&tbnh=127&tbnw=229&start=0&ndsp=31&ved=1t:429,r:1,s:0&tx=76&ty=27 (accessed December/09.12.2011, .
- (110) Hyka, P.; Zuellig, T.; Ruth, C.; Looser, V.; Meier, C.; Klein, J.; Melzoch, K.; Meyer, H.; Glieder, A.; Kovar, K. Combined use of Fluorescent Dyes and Flow Cytometry to Quantify the Physiological State of *Pichia Pastoris* during the Production of Heterologous Proteins in High-Cell-Density Fed-Batch Cultures. *Appl. Environ. Microbiol.* **2010**, 76, 4486-4496.
- (111) Morawski, B.; Lin, Z.; Cirino, P.; Joo, H.; Bandara, G.; Arnold, F. Functional Expression of Horseradish Peroxidase in *Saccharomyces Cerevisiae* and *Pichia Pastoris* RID A-7232-2011. *Protein Eng.* **2000**, 13, 377-384.
- (112) AnonymousDelta ALA. <http://www.google.at/imgres?q=%CE%B4-ALA+porphyrin&hl=de&biw=1680&bih=901&tbm=isch&tbnid=4crli2f5YiMAMM:&imgrefurl=http://www.aacc.org/publications/cln/2010/april/Pages/series.aspx&docid=khtdIArVFI7SsM&imgurl=http://www.aacc.org>

g/publications/cIn/2010/april/PublishingImages/Hemoglobin-Fig1.jpg&w=800&h=513&ei=ZqXiTo62Llaj4qSDovmaBQ&zoom=1&iact=rc&dur=180&sig=102809386527884128660&page=4&tbnh=140&tbnw=219&start=89&ndsp=33&ved=1t:429,r:18,s:89&tx=129&ty=101
(accessed December/09.12.2011, .

Appendices

Fermentation HRP A2 mut 28.03.-01.04.2011



Fermentation HRP A2 syn 28.03-01.04.2011

